ULTRASONIC PROPAGATION PROPERTIES OF CANINE MYOCARDIUM AT 100 MHZ

BY

SHARY YUN CHEN

B.S., University of Illinois, 1988

THESIS

Submitted in partial fulfillment of the requirements
for the degree of Master of Science in Electrical Engineering
in the Graduate College of the
University of Illinois at Urbana-Champaign, 1990

Urbana, Illinois

UNIVERSITY OF ILLINOIS AT URBANA-CHAMPAIGN

GRADUATE COLLEGE DEPARTMENTAL FORMAT APPROVAL

THIS IS TO CERTIFY THAT THE FORMAT AND QUALITY OF PRESENTATION OF THE THESIS SUBMITTED BY SHARY YUN CHEN AS ONE OF THE REQUIREMENTS FOR THE DEGREE OF MASTER OF SCIENCE ARE ACCEPTABLE TO THE DEPARTMENT OF ELECTRICAL AND COMPUTER ENGINEERING.

Full Name of Department, Division or Unit

7 December 1989

Date of Approval

Lilian H. Eckhouse

Departmental Representative

UNIVERSITY OF ILLINOIS AT URBANA-CHAMPAIGN

THE GRADUATE COLLEGE

JANUARY 1990

WE HEREBY RECOMMEND THAT THE THESIS BY

SHARY YUN CHEN

ENTITLED ULTRASONIC PROPAGATION PROPERTIES OF

CANINE MYOCARDIUM AT 100 MHZ

BE ACCEPTED IN PARTIAL FULFILLMENT OF THE REQUIREMENTS FOR

THE DEGREE OF MASTER OF SCIENCE

W. D. O'Brien
Director of Thesis Research

O. L. Dodd
for Head of Department

Committee on Final Examination†

Chairperson

† Required for doctor's degree but not for master's.

O-517

ACKNOWLEDGEMENTS

The author would like to express her appreciation to her advisor, Prof. William D. O'Brien Jr., for his encouragement, guidance and funding throughout this investigation. His optimistic attitude and sound advice have helped the author through many of the difficulties encountered in her research.

Also, much assistance has been extended by Dr. Kiran Sagar, Dr. Lorie Pelc and Jeanne Howard from the Medical College of Wisconsin.

The author would like to thank Wanda Elliott, Bob Cicone, Billy McNeill and Joe Cobb for providing advice and much needed assistance throughout the past two years.

Special thanks are extended to the author's family especially to her sister, Marilyn, for their unfailing encouragement and support throughout the author's education, and to Bob Camello, Ellen Cheng, Diane Agemura, Nadine Smith, Ilmar Hein, Felice Chu, Jian Zhang, and Frank Ngo for their help and moral support.

TABLE OF CONTENTS

CHAPTER 1

INTRODUCTION

1.1 Introduction

Ultrasound is currently one of the most popular and productive noninvasive diagnostic imaging techniques in medicine. Different ultrasonic techniques are used to obtain information about the structure and functions of the organs of the body. The propagation phenomena of ultrasound are the same as those of the audible sound. It occurs when mechanical vibrations in a region of a medium are transmitted to other regions by the mechanical interaction of the atoms and molecules in the medium.

One of the important applications of ultrasound is to produce images of tissue structures. The information supplied by ultrasound transmission is essentially different from that obtained by other diagnostic tools such as X-rays or isotope scanning. The clinical ultrasonic images are created by the backscatter of ultrasound energy from discontinuities wherever ultrasonic propagation properties are different. These images then convey the size and the nature of tissue structure. Information can be gathered for soft-tissue organs and lesions. In particular, currently available ultrasonic imaging techniques as used in cardiology have focused primarily on imaging the anatomy of the heart. These noninvasive methods allow the physician to observe the beating heart in real time and to define the size of the chambers and abnormalities of the valves and their motion. Ultrasonic waves possess the unique ability to

traverse soft tissue and to be partially reflected from soft-tissue interfaces. This interaction between ultrasound and tissue produces information which can be visually displayed. As a result, this image is directly related to the acoustic properties of the tissue. However, quantitative measurements of tissue properties can not be easily made from these images.

In contrast to ultrasonic imaging, ultrasonic tissue characterization allows for quantitative analysis of acoustic properties. The hypothesis underlying the characterization of tissue is that pathological changes alter the physical properties of the tissue and these changes can be detected and quantified by ultrasound [1]. In other words, measurements of material properties contain information about tissue composition, structure and mechanical characteristics. An application of ultrasonic tissue characterization is the detection of vascular pathology. The ability to detect variation in ultrasonic characteristics of vascular tissue due to calcium or lipid deposits or fibrous connective tissue would allow the monitoring of the development of atherosclerotic lesions in specific vessels. Another possible clinical use is the improved detection of cardiac tumors and mural thrombi (blood clots). Ultrasonic tissue characterization allows more precise identification than conventional echocardiography.

As one of the steps in the development of utilizing ultrasonic tissue characterization in clinical cardiology, an experiment was designed to study the relationship between ultrasonic propagation properties and biochemical changes in

myocardium tissue utilizing a 100 MHz scanning laser acoustic microscope (SLAM). The first group of experiments to be described in this thesis involves the studying of the properties of normal and ischemic canine myocardia analyzed by the SLAM and a clinical integrated backscatter technique. The second group of experiments studies the properties of rat liver and myocardium in order to better understand the results from the first group. Chapter 2 describes the SLAM and the ultrasonic backscatter instrumentation. Chapter 3 describes the preparation of canine myocardium and rat liver and myocardium. Chapter 4 includes the presentation and discussion of the results of the experiments. The main objective of these experiments is to compare the attenuation coefficient, ultrasonic speed, and heterogeneity index of ischemic myocardium with those of normal myocardia.

1.2 Background

The use of ultrasound in medicine makes it desirable to know the process responsible for altering the propagation of ultrasonic wave as it passes through biological tissue. However, this complicated process is little understood. Efforts have been made by studying the tissue properties associated with the propagation of sound in biological material. In particular, studies involving the ultrasonic characterization of myocardium tissue have been conducted.

1.2.1 Tissue constituents

The measurement of ultrasonic attenuation in tissue was first made by Pohlman in 1939 [2]. He found some differences among the measurements of body tissues and organs, observing a factor of two difference between fat and muscle tissues. Later, several publications discovered that ultrasonic properties of tissues, namely attenuation and speed, are largely determined at the macromolecular level. In 1953, Carstensen et al. [3] were the first to make the identification of the role of macromolecular constituents in the absorption process in their studies involving acoustic properties of blood. It was found that the attenuation of sound is directly proportional to protein concentration. Later, in 1959, Carstensen and Schwan showed that a small fraction of the attenuation is due to the cellular organization of the blood [4]. In 1971, Pauly and Schwan investigated the importance of structures in determining the attenuation properties of tissue [5]. It was found, in their studies on liver tissue, that two-thirds of the attenuation was attributed to protein at the macromolecular level, while one-third was to tissue architecture at the microscopic level. A study which compares the ultrasonic attenuation coefficient and the mean backscatter amplitude in different tissues as a function of time after excision shows that, while the attenuation coefficient does not vary significantly, the mean backscatter amplitude decreased considerably [6]. This result implies that backscatter signals are associated with large parenchymal structures which disintegrate first, while attenuation is

associated with the macromolecular structures which decompose more slowly. Ultrasonic speed measurements on various tissues were made by Frucht in 1953 [7] and described by [8]. Frucht found that velocity differences were related to tissue water content, tissue morphology and physiological function. Additional research was conducted which greatly expanded on the importance of tissue constituents and physiological function in relation to attenuation and speed parameters [9], [10]. A more recent study involving a comparison of ultrasonic attenuation and speed to the concentration of water, proteins, and fat reinforces the hypothesis that the propagation properties of tissue are functions of the constituent concentration [11]. The following will discuss the effects that each of these constituents has on the ultrasonic propagation properties in tissues.

Water comprises 70-80% of many biological tissues and exhibits a low attenuation coefficient [12]. Its overall effect is to dilute the macromolecular concentration and thus it does not by itself contribute to the acoustic properties of the tissue. Ultrasonic attenuation in the infant brain is approximately one-third that of the adult brain. Correspondingly, the infant brain has a much higher water concentration (approximately 90%) than the adult brain (76-79%). Additionally, in the fetal brain, the speed increases as water concentration decreases with age. These changes are caused by an increased concentration of solids, or conversely, a decreased concentration of water.

The protein constituents of tissues can be divided into the globular and the structural proteins. The structural protein, collagen, is a high tensile strength insoluble fiber found in most connective tissues. Collagen plays an important role in the acoustical properties of tissues for the following reasons: first, it is the most abundant protein in the human body (about six percent of total body weight); second, it exhibits widely different acoustic properties from those of other common tissue constituents [13], [14]. For example, collagenous fibers exhibit a static elastic modulus (Young's modulus) approximately 1000 times greater than that of other tissues [13]. Since ultrasonic speed is proportional to the square root of Young's modulus, the speed for collagen would be greater than for other constituents. Direct measurement of ultrasonic speed in tendon threads show that this is the case [14]. The higher speed in collagen implies that collagen also has a higher characteristic impedance which causes impedance mismatching with its surrounding tissues. As a result, collagen is responsible for most of the reflection and scattering within the tissues. Based on the examinations of articular tissues by [9], [10], a conclusion is drawn that tissues with high collagen concentration exhibited higher ultrasonic attenuation and speed than soft tissues containing less collagen.

Fat, or lipid, is an almost water-free tissue. Therefore, the total amount of water in the body is inversely dependent on the total amount of fat. Studies done on orotic acid treated rat liver [15] show that the ultrasonic speed is lower with an

increase in lipid concentration. The same studies also show a decrease in speed with decreasing water concentration, which contradicts the result reported above. A possible explanation is that there is a one-to-one replacement of water with fat and thus the low speed associated with lipid decreases the overall speed [16].

1.2.2 Canine myocardium

Acute myocardial infarction (death of heart tissue) is one of the major causes of deaths in the United States; 25% of infarctions occur abruptly and unexpectedly, usually within one hour of the first clinical symptoms [17]. Often, there is no time to make a firm clinical diagnosis. Thus, it is a challenge to recognize an infarct within a short period of time of its occurrence. The use of ultrasound can be a promising way to diagnose cardiac disease. The first exploration of ultrasonic signals through normal and diseased tissues from excised human heart dates back as early as 1957 [18]. Early methods of tissue characterization utilized two-dimensional and Doppler echocardiographic displays of abnormal tissue. Regions of "brightness," "speckling" and changes in grey scale were seen in patients with old myocardial infarction [19], amyloid heart disease (accumulation of a starch-like glycoprotein in the heart tissue) [20], and idiopathic hypertrophic cardiomyopathy (unknown increase in the size of the heart) [21]. Since the result was highly dependent on the user's experience in observing slight changes in the grey scale of the images, quantitative

representation of alterations of ultrasonic signals indicating their interactions with the normal or diseased myocardium was not readily attainable with conventional echocardiography.

As a solution to the problem of subjectivity, regional average echo amplitude and spatial distribution of amplitude were analyzed by computer [22]-[24]. Although this technique successfully differentiated normal, ischemic and post-ischemic reperfused myocardium, it was sensitive to the individual's adjustment of the instrument.

In contrast to conventional two-dimensional and Doppler echocardiography, cardiac ultrasonic tissue characterization is used to 1) quantitatively define the physical state of the cardiac muscle with ultrasonic parameters that relate to the structural components of the cardiac muscle; 2) differentiate functionally normal myocardium from tissue impaired structurally or functionally as a result of primary or secondary myocardial insults and 3) provide computer assisted images characterizing the tissue rather than the chamber dimensions alone, with the use of the quantitative approximation of backscatter and attenuation [25].

Important developments in ultrasonic tissue characterization involve the use of the "raw" radio frequency ultrasound and the measurement of changes in ultrasound attenuation and backscatter. In 1974, Lele and Namery [26] proposed that the tissue impedance and the frequency dependence of ultrasonic attenuation might be useful for identification of the characteristics of the myocardium with ultrasound. They found that an infarcted

myocardium has a lower acoustic impedance than a normal myocardium.

In 1977, Mimbs and co-workers performed in vitro experiments using the "through" transmission ultrasonic technique [27]. This method required two transducers, one on each side of the tissue. One of them was for transmitting and the other, for receiving. It was found that after a myocardial infarction, attenuation decreased followed by periods of increase. Although they had successfully differentiated ischemic from nonischemic myocardia, this technique could not be applied in vivo.

In 1979, using ultrasound reflection (backscatter), O'Donnell, Mimbs, and Miller developed experiments to study ultrasonic characterization of myocardium in vivo with open-chested dogs [28]. They developed an index called the Integrated Backscatter (IB) in order to distinguish normal and ischemic myocardia. The IB represents the frequency average of the backscatter transfer function over the bandwidth of the insonified transducer. The backscatter transfer function describes the efficiency with which ultrasound is backscattered at each frequency. The results of these studies showed that IB increased significantly after myocardial infarction both in vitro and in vivo [29]. Additionally, an increase in collagen, an increase in cardiac fluid content and a change in coronary blood flow were observed with increased IB.

In 1986, Rhyne and associates studied the absolute myocardial backscatter as a function of the frequency and phase of the cardiac cycle [30]. A first-order model was discovered in

which the scattering from the myocardium is Rayleigh scattering with a cardiac cycle variation in the scattering cross section. The statistics were approximately those of a radio frequency waveform with two independent Gaussian components (Rayleigh envelope). Their data suggested amplitude modulation which has minimal backscatter in systole and maximal in diastole. During ischemia, the amplitude modulation is reduced and phase shifted with respect to the cardiac cycle. In addition, it was found that during ischemia, the time average of the backscatter increases.

Due to the desire to extend cardiac backscatter measurements to the intact human chest and the discovery of the Rayleigh scattering model, Rhyne and associates introduced a new integrated backscatter parameter called the Integrated Backscatter Rayleigh 5 MHz corrected (IBR5), which is an absolute measure of the backscatter per cm, independent of the instrumentation and diffraction [31]. The measurement method consists of filtering the backscatter to achieve equal spectral weighting followed by squaring and averaging, which yield the average power of the signal. The IBR5 measurement is a maximum likelihood optimal estimator for the backscatter and for amplitude variation. This estimator is similar to that of O'Donnell, Mimbs and Miller [28], the differences being the establishment of an absolute scale factor, minimum variance, and a maximum likelihood estimate of the amplitude modulation.

Sagar and associates [32] characterized regional myocardial alterations of integrated backscatter during the cardiac cycle in

normal, ischemic, and post-ischemic reperfused myocardia. Their result showed that cardiac cycle-dependent amplitude modulation of integrated backscatter is dependent on myocardial contraction. Furthermore, it was observed that changes in amplitude modulation with the cardiac cycle were followed by changes in systolic segmental shortening and systolic muscle thickening during ischemia and reperfusion. This demonstrates that IB detects both the pathological abnormalities and the functional alterations in the myocardium during acute ischemia and reperfusion.

These studies show that the mechanics by which ultrasound interacts with the myocardium depend on the myocardial microstructures. However, few other facts are yet known about this mechanism. An approach to gain better understanding of this process is to study the ultrasonic properties of the myocardium at very high frequency, i.e., using the SLAM at 100 MHz. This technique permits the opportunity to study the ultrasonic myocardial microstructure and to relate modified backscatter amplitude to pathophysiological changes.

CHAPTER 2

SYSTEM DESCRIPTIONS

2.1 Scanning Laser Acoustic Microscope (SLAM)

A scanning laser acoustic microscope (Sonomicroscope 100^R, Sonoscan, Inc., Bensenville, IL), is utilized to make quantitative measurements on the biological specimens. It is used to determine the attenuation coefficient, the speed and the heterogeneity index of ultrasound at 100 MHz. A more detailed description of the SLAM and its operation can be found in References [33]-[40]. The following is a summary.

A block diagram of the SLAM is shown in Figure 1. A specimen is placed on the microscope stage. Inside the stage, there is a piezoelectric transducer which produces plane acoustic waves at a frequency of 100 MHz. On top of the stage, the specimen is submerged in a thin layer of saline and supported by a 25 μm sheet of mylar. Then, the specimen is covered by a semi-reflective gold-coated cover slip.

There are two types of stages: a fused-silica stage and a water stage. Both the fused-silica and the water act as low loss coupling media between the stage and the specimen. Even though the water stage gives a more uniform sound field, it is more fragile. The sound source of the 100-MHz continuous plane wave propagates through the coupling medium and then travels upward through the the specimen region. Within the sample, the sound is scattered or absorbed according to its internal microstructure. Thus, a distortion, or dynamic ripple, is

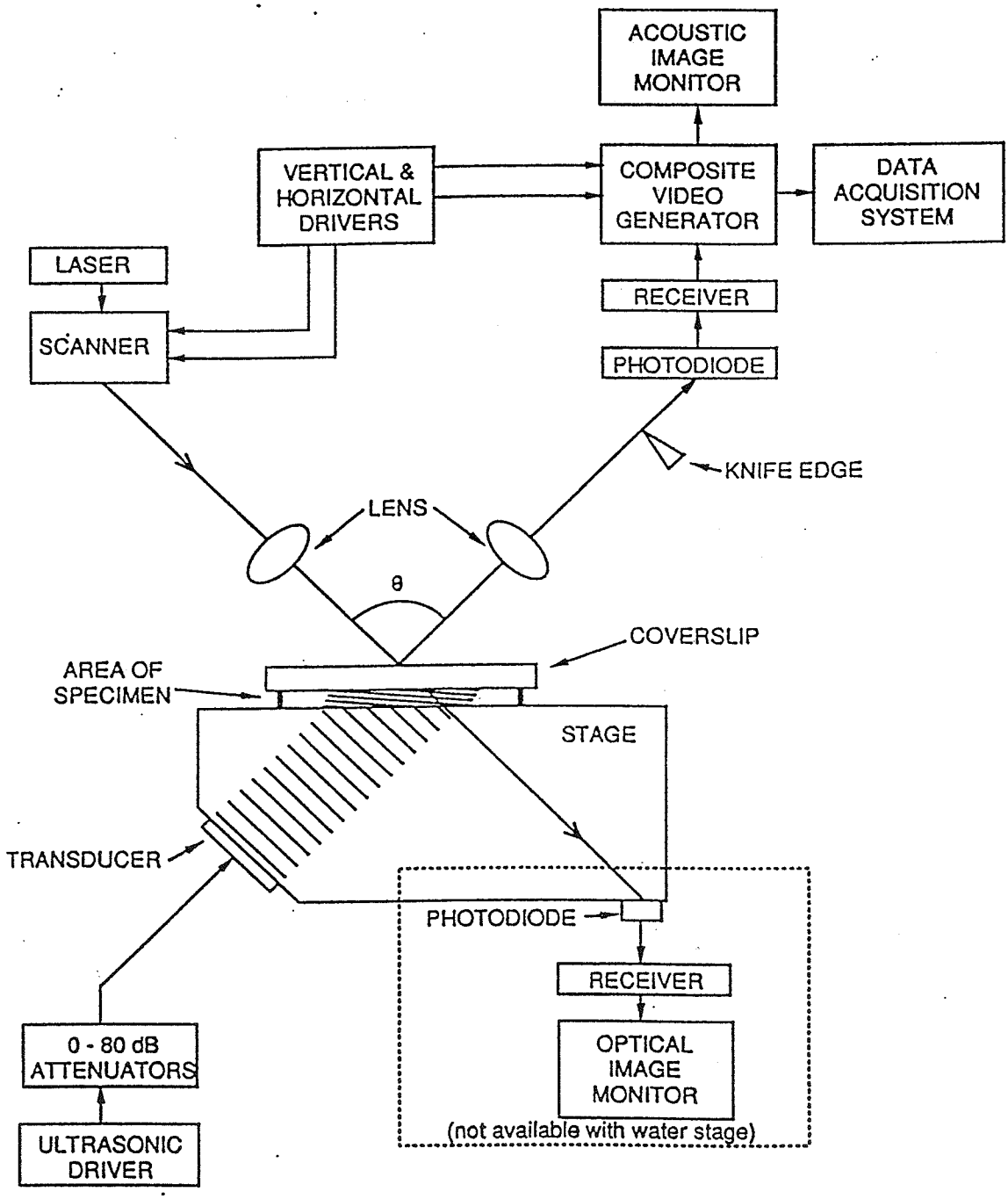

Figure 1. SLAM block diagram.

produced at the interface between the specimen and the coverslip. This ripple oscillates at the frequency of the sound and has an amplitude proportional to the acoustic pressure incident upon the interface. A focused laser beam is used to measure the degree of regional distortion which approximates the localized sound pressure.

Scanning at the rate of thirty images per second, the beam covers an area of 3 mm horizontally by 2 mm vertically. The laser beam reflected from the coverslip gold-film surface is angularly modulated by the changing slope of the ripple surface. A knife edge, placed in the path of the reflected beam, blocks a portion of the light depending on the angle of reflection. A photodiode detects the unblocked laser beam and converts it into electrical signal which is proportional to the ripple amplitude. This process can be thought of as amplitude modulation. The electrical signal is then passed through a receiver to a video signal generator which electronically magnifies the area being scanned and displays a two-dimensional image on a television monitor.

The SLAM is capable of displaying three different images with the fused-silica stage and two with the water stage. The first is an acoustic amplitude image shown in Figure 2. It is available for both stages. This image displays the spatial amplitude of the acoustic field after passing through the specimen. This image can be used to determine the attenuation of a sound in a specimen. On the monitor, the bright areas correspond to low attenuation while dark regions correspond to

high attenuation. The spatial resolution is limited by the acoustic wavelength and the laser beam size, approximately 20 μm.

The second type of image generated by the SLAM is an acoustic interference image shown in Figure 3. This image is also available for both stages. Mixing the output signal of the photodiode with a 100 MHz reference signal creates an electronic image which consists of approximately thirty-nine light and thirty-nine dark attenuating vertical bands or fringes. These bands correspond to constant phase fronts of the ultrasonic field. A change in phase due to a change in the ultrasonic speed will cause a shift in the fringes. For example, if a homogeneous material such as saline was placed between the stage and the coverslip, the lines would be straight and equally spaced as seen in the top and bottom areas of Figure 3. However, when a tissue specimen is placed in the saline, the interference lines would shift at the interface between the specimen and the saline, as seen at the interfaces between the top and center regions and the center and bottom regions in Figure 3. The magnitude and direction of this fringe shift are dictated by the localized speed of sound in the specimen relative to that in the saline. The interference lines will shift to the right if the speed of sound in the specimen is greater than that in the reference and to the left if the speed of sound in the specimen is less than that in the reference.

The third type of image generated is an optical image shown in Figure 4. The semi-transparent coverslip allows a fraction

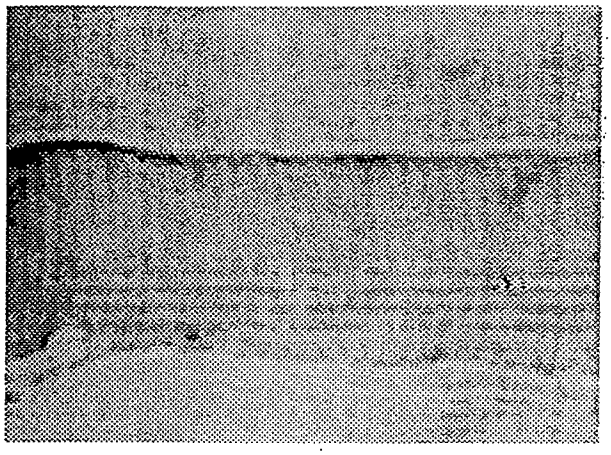

Figure 2. SLAM acoustic amplitude image of rat liver.

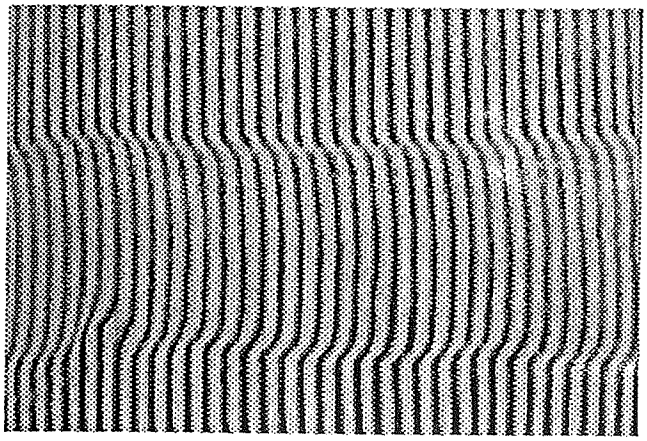

Figure 3. SLAM interference image of rat liver.

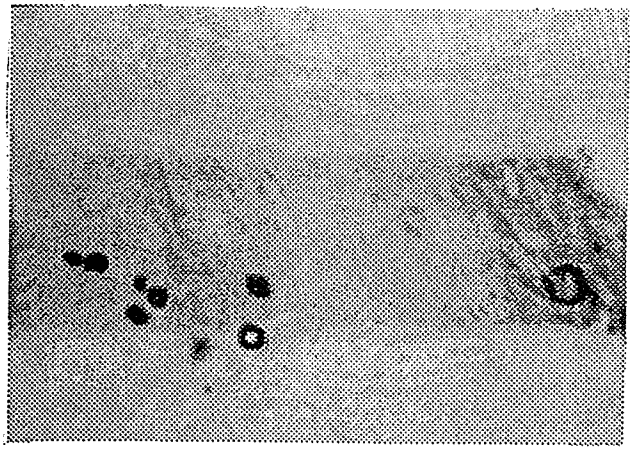

Figure 4. SLAM optical image of canine myocardium.

of the laser beam energy to penetrate through the sample from above. Inside the fused-silica stage, there is a photodiode which collects the transmitted light. The processed signal is then displayed on a second TV monitor as the optical image (magnified about seventy-five times). This optical image is not available with the water stage since there is no photodiode inside this stage. The optical image is used to position the specimen and identify optically transparent structures such as air bubbles which are shown as black regions in the acoustic image.

The data acquisition system developed for the quantitative measurement of the ultrasonic propagation properties will be described next. The system has been described previously [41] and will only be summarized here.

2.2 The SLAM Data Acquisition System

In order to determine quantitatively the attenuation coefficient and the ultrasonic speed, a computer and a frame grabber are used to acquire and analyze data from the SLAM's acoustic image and interference-mode image. This acquisition system was developed in 1986 [42] and greatly modified in 1989 [41].

2.2.1 Hardware

In the current system, an IBM Personal Computer AT (AT) with an 8 MHz 80286 microprocessor is used. The AT has a 640 kByte main memory and a 30 MByte hard drive. For computational

purposes, an 80287 mathematics coprocessor enhances the speed of floating point operations. In addition, there is an Archive XL 5540 40 MByte tape backup system for the storage of large image files. An enhanced Graphics Adapter (EGA) allows some graphics capabilities.

A Data Translation DT2851 video, plugged directly into an expansion slot of the AT, digitizes and stores video images. The AT communicates with the frame grabber through the standard IBM PC registers. The DT2851 has an 8-bit 10 MHz A/D converter. It acquires one full frame from the SLAM image. A full image is 512 pixels by 480 lines and requires 256 kBytes of memory. The DT2851 has memory for two such frames consisting of dual-ported random access memory (RAM). Thus, both the computer and the frame grabber can access the memory simultaneously. The DT2851 can output the contents of either of its buffers to a standard analog video monitor. A Data Translation DT2858 frame processor board with a memory of 256 K by 16-bit words is used to increase the speed of some imaging functions. It communicates with the AT through a pair of 10 MHz asynchronous parallel I/O ports. The image processor, through its logical and arithmetic functions, allows for frame averaging of up to 256 frames, convolution to perform filtering, and histograms to show the distribution of pixel values in an image. A pixel is an abbreviation for picture element.

2.2.2 Software

Algorithms for SLAM tissue characterization are implemented by computer programs written in language "C." These programs call subroutines from the Data Translation's DT-IRIS software package written specifically for accessing the Data Translation hardware such as the DT2851 and DT2858.

The following sections describe the algorithms and the software implementation for the attenuation measurement, ultrasonic speed, and heterogeneity index.

2.2.2.1 Attenuation coefficient measurement

The attenuation coefficient represents the decrease in acoustic energy after passing through the specimen. The method involved in its calculation utilizes the acoustic image and determines the difference between the received signal amplitude of a specimen of known thickness in the sound and that of the reference medium, low-loss normal saline solution. The procedure involves acquiring several amplitude values (V) in dB which represent the brightness of a boxed-in area on the acoustic image in both the saline and the specimen regions. The sample and its surrounding saline are moved around on the stage so that five to seven values can be taken from both regions for each thickness of the specimen. Insertion values are then calculated by taking the difference between the amplitudes for the specimen area and the average of those for the saline area. To determine the attenuation coefficient, the IL for three to nine different thicknesses are calculated.

These IL values are then plotted against the thicknesses. The attenuation coefficient is the slope of the best-fit line determined by the least squares method. A more detailed description of the procedure in determining the attenuation coefficient follows.

The AT uses a C program named "atten" to take data for the calculation of the IL. To reduce the effects of ultrasonic field nonuniformity over the 2 mm x 3 mm image, these data are taken from a subimage area of about 96 pixels horizontally and 32 pixels vertically (about 400 μm x 250 μm) . An image monitor which displays the same image, in real time, as the SLAM monitor shows an outlined box which encloses a portion of the acoustic image. This box represents the subarea from which data are taken. The operator then is able to try to make the boxed region as bright and uniform as possible by adjusting the SLAM stage forward and backward and also sideways until the optimal area is found. This procedure is necessary since the SLAM acoustic image is not consistently uniform across the monitor.

Since IL measurements need to be taken in several areas of the tissue specimen and the saline solution, and since the imaging area is fixed, there needs to be a way to move the specimen around. As a result, the specimen is place on a 25 μm sheet of mylar, coupled to the stage by water to provide mobility. Each subimage area is digitized to give an average amplitude value (V). This value represents the acoustic illumination of the image area. The procedure involved in finding V is as follows: first, an image is acquired, including

the reference signal; then, the reference signal for each raster line used in the subarea is averaged using ten samples and then subtracted from the pixel values on that raster line; finally, all the pixels in the subarea are averaged. The above procedure is repeated eight times and the overall average is taken. This value was converted to decibels and then displayed on the screen every five seconds. Equation (1) describes this process mathematically.

$$V = 10 \log \left\{ 1/n \sum_{1}^{n} \left[(1/3072) \sum_{i=y}^{y+31} \sum_{j=x}^{x+95} \left(v_{ij} - r_i \right) \right] \right\} \qquad (1)$$

where V = the overall average of the image areas in dB,

n = the number of times an image area is averaged,

y = the starting row number of the subarea,

x = the starting column number of the subarea,

i = the image row index,

j = the image column index,

v_{ij}= the value of the pixel at position (i,j), and

r_i = the average reference signal level of the i^{th} raster line.

The insertion loss is measured by first moving the saline on the mylar into the subarea to be measured. Using the image monitor as a visual aid, the SLAM is adjusted so that optimal brightness and uniformity are in the box as mentioned above. The user then moves a piece of thick plastic into the

leftmost area on the image monitor. This is done to block the laser beam in that region to establish the reference signal r_i which represents maximum attenuation. This procedure is necessary, because in the current system, the reference signal is no longer available. This is due to the fact that since the DT2851 samples a video signal, that portion of the receiver signal has been replaced by the horizontal sync pulse and the horizontal blanking signal. Next, a histogram of the pixel values is displayed on the monitor. This provides the user with both a graphic representation of the pixel value distribution as well as the absolute minimum, absolute maximum, average, and most prevalent pixel values. The user then adjusts the receiver gain to allow the maximum dynamic range of the frame grabber without saturation.

When the program "atten" is run, as many as desired V values can be recorded from both the saline and sample areas. Since the saline is assumed to be acoustically uniform, its V values are averaged and denoted by V_r. Each V measured in the specimen is denoted by V_s. The insertion loss is a measurement of the energy loss in decibels through the specimen. In dB, the insertion loss is given by

$$IL = V_s - V_r \tag{2}$$

A program in C named "regress" has been developed to calculate the IL. The program imports the V values from "atten." It prompts the user for the number of thicknesses and thickness

values. The program then calculates the reference average for each thickness and subtracts it from each of the sample intensity values to arrive at IL values as in Equation (2). The number of intensity values per thickness for the reference and sample need not be the same. Then, regress analysis on data pairs is performed. The output includes a data array of the thickness and insertion values, slope (attenuation coefficient), intercept, standard error, 95% confidence interval of both slope and intercept, number of data pairs, F test, and correlation coefficient. The data are plotted and the regression line is graphed.

2.2.2.2 Speed of sound measurement

The speed of ultrasound through a specimen can be obtained from the SLAM's interference image described in Section 2.1. The field of view, 3 mm x 2 mm, consists of thirty-nine vertical lines or fringes, equally spaced and having a center-to-center distance of 85 μm. The specimen is placed in the center of the field of view surrounded by a reference medium of known speed such that the image is divided into three parts. The top and bottom regions contain the reference medium (normal saline) while the center area contains the specimen (see Figures 2 and 3). Since the interference lines represent equal phase fronts, they shift upon entering the specimen region and shift back upon re-entering the reference. Abrupt shift in the interference lines should be avoided to allow the SFDT algorithm to track the phase values correctly. This can be achieved by

properly preparing the tissue samples. If the speed of sound of the reference and the thickness of the specimen are known, the speed of sound in the specimen can be calculated from the normalized fringe shift, N, using Equation (3) [14].

$$C_x = \left(C_o/\sin\ \theta_o\right) \sin\left\{\arctan\left[\frac{1}{(1/\tan\ \theta_o) - (N\lambda_o/T\ \sin\ \theta_o)}\right]\right\} \qquad (3)$$

where C_x = the speed of sound in the specimen,

C_o = the speed of sound in the reference medium,

λ_o = the wavelength of sound in the reference medium,

θ_o = the angle of sound, measured from the normal, in the reference medium,

N = the normalized fringe shift,

T = the thickness of the specimen.

The λ_o is given by $\lambda_o = C_o/f$ where f = 100 MHz. The θ_o is calculated for the reference medium using Snell's Law (4)

$$\theta_o = \sin^{-1}\left[\frac{C_o}{C_s}\ \sin\ \theta_s\right] \qquad (4)$$

where for the fused-silica stage, C_s = 5968 m/s is the speed of sound in the stage, θ_s = 45° is the angle at which the generated sound wave travels through the stage, and C_o = 1520 m/s is the speed of sound in normal saline. Thus, θ_o is calculated to be 10.37° at 22°C. For the water stage, C_s = 1509 m/s, θ_s = 10° and qo is calculated to be 10.07°. The only value left to be determined from Equation (3) is N.

Different methods have been developed to calculate the normalized fringe shift which refers to the lateral fringe shift relative to the fringe spacing. The first technique involved manually using a ruler to measure the fringe shift and fringe spacing directly from the TV monitor or a photograph. There were several disadvantages associated with this method: the readings were subjective and dependent on the operator's experience; additionally, the method was time consuming and yielded few speed measurements per specimen. As a result, an automated data acquisition system and the spatial domain technique were developed [43]-[45]. This method utilized a correlator to track each interference line and allowed for computer determination of fringe shift. Using this system, a fringe shift of down to 0.03 could be detected compared to the 0.1 from before. Also, 30 to 39 speed values could be determined to allow for statistical calculation of the mean, standard deviation, mode, median, skewness and kurtosis. In analyzing homogeneous material such as the liver which has smooth interference lines, the SDT worked well. However, for heterogeneous specimens, it sometimes failed.

In order to analyze heterogeneous specimens, the present technique, the spatial frequency domain technique (SFDT) was developed [46]. While the SDT determines the fringe shift, N, in the spatial domain, the SFDT determines it in the spatial frequency domain. Figure 5 illustrates the technique under the

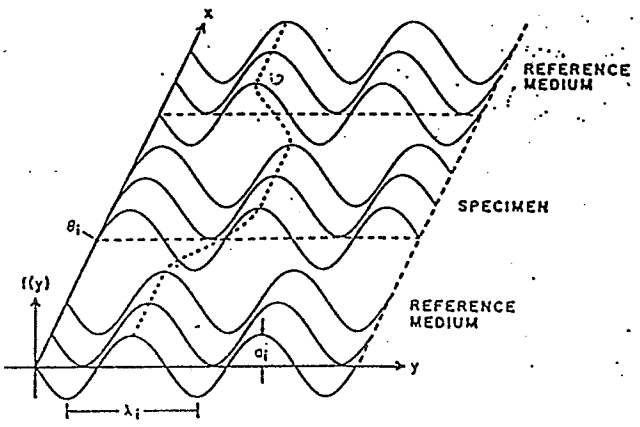

Figure 5. Illustration of the creation of a simulated interference image.

ideal conditions. Each sine wave depicts the pixel values for one raster line of an interference image versus their corresponding column index. This is due to the fact that the interference image consists of alternating bright and dark bands. Raster line plots from the reference regions and the specimen region are plotted. Even though, in all regions, the frequencies of the sine waves are the same, those of the specimen have a shift in phase relative to the reference regions. The SFDT is based on this shift in phase. For sine wave frequency ξ_o, the phase shift $\Delta\varphi(\xi_o)$, is given by

$$\Delta\varphi\left(-\xi_o\right) = 2\pi y_o/\lambda_y \tag{5}$$

where y_o is the amount of horizontal shift, and λ_y is the fringe line spacing. By definition, y_o/λ_y is the normalized fringe

shift N. Therefore,

$$N = \Delta\varphi(-\xi_o)/2\pi \tag{6}$$

The following is a description of the calculation of the phase shift. First, the Fourier transform of each raster line is taken to find its spatial frequency spectrum (or plane wave spectrum). Then, the phase for each line is found by choosing the phase at the frequency where the spectrum is a maximum (ξ_o), and taking the negative of that value. The negative of ξ_o is taken since the sampled data are real, and from the Fourier transform theory, the magnitude is symmetrical about the imaginary axis while the plane is symmetrical about the origin. Due to the cyclic nature of the Fourier transform, there is a 2π ambiguity in determining the phase. The solution developed for this problem involves a phase unwrapping algorithm. Lastly, the phase values for the reference region are averaged and subtracted from each specimen phase value to give the phase shift $\Delta\varphi(-\xi_o)$.

The Discrete Fourier Transform (DFT) is used since the data are discrete. The DFT is given by

$$X_k = \sum_{l=0}^{n-1} x_e e^{-j\frac{2\pi}{N}kl} \qquad k=0,1,2,\ldots,N-1, \tag{7}$$

where X_k = the discrete frequency domain variable with index k,

x1 = the discrete space or time domain (depending on the basis used) variable with index 1, and

N = the number of points used in calculating the transform.

There are several advantages of SFDT over the previous SDT method. As mentioned before, it works for heterogeneous specimens where SDT fails. This is accomplished by taking into account the variation in the spacing of the interference lines. In addition, it is twice as fast and more noise tolerant. Since the SFDT analyzes the SLAM image vertically, a contour or speed profile of speed versus data point can be constructed giving an illustration of the change in the speed of sound from saline to specimen.

The original SFDT used a 32-point Fast Fourier Transform (FFT), which is a fast DFT algorithm that requires N to be a power of 2. It assumed a constant fringe line spacing (raster signal wavelength) of approximately 84.5 μm (about 1.5 μs in the time domain), and thus a constant spatial frequency of about 11.8 km^{-1} (660 kHz in the time domain). However, this is not necessarily the case for heterogeneous specimens. As a result of this assumption, the phase for each raster line was always determined at a fixed frequency. However, due to leakage when using the DFT, this fixed frequency is not exactly the desired frequency ξ_o. An investigation of the digitized data for several interference images indicated that the assumption of constant fringe line spacing for heterogeneous materials was wrong. The actual spacing of the interference lines can vary significantly. Depending on the position of the image, saline was found to have maximum frequency components between 700 and

800 kHZ. However, examination of the heterogeneous specimen showed maximum frequency components between 600 and 800 kHz.

To compensate for the variation in fringe spacing, modification of the algorithm was necessary [42]. The new algorithm would seek the maximum spectral component within a band of frequencies known to be the limits of the variations. To achieve this, a normal DFT was calculated for the specified frequency components, and the phase for the frequency with maximum amplitude was used to compute N. Due to system nonlinearities, the interference lines have a slight slope from top to bottom of the screen. Therefore, instead of finding an average phase value, the algorithm used the linear least squares method to calculate the slope and intercept from the reference phase values. Then, the phase shift was found for each raster line by subtracting the corresponding reference phase from the current phase. A 728-point DFT, 18 discrete frequency components between 600 and 915 kHZ, and a window length of 20 data points were used. This modified SFDT not only reduces the overall time in speed data calculation but also produces speed values for each raster line (255 values).

In the current system [41], since the DT2851 samples a full video frame, 480 instead of 255 speed values are available. In addition, the user has more control over where and how the ultrasonic speed analysis is performed. However, modification is made mainly in the DFT calculation. The current system uses 512-point DFT, 21 discrete frequencies, and a window length of 26 data points to compute N. The window length was expanded

from the previous 20 data points since in the previous algorithm, DFT had a skewing problem which arose from discrepancies between the real sampled waveform and the predicted complex sine waves. Increasing the window length minimized this problem.

The software utilized to perform the speed analysis "speed," as "atten" and "regress," is also written in C. It allows the user to choose different values for the parameters in Equation (3). Using Equation (3) and the SFDT, the program then calculates the speed. The parameters include the thickness of the specimen, the speed of sound in the reference, and the type of stage used (affects θ_o). Furthermore, skip values can be chosen to skip some raster lines and speed up the analysis on a questionable specimen. Other important user-defined inputs include: first, the vertical region of the image where the speed is to be calculated and second, the reference regions. These regions are specified by using the cross-hair on the monitor. After the parameters are entered, calculation takes place and as a result, a plot of speed versus raster line is displayed on the image monitor. Data are stored in specified files.

2.2.2.3 Heterogeneity index (HI)

The variation in speed, depicted by HI, characterizes how heterogeneous a specimen is. The HI is calculated from the speed data using the modified SFDT [42]. Ideally, the standard deviation σ, a statistical measure of values about the mean of

the speed, can be used to determine HI. However, the SLAM system may add to this deviation from the mean speed value due to different sources such as electrical noise, a nonuniform sound field, etc. As a result, even homogeneous material such as saline would have variation in its speed value. To compensate for this difference, the deviation in speed due to the SLAM system is subtracted to give only the variation due to specimen heterogeneity. To measure the SLAM system variation, the standard deviation of the homogeneous reference saline is used. This standard deviation is then subtracted from that of the specimen. A mathematical description of the calculation of HI is

$$HI = (\sigma_s - \sigma_r) \times 100 \qquad (8)$$

where σ_s is the standard deviation (SD) of speed in the specimen and σ_r is the SD of speed in the reference. As discovered by Steiger [42], the SD is dependent on the number of times the image is averaged, the thickness of the sample, and the number of speed values averaged. A computer program named "stats" has been written to calculate the HI. From the graphical display of speed versus raster line (Figure 6), the user can use the cross-hair to choose the region where the mean and standard deviation are to be calculated.

2.2.2.4 Uncertainty in the SLAM assessment

Using a solution of known acoustic properties and duplicate samples of skin and healing wound tissue, uncertainty in the SLAM assessment of the sound speed and the attenuation

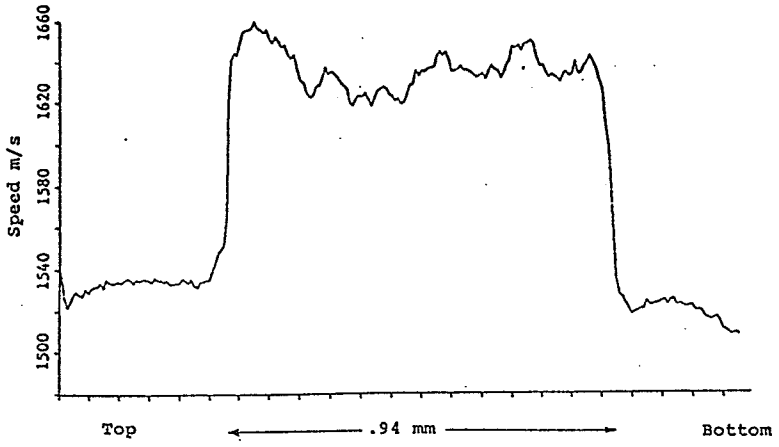

Figure 6. Graphical display of speed versus raster line.

coefficient was determined [47]. Using an aqueous solution of bovine serum albumin, a homogeneous material, the speed accuracy (proximity to the true value) and precision (reproducibility of successive independent measurements) are ±2.9% and ±4.0%, respectively; the attenuation coefficient accuracy and precision are ±12% and ±15%, respectively. Using canine skin and wound, a heterogeneous material, the estimated precision in the measurement of the attenuation coefficient and the speed are ±16% and ±1.7%, respectively.

2.3 Ultrasonic Backscatter Instrumentation

A portable research instrument, Marquette Electronic Computed Tissue Characterization System (CTC-II), is used to measure ultrasonic backscatter [30]-[32]. The CTC-II consists

of a transmitter-receiver, high resolution display, control panel, ECG monitor, and microprocessor circuitry. Two μsec duration carrier bursts are transmitted. The receiver amplifies and demodulates the returned echoes for analog-to-digital conversion to allow a computer-automated data-taking procedure. The CTC-II is programmed to perform a frequency scan at frequencies between 5.0 and 6.8 MHz, in 0.1 MHz steps. Six frequency scans, 15 msec each, are performed during each cardiac cycle.

The hand-held transducer is a 6 mm diameter, 5 MHz, unfocused disk. Fitted with a 2 cm degassed water-filled fixture closed by a finger cot, the transducer is applied directly to the cardiac surface. By observing echo patterns on the A mode display, range gates are positioned to encompass the entire myocardiac wall. Ultrasonic sampling extends over 16 cardiac cycles at each site. Then, digitized echoes, ECG waveform, transmitter level, and receiver gain are stored on floppy disks.

A marking signal which is coincident with each frequency scan is added to the electrocardiogram to determine the timing of the frequency scan relative to the cardiac cycle. The frequency scans are repeated according to the heart rate. Phase annotation for each frequency scan is read off the electrocardiogram manually and entered into data disks.

The information contained by the disks such as frequency scan echoes, transmitter level, gain setting, and ECG waveform are analyzed with an IBM PC. The magnitude of the echo signal

is scaled by adjusting 1) the transmitter level, 2) the receiver gain setting, 3) the transducer frequency calibration, 4) the diffraction calibration, 5) the bulk attenuation (1.0 dB/cm-MHz), and 6) the Rayleigh scattering spectrum of the tissue. Then, five of the echoes from each frequency scan, each having a 2 μs resolution (0.5 MHz bandwidth), are combined coherently to form a composite echo signal with a 0.5 μs resolution (2 MHz bandwidth). The resulting echoes from this process have an absolute magnitude, and a perfectly flat frequency content (whitened spectrum) over the frequency range from 4.0 to 7.0 MHz. The construction of the Integrated Backscatter Rayleigh Five MHz (IBR5) is done by sampling the corrected echoes at selected ranges and averaging the squared magnitudes. After averaging, the magnitude is expressed in decibels as an absolute measure of the backscatter in square centimeters of reflecting material per cubic centimeter of volume.

To analyze the subendocardial region, for each frequency scan, two successive data points spaced 1 μsec apart (approximately 0.77 mm/μsec time of flight) are averaged. Since the resolution of the echoes is 0.5 μsec, this represents two samples with a duration of 0.39 mm, spaced 0.77 mm apart. The large epicardial wall echo automatically tracks and positions the subendocardial region to begin 5.4 mm from the epicardial surface. Sixteen heart beats were recorded with six frequency scans per beat at each data site. The mean IBR5 is found by averaging the data at that site and for the selected range.

CHAPTER 3

METHODS

3.1 Tissue Preparation: Canine Myocardium

The canine myocardium tissues were prepared by Sagar and associates at the Division of Cardiology, Medical College of Wisconsin [32]. Thirteen adult mongrel dogs of both sexes weighing 15 to 25 kg were anesthetized with sodium pentobarbital (30 mg/kg i.v.) initially and supplemented with 5 mg/kg/hr. They were ventilated with room air supplemented with oxygen (1 to 2 liters/min) with a respirator (Harvard model 607). An end-expiratory pressure of 5 to 7 cm of water was maintained to prevent atelectasis (collapse of the lung tissue). In addition, throughout the experimental procedure, Po_2, Pco_2, and pH were maintained at physiologic levels. Body temperature was controlled at 38° C with a heating pad and servomechanical controller.

A thoractomy (an opening into the thoracic cavity) in the left fifth intercostal space (the space between two ribs) was performed. The lungs were gently retracted and the heart suspended in a pericardial cradle. Left ventricular pressures were monitored by inserting a double pressure transducer-tipped catheter (Millar PC 380, 8F) into the left ventricle via the left carotid artery. The left ventricular pressure pulse was electronically differentiated to obtain peak positive left ventricular dP/dt. The differentiator was calibrated by using a triangular waveform of known slope. Phasic and mean aortic

pressures were recorded by a catheter inserted into the right femoral artery, advanced to the ascending thoracic aorta, and connected to a strain gauge pressure transducer (Statham P50). Supplemental anesthetic was injected into the right femoral vein through a cannula.

A 1.0 to 1.5 cm segment of the left anterior descending coronary artery (LAD) (Figure 7) was isolated and a calibrated electromagnetic flow probe was positioned around the vessel for measurement of coronary blood flow (Statham 2202). A micrometer-driven mechanical vascular occluder was placed distal to the flow probe to produce total coronary occlusion and subsequent reperfusion. The electrocardiogram (limb lead II) was monitored and all hemodynamic variables were continuous recorded on a Grass (model 7) polygraph.

The thirteen dogs were divided into two groups. In the first group (N=8), the LAD was occluded for 15 minutes and subsequently reperfused for 3 hours. Control measurements of hemodynamics, segmental shortening, blood flow, and ultrasonic backscatter were made before and after the occlusion and also after reperfusion of the LAD. This experiment resulted in a decrease in amplitude modulation of the backscatter and segmental shortening immediately after occlusion of the LAD, with recovery during reperfusion [48].

In the second group (N=5), total occlusion of the left anterior descending coronary artery for 90 minutes produced myocardium ischemia which caused a decrease of blood supply to the heart tissue. Myocardium ischemia was documented by

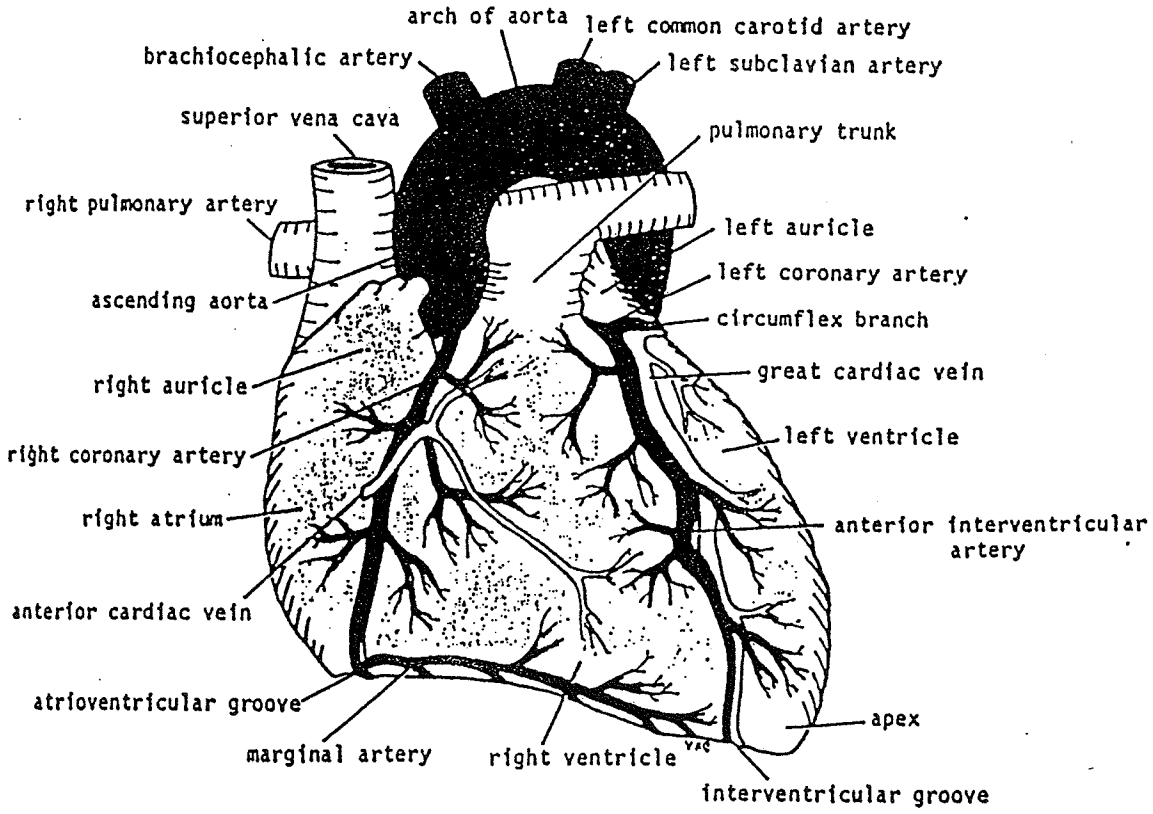

Figure 7. Anterior view of myocardium showing the locations of the left anterior descending coronary artery and the circumflex branch.

paradoxical segmental lengthening and measurements of LAD blood flow in all animals. In two animals, myocardial blood flow was also determined by the radioactive microspheres technique. Measurements of IBR5, systolic segmental shortening and systemic hemodynamics were recorded before and after 90 minutes of coronary artery occlusion. At the end of each experiment, the dog was killed, and tissue specimen (5 mm x 5 mm) were obtained from the subendocardium of the left anterior descending and the left circumflex coronary artery perfusion regions (CCX) for SLAM study. The CCX served as a control.

The samples for the SLAM were mounted on a circular cork (22 mm diameter, 3 mm thickness) with Ames Tissue-Tek OCT^{R}, frozen in liquid nitrogen, placed in Ziploc^{R} bags and shipped on dry ice from the Medical College of Wisconsin to the Bioacoustics Research Laboratory at the University of Illinois. There, they were stored in a -70°C Revco freezer until ready to be analyzed. Orientation of the endocardial and epicardial surfaces was marked and the corks were coded so that those who made ultrasound measurements were unaware of the tissue type.

3.2 Tissue Preparation: Rat Liver and Myocardium

Eight female rats from two litters were used for this study. The first litter consisted of four Fischer 344 rats 22-months old while the second group consisted of four Sprague Dawley rats 12-months old. The rats were anesthetized with an overdose of carbon dioxide and killed. Both the livers and hearts were quickly removed (only the myocarcium was studied in the second

litter). From the left ventricle of the heart and the main lobe of the liver, four adjacent specimens (5 mm x 5 mm) were taken. Then, they were mounted on the corks, frozen in liquid nitrogen and stored in the freezer as described in Section 3.1.

3.3 Experimental Protocol

Immediately before the SLAM measurements, each tissue specimen was mounted on the object disk of a Lipshaw cryostat maintained at -20° C. About 50-100 μm of the surface of the specimen was sectioned and discarded to create a flat and even surface for additional cutting.

Previous studies have shown that rapid freezing in liquid nitrogen has no effect on the ultrasonic impedance and other mechanical properties of several different tissues [49], [50]. The freezing procedure for the canine myocardium was necessary for the transportation and sectioning of the specimens. The rat liver and myocardium were also frozen so that the results from both studies could be compared. The procedure was designed so that all experiments could be accomplished in one freeze-thaw cycle.

From each of the samples, the thinnest specimen was cut first and the thickest, last. In the case of the canine myocardium, three thicknesses (75, 100, and 125 μm) were studied. In the case of the rat liver, thicknesses ranging from 100 μm to 400 μm were used and for rat myocardium, nine thicknesses ranging from 75 μm to 400 μm were studied. Each specimen was trimmed to

a size 2-3 mm horizontally by 1-1.5 mm vertically to fit into the field of view of the SLAM.

3.4 Statistical Procedures

Statgraphics, a statistical graphics program, was used to compare normal and ischemic canine myocardia. An analysis of variance (ANOVA) was used to compare the variance between these tissues. Comparisons were considered significant at the $p<0.05$ level. In the rat tissues, regression analysis which analyzes the insertion loss data in addition to ANOVA was used.

CHAPTER 4

RESULTS AND DISCUSSION

4.1 Canine Myocardium

Infarcted and normal tissue specimens from thirteen dogs were analyzed by the SLAM. Out of the thirteen, eight were stunned (15 minute occlusion, 3 hour reperfusion) and five were ischemic (90 minute occlusion). From the eight stunned dogs, 28 normal (CCX) and 28 stunned (LAD) specimens were analyzed; from the five ischemic dogs, 19 normal (CCX) and 19 ischemic (LAD) specimens were studied.

4.1.1 The SLAM ultrasonic propagation results

For each of the stunned and ischemic tissue groups, an analysis of variance (ANOVA) was performed to assess the effects of tissue type and thickness on the attenuation coefficient, ultrasonic speed and heterogeneity index. In addition, an ANOVA was performed to evaluate the effect of occlusion time on the propagation properties by combining the results from both groups of dogs.

An ANOVA separates the total variance of a dependable variable into components due to the independent factors through comparison of group means. It is assumed that the data are normally distributed. The F-test is used to determine the significance of the effect of a factor on the variance of the dependent variable. The F-ratio is the ratio of the mean squared variance between the factor category means and the mean squared

variance within all the categories of the factor. In other words, the F-ratio measures the degree of variation between factor groups in comparison to variation within factor groups. Thus, a large F-ratio means that the factor makes a significant differentiation among the different categories under consideration. In addition, the degrees of freedom are given for each of the F-ratios. They represent the total number of samples evaluated minus one. The significance level, or p, measures how important the variation is between groups. A p value of less than 0.01 is considered significant. The data files used by ANOVA containing all the raw data are found in Appendix I. The results of the ANOVA on the myocardium are presented in Appendix II. Table 1 lists factors and categories for each factor included in the ANOVA. The effect of thickness and tissue type are evaluated for both the stunned myocardium and its control (normal), and the irreversibly ischemic tissue and its control.

Table 1. Factors and categories included in the ANOVA of the canine myocardium attenuation coefficient, ultrasonic speed and heterogeneity index.

Factor	Categories
Thickness (μm)	1) 75 2) 100 3) 150
Tissue	1) Normal 2) Ischemic
Occlusion time (min)	1) 15 2) 90

4.1.1.1 Stunned myocardium (15 min occlusion)

An ANOVA is performed on the speed and heterogeneity index data of the stunned myocardium to assess the effect of thickness. Table 2 shows the result. Parameters included are tissue type, propagation property, degrees of freedom, F-ratio and significance level of the factor.

Table 2. The ANOVA results showing the effect of thickness on the ultrasonic speed and heterogeneity index for the stunned myocardium.

Tissue	Property	Degrees of freedom	F-ratio	Significance
Normal	Speed	81	1.29	0.28
	HI	81	0.94	0.39
Stunned	Speed	78	1.17	0.31
	HI	78	1.36	0.26

The results of Table 2 show that thickness has no significant effect on either the speed or the HI for both the normal and the stunned tissues. Figures 8 to 11 in Appendix II are plots of speed and heterogeneity index versus thickness for both the normal and the stunned tissues. The vertical brackets about the data point, the mean, represent its 95 percent confidence level interval. These brackets are an indication of the uncertainty in the measured speed and heterogeneity index. These figures suggest that there is a decreasing trend in both the speed and the heterogeneity index with increasing thickness.

Since the differences were not significant (all p values greater than 0.25), the data for all four thicknesses could be pooled without affecting the results.

The speed and heterogeneity index data from all the thicknesses were combined for each tissue and a separate ANOVA was performed to assess the effect of tissue type. The results of the variance in ultrasonic propagation properties due to tissue type are listed in Table 3. The corresponding mean ± SDs are listed in Table 4.

Table 3. The ANOVA results for the effect of tissue type on the attenuation coefficient, ultrasonic speed and heterogeneity index for the stunned myocardium.

Property	Degrees of freedom	F-ratio	Significance
Attenuation Coefficient	54	0.47	0.50
Ultrasonic Speed	160	0.14	0.71
Heterogeneity Index	160	1.67	0.20

Table 4. The SLAM attenuation coefficient (dB/mm), ultrasonic speed (m/s), and heterogeneity index (m/s) ± SD for normal and stunned tissues.

Tissue	Attenuation Coefficient	Ultrasonic Speed	Heterogeneity Index
Normal	34.6 ± 10.6	1574 ± 21	4 ± 3
Stunned	36.9 ± 14.9	1575 ± 21	4 ± 4

Tissue type did not have a significant effect on the propagation properties. However, there was a small increase in the mean of the attenuation coefficient; it was 34.6 ± 10.6 dB/mm in the normal and 36.9 ± 14.9 dB/mm in the stunned tissue. The speed and the heterogeneity index, on the other hand, remained about the same. The standard deviations for the heterogeneity index are very large due to skew in the data distribution. The skew coefficient is a measurement of how asymmetric the data distribution is. Positive values of skewness indicate that the upper tail of the distribution curve is longer than the lower tail. For the HI of the normal tissue, the skew coefficient is 4.1, and for the HI of the stunned tissue, it is 3.3. These high skew coefficients indicate that both distributions are greatly skewed.

4.1.1.2 Ischemic myocardium (90-minute occlusion)

As in the stunned myocardium, an ANOVA was performed on the speed and heterogeneity index to determine the effect of thickness in the irreversibly ischemic tissues. Analysis was done for both the normal (control) and the infarcted tissues. Table 5 lists the results.

Table 5. The ANOVA results showing the effect of thickness on the ultrasonic speed and heterogeneity index for the 90-minute infarction.

Tissue	Property	Degrees of freedom	F-ratio	Significance
Normal	Speed	56	0.45	0.64
	HI	56	1.06	0.35
Ischemic	Speed	52	1.35	0.27
	HI	52	4.02	0.02

The results show that for the ischemic tissue, thickness has a significant effect on the heterogeneity index ($p<0.024$). Figure II.5 in Appendix II demonstrates the decreased heterogeneity index due to the increased thickness in ischemic tissue. Although the effect of thickness is not significant for the heterogeneity index of the normal tissue ($p<0.36$), Figure II.6 shows that the same decreasing trend also exists for the normal tissue. From Figures II.7 and II.8, no significant effect on the speed is observed for either tissue.

Another ANOVA was performed to assess the effect that tissue type has on the ultrasonic propagation properties for the 90-minute occlusion samples. Table 6 lists the results. In addition, the corresponding mean and standard deviation are listed in Table 7.

Table 6. The ANOVA results for the effect of tissue type on the attenuation coefficient, ultrasonic speed and heterogeneity index for the 90-minute infarcted myocardium.

Property	Degrees of freedom	F-ratio	Significance
Attenuation Coefficient	37	0.45	0.51
Ultrasonic Speed	109	0.31	0.58
Heterogeneity Index	109	1.55	0.22

Table 7. The SLAM attenuation coefficient (dB/mm), ultrasonic speed (m/s), and heterogeneity index (m/s) $\pm$ SD for normal and ischemic tissues.

Tissue	Attenuation Coefficient	Ultrasonic Speed	Heterogeneity Index
Normal	34.5 $\pm$ 16.6	1575 $\pm$ 20	5 $\pm$ 4
Ischemic	31.5 $\pm$ 10.5	1578 $\pm$ 26	4 $\pm$ 3

Table 6 shows that tissue type has no significance for any of the ultrasonic propagation properties. The means of both the attenuation and the heterogeneity index are a little higher for the normal tissue than the ischemic tissue, as shown in Table 7. Again, the standard deviations for the heterogeneity indices are high. The skew coefficient for the HI of the normal tissue is 3.6, and for the HI of the ischemic tissue, it is 1.8.

4.1.1.3 Stunned and ischemic myocardium: combined results

Further steps were taken to analyze the effect that occlusion time has on the propagation properties. Table 8 presents the results of the ANOVA while Table 9 lists the corresponding mean and standard deviation.

Table 8. The ANOVA results of the effect of occlusion time on the attenuation coefficient, ultrasonic speed and heterogeneity index for the canine myocardium.

Tissue	Property	Degrees of freedom	F-ratio	Significance
Normal	Atten. Coeff.	45	0.00	0.99
	Speed	138	0.22	0.64
	HI	138	4.68	0.03
Ischemic	Atten. Coeff.	46	1.91	0.17
	Speed	131	0.49	0.49
	HI	131	0.16	0.69

Table 9. The SLAM attenuation coefficient (dB/mm), ultrasonic speed (m/s), and heterogeneity index (m/s) ± SD for the 15-min stunned myocardium and its control, and for the 90-min ischemic myocardium and its control.

Tissue	Attenuation Coefficient	Ultrasonic Speed	Heterogeneity Index
Normal(15 min)	34.6 ± 10.6	1574 ± 21	4 ± 3
Normal(90 min)	34.5 ± 16.6	1575 ± 20	5 ± 4
Stunned(15 min)	36.9 ± 14.9	1575 ± 21	4 ± 4
Ischemic(90 min)	31.5 ± 10.5	1578 ± 26	4 ± 3

For the normal tissue, there was no significant effect of occlusion time on the attenuation coefficient. This is expected since the normal tissue serves as a control and should not be affected by the infarction. However, the heterogeneity index of the normal tissue was significantly affected by the occlusion time. The mean HI for the normal of the 90-minute occlusion is 5 m/s while that for the normal of the 15-minute occlusion is 4 m/s (see Table 7). Since the standard deviations for these heterogeneity indices are large (3 and 4 m/s for the 15-min normal and 90-min normal, respectively), the difference of 1 m/s may not be as significant as suggested by the p value. Table 8 does not show any significant effect of occlusion time on the properties for the infarcted tissue. However, from Table 9, it is seen that the ischemic tissue has an attenuation coefficient about 5.4 dB/mm lower than the stunned tissue. The p-value for

the attenuation coefficient ($p<0.18$) shows that the occlusion time has an almost significant effect on the attenuation coefficient of the infarcted tissue. The mean of the heterogeneity index for the ischemic tissue is the same as that of the stunned tissue.

4.1.2 The IBR5 and Biochemical Results

A listing of the IBR5 for four of the stunned dog myocardia and three of the ischemic tissues can be found in Appendix III. Myocardial fat, water, and protein concentration for three of the stunned myocardia and the control are listed in Appendix IV. A summary is presented in Table 10.

Table 10. Mean and SD of IBR5 (dB), myocardial water, fat and protein content for normal, stunned and ischemic tissues.

	Normal (15 min)	Stunned (15 min)	Normal (90 min)	Ischemic (90 min)
IBR5	-48.3 ± 0.5	-45.6 ± 0.5	-49 ± 1	-45 ± 1
% Water	77.0 ± 0.2	77.4 ±0.4	--	--
% Protein	15 ± 3	16.0 ± 0.6	--	--
% Lipid	11 ± 5	6.5 ± 0.8	--	--

The IBR5 in the infarcted zone is higher than that in the normal region for both the 15-minute and 90-minute occlusions. For the 15-minute occlusion samples, the IBR5 is -48.3 ± 0.5 dB in the normal tissue and -45.6 ± 0.5 dB in the stunned tissue. For the 90-minute occlusion, the IBR5 is -49 ± 1 dB in the normal

region and -45 ± 1 dB in the ischemic region. Information on the water, protein and lipid contents is available only for the 15-minute occlusion tissues. The water content is about the same for both the normal and the stunned tissues. The protein content is slightly higher in the stunned tissues than in the normal tissues. The most noticeable difference between the two tissues, however, is in the lipid content: 11 ± 5 % for the stunned tissue and a significantly lower 6.5 ± 0.8 % for the normal tissue.

4.1.3 Discussion

Several observations have been made in the present investigation in both the reversibly stunned and the irreversibly infarcted tissues. In the stunned myocardium, the attenuation was found to be slightly higher in the infarcted region than the normal area. Also, the heterogeneity index demonstrated a slight decreasing trend with increasing thickness for both the normal and the stunned tissues. In the ischemic myocardium, the irreversible damage in the tissue caused a slight decrease in the attenuation coefficient. More noticeable, however, was the significant decrease in the heterogeneity index with increased thickness for both the normal and the ischemic tissues. This same trend, though not as pronounced, was observed in the stunned tissue. When the stunned tissue was compared to the ischemic tissue, the ischemic myocardium again showed a lower attenuation coefficient. An increase in the integrated backscatter was associated with both the stunned and ischemic tissues. A slight

increase in the myocardial protein content and a significant decrease in the lipid content are also associated with the stunned tissues.

Since the 1950s, it has been know that the ultrasonic propagation properties, the attenuation coefficient in particular, of biological materials are strongly affected at the macromolecular level [3], [4]. In later studies [11], it was suggested that the ultrasonic propagation of tissue can be modelled as a function of constituent concentrations. The four tissue constituents of particular acoustical importance are water, protein, collagen and lipid. A study done on orotic acid treated rat liver [15] gives a graphical representation of attenuation coefficient versus fat concentration. This result showed positive correlation between the two. Quantitatively, the attenuation coefficient was found to increase at a rate of 1.08 dB/mm/%fat. Another study [11] also showed that in some tissues, the attenuation coefficient and fat concentration are positively correlated. Since the lipid concentration was determined to be low in the stunned tissue, it may be possible that the decrease in the attenuation coefficient is caused by the infarction of the tissue even though reperfusion took place afterwards. Thus, it would not be surprising to find the same decrease in the ischemic tissue. If this were the case, the low fat concentration would have caused a decrease in the attenuation coefficient. This assumption holds for the data of the ischemic but not the stunned tissue. In any case, since the biochemistry data are limited, more studies on the tissue constituents need to be done before

any conclusion can be drawn about their effects on the attenuation coefficient of the ischemic myocardium. The significant change in fat concentration seen here dictates a more careful examination of the relationship between fat concentration and the propagation properties of the infarcted myocardium.

A negative correlation between the heterogeneity index and the thickness is demonstrated in both the ischemic and stunned tissues. However, since only three thicknesses are involved here, definite conclusions should not be drawn. More about this subject will be discussed in Section 4.2.

The IBR5 data are higher in the area of infarction compared to the normal region for both the stunned and the ischemic studies. A previous study reported a similar result for the ischemic tissue [32]. It showed that the primary mechanics involved are the altering of the framework of the myocardium due to increased water concentration, which creates a larger distance between adjacent muscle fibers and thus explains the increase in the scattering of the ischemic tissue. Other studies have shown that geometric configuration also affects the acoustic properties of the scatters [30], [51]. It has been determined that after 60 to 180 minutes of acute occlusion of the coronary artery, intercellular edema is more prominent, mitochondrial dense bodies are more numerous and breaks in the sarcolemma are present [52]. All of these may be contributing in the increase of scattering by altering the size and density of possible scatterers.

Since the standard deviation of the attenuation coefficient was very high, a study was conducted to examine the myocardium

with the SLAM more carefully. This experiment involved eight rats. Normal heart and liver tissue specimens were analyzed by the SLAM to obtain their ultrasonic propagation properties. In four of the rats, both the heart and the liver were studied, and in the other four, only the heart was studied. The large standard deviation of the canine myocardium attenuation coefficient being the main concern, the experiment was designed to find a dynamic range of thicknesses which might yield more consistent attenuation coefficients.

4.2 Rat Myocardium

The thicknesses used for the rat heart study ranged from 75 μm to 400 μm in most cases. Occasionally, thicknesses up to 600 μm were analyzed. For each rat, data were taken from nine thicknesses. Sections 4.2.1 and 4.2.2 contain the results and discussion of the rat heart, respectively.

4.2.1 Rat myocardium results

Regression analysis was performed on the insertion loss values versus thickness to calculate the attenuation coefficients. All of the data files used for the analysis are presented in Appendix I. Appendix V displays the detailed results of the analysis. A summary and observations will be presented here. Figures V.1 to V.8 in Appendix V show the insertion loss versus thickness graph for each of the eight rats evaluated. The slope of the line is the attenuation coefficient. Table 11 lists the results of the regression analysis which

include the attenuation coefficient (A), correlation coefficient (R), the mean squared variance and the degrees of freedom.

Table 11. The attenuation coefficient, correlation coefficient, mean squared variance and degrees of freedom of rat myocardium evaluated for thicknesses 75 μm to 400 μm.

Rat ID	A(dB/mm)	R	Mean Square	Degrees of freedom
1	9.17	0.86	0.42	149
2	9.28	0.76	0.59	152
3	11.4	0.82	0.65	179
4	10.6	0.78	0.73	155
5	11.9	0.87	0.54	110
6	13.4	0.91	0.56	114
7	10.7	0.81	0.59	98
8	15.5	0.89	0.72	90
mean ± SD	12 ± 2	0.84 ± 0.05	0.6 ± 0.1	

The mean square variance indicates the variation of insertion loss values about their mean for each of the thicknesses. The larger the mean squared variance, the wider the range of insertion loss within the thicknesses. Note that in the study of the myocardium, an inhomogeneous material, the spread of IL values for a given thickness is due to the specimen heterogeneity, since each IL value represents a different area of the specimen. The mean ± SD of the mean squared variance for the rat heart is 0.6 ± 0.1. For the attenuation coefficient, the standard deviation is ±2 dB/mm or ±16.7% of the mean (12 dB/mm).

This result shows fairly good consistency since the precision for the SLAM attenuation coefficient measurement is evaluated at ±16% for canine skin and wound, inhomogeneous materials, as mentioned previously in Section 2.2.2.4. The correlation coefficient represents how well the insertion loss data fit the slope of the line, with the perfect fit being R = 1. For the rat heart, its mean ± SD is 0.84 ± 0.05.

Since the rat experiment was designed to better understand the canine myocardium results, regression analysis of the rat heart was repeated for only the thickness range used for the canine study, namely, 75 μm to 150 μm. This range will be referred to as thickness range I hereafter. Table 12 contains the attenuation coefficient results.

Table 12. The attenuation coefficient, correlation coefficient, mean squared variance and degrees of freedom of rat myocardium evaluated for thickness range I.

Rat ID	A(dB/mm)	R	Mean Square	Degrees of freedom
1	26.0	0.80	0.29	62
2	32.4	0.82	0.50	54
3	24.7	0.68	0.59	72
4	24.2	0.56	0.85	78
5	3.2	0.48	0.47	47
6	16.3	0.67	0.25	50
7	3.8	0.13	0.75	42
8	23.3	0.67	0.59	41
mean ± SD	20 ± 9	0.6 ± 0.2	0.5 ± 0.2	

The mean of the attenuation coefficient (20 dB/mm) is 8 dB/mm higher than that for thickness range of 75 μm to 400 μm (Table 11). Additionally, the standard deviation about this mean is ±9 dB/mm or ±45%, significantly above the SLAM's precision of 16%. Careful inspection of Figures V.1 to V.8 (regression plots of insertion loss versus thickness for the eight rats) shows that, indeed, in the thickness range of 75 μm to 150 μm, if a slope were to be fitted for the insertion loss values, it would vary significantly among the eight rats and would usually be steeper than the fitted line in the figures.

Regression analysis of the insertion loss for the thickness range from 200 μm to 400 μm was performed next to see if better agreement exists among the attenuation coefficients. In the future, this thickness range will be designated as thickness range II. Table 13 summarizes the results.

Table 13. The attenuation coefficient, correlation coefficient and mean squared variance of rat myocardium evaluated for thickness range II.

Rat ID	A(dB/mm)	R	Mean Square	Degrees of freedom
1	10.1	0.83	0.60	76
2	8.2	0.54	0.72	89
3	11.4	0.69	0.74	106
4	11.8	0.71	0.73	76
5	10.1	0.70	0.58	62
6	15.1	0.82	0.55	63
7	9.6	0.68	0.44	55
8	9.9	0.70	0.58	48
mean ± SD	11 ± 2	0.71 ± 0.09	0.6 ± 0.1	

The attenuation coefficients shown in Table 13 are very close to those obtained for the thickness range from 75 μm to 400 μm in Table 11; there is a difference of only 1 dB/mm in their mean values. However, compared to those for the thickness range I, the attenuation coefficients are much lower; there is a difference of 9 dB/mm in their means. The standard deviation of the attenuation coefficient in Table 13 is ±2 dB/mm or ±18% of the mean (11 dB/mm). This value shows that more consistent measurements of the attenuation coefficient exist in thickness range II than in range I (±45%).

ANOVA was performed to evaluate the effect of thickness on the speed and the heterogeneity index of the rat myocardium. The results for the analysis are presented in Appendix V. A summary

of the results is given in Table 14. The mean ± SD of the speed and the HI for all the thicknesses is also presented.

Table 14. The ANOVA results showing the effect of thickness on ultrasonic speed and heterogeneity index for the rat myocardium (75 μm to 400 μm).

Property	Degrees of freedom	F-ratio	Significance	Mean ± SD (m/s)
Speed	142	2.66	0.003	1572 ± 4
HI	142	14.8	0.000	2.4 + 1.0

Table 14 shows that thickness has a significant effect on the ultrasonic speed in the heart ($p<0.003$). However, Figure V.9 indicates no trend of increase or decrease of the speed with increasing thickness. The mean ± SD of the speed is 1572 ± 4 m/s. The low standard deviation of ±0.25% is well within the error of the SLAM's speed determination of heterogeneous materials (1.7%), as mentioned in Section 2.2.2.4. Therefore, even though the p-value indicates significant variation in the speed due to thickness, this variation is contributed mostly by the errors in the reference medium velocity, the normalized fringe shift, the specimen thickness, noise, and other unknown variations in the SLAM system.

The significance level of the heterogeneity index ($p<0.000$) suggests that it is very much affected by the thickness. An examination of the corresponding ANOVA variance plot (Figure

V.10) reveals decreasing HI with thickness in the range from 75 μm to 150 μm. However, from 175 μm to 400 μm, this decreasing trend appears to level off. The 95% confidence level intervals (indicated by the vertical brackets) for thicknesses 175, 450, 500, and 600 μm are much larger than those for the other thicknesses due to the small number of samples evaluated at these thicknesses (1-4 compared to 13-15 at other thicknesses). Therefore, these measurements will not be considered further. To investigate whether the HI really levels off above 150 μm, an ANOVA for the speed and the HI was repeated for the thickness range of 200 μm to 400 μm, or range II. The results appear in Table 15.

Table 15. The ANOVA results showing the effect of thickness on ultrasonic speed and heterogeneity index for the rat myocardium (200 μm to 400 μm).

Property	Degrees of freedom	F-ratio	Significance	Mean ± SD (m/s)
Speed	73	1.59	0.16	1575 ± 3
HI	73	1.86	0.10	1.6 ± 0.2

The analysis yielded higher p-values for both the speed and the HI versus thickness ($p<0.16$ and $p<0.10$, respectively) compared to those from Table 14 ($p<0.003$ and $p<0.000$). These higher values suggest that there is no significant correlation between either the speed or the HI and the thickness in the thickness range from 200 μm to 400 μm. Also, the low SD of the

HI (±0.2 or ±12%) shows that the HI is consistent between thicknesses.

In this section, several observations have been made about the rat myocardium from the statistical analysis of its ultrasonic propagation properties. A summary of these observations will be presented here. The evaluation of the attenuation coefficient is much more consistent when it is performed for thicknesses 200 μm to 400 μm than for thicknesses 75 μm to 150 μm (±18% compared to ±45%). The mean of the attenuation coefficient for the thicker range is about one-half that of the thinner range (11 dB/mm compared to 20 dB/mm). For the range from 75 μm to 60 μm, the speed was found to be varying significantly with thickness, though, for the range from 200 μm to 400 μm, it was not. It was also observed that between 75 μm and 150 μm, the heterogeneity index decreased significantly with thickness. However, thickness does not have a significant effect on the HI from 200 μm to 400 μm. Thus, the observation that the HI versus thickness plot levels off after 150 μm is correct.

4.2.2 Rat myocardium discussion

The study of rat myocardium provided insight into a better understanding of the canine myocardium results. Both the high attenuation coefficient and its large standard deviation found in the rat myocardium for the thickness range I are also characteristic of the canine myocardium in the same range. A reasonable hypothesis is that as in the case of rat heart, canine myocardium may also demonstrate a lower attenuation coefficient

and standard deviation in thickness range II. A possible explanation for the difference in the attenuation coefficients between the two thickness regions is the spatial averaging of the heterogeneous tissue with thickness. The lower standard deviation in the higher thickness region indicates that the attenuation coefficient measurement is more repeatable in range II than in range I. This is because thickness range II provides a larger dynamic range over which to evaluate the insertion loss versus thickness plot than range I.

The speed measurements for thickness range II are more consistent between thicknesses than those in range I. The combined result shows a significant difference in the speed with thickness while for thickness range II alone, there is no significant difference. However, either way, the difference is still within the system error. Therefore, no definite conclusion should be drawn about any difference in speed between the two regions.

The heterogeneity index data suggested a very interesting relationship with thickness. In thickness region I, the HI decreased with thickness and upon reaching 200 μm, it leveled off and stayed fairly constant through region II. It is not reasonable to expect the thinner specimens to be more heterogeneous since the thicker sections contain more interfering structures. A possible explanation involves the calculation of the HI. The HI is computed by subtracting the system SD (for the appropriate thickness) from the SD of the speed values determined for the sample. The system SD represents the standard deviation

of the speed in the saline area. It may be that the system SDs for the thinner sections were underestimated, thus creating higher HI than expected. In canine myocardium, the HI also showed a decrease with increased thickness in thickness range I. This trend may very well be caused by the same system SD error. A more detailed discussion will be presented in Section 4.4.

4.3 Rat Liver

The thicknesses range between 75 mm and 400 mm from four rats was used for the rat liver study. Nine different thicknesses were analyzed, as for the rat myocardium. Sections 4.3.1 and 4.3.2 present the rat liver results and discussion, respectively.

4.3.1 Rat liver results

Attenuation coefficients were calculated via regression analysis on the insertion loss versus thickness. Data files used for the analysis are presented in Appendix I. The results are shown in Appendix VI. Figures VI.1 to VI.4 in Appendix VI are graphs of the insertion loss versus thickness for each of the four rats evaluated. Table 16 summarizes the results of the analysis.

Table 16. The attenuation coefficient, correlation coefficient, mean squared variance and degrees of freedom of rat liver evaluated for thicknesses 75 μm to 400 μm.

Rat ID	A(dB/mm)	R	Mean Square	Degrees of freedom
1	9.03	0.86	0.33	140
2	9.08	0.85	0.30	132
3	9.87	0.90	0.22	141
4	10.3	0.87	0.32	129
mean ± SD	9.6 ± 0.6	0.87 ± 0.02	0.29 ± 0.05	

The low mean squared variance compared to that of the rat myocardium (Table 10) is a good representation of the homogeneity of the liver tissue. The standard deviation of the attenuation coefficient is ±0.6 or ±6.2% of the mean (9.6 dB/mm). This shows excellent agreement among the attenuation coefficient measurements since the system precision for bovine serum albumin (BSA) solution, a homogeneous material, is evaluated at ±15%. The mean correlation coefficient, indicative of how well the ILs fit the slope of the line in Figures VI.1 to VI.4, is 0.87 ± 0.02. This is a little better than that for the myocardium (0.84 ± 0.05).

Since interesting results were observed when the myocardium data from two thickness ranges were analyzed separately, the same procedure was repeated for the liver. Thickness range I (75 μm to 150 μm) and thickness range II (200 μm to 400 μm) were used. Table 17 contains the result for range I.

Table 17. The attenuation coefficient, correlation coefficient, mean squared variance and degrees of freedom of rat liver evaluated for thickness range I.

Rat ID	A(dB/mm)	R	Mean Square	Degrees of freedom
1	9.7	0.41	0.41	58
2	18.0	0.77	0.22	44
3	7.9	0.44	0.19	59
4	6.2	0.24	0.42	53
mean ± SD	10 ± 5	0.5 ± 0.2	0.3 ± 0.1	

The mean of the attenuation coefficient (10 dB/mm) is about the same as that of the thickness range from 75 μm to 400 μm. It does show the high values associated with rat myocardium in thickness range I. However, the standard deviation, like the myocardium, is large (±50%), much higher than the SLAM's measurement uncertainty of 15%. In particular, the attenuation coefficient for rat 2 (18 dB/mm) is very high. As in the rat myocardium (Table 12), the correlation coefficient in thickness range I is also low for the liver (0.5 ± 0.2).

Next, regression analysis of the insertion loss for thickness range II was executed. The results appear in Table 18.

Table 18. The attenuation coefficient, correlation coefficient, mean squared variance and degrees of freedom of rat liver evaluated for thickness range II.

Rat ID	A(dB/mm)	R	Mean Square	Degrees of freedom
1	10.2	0.80	0.29	81
2	9.8	0.75	0.37	87
3	11.5	0.83	0.32	81
4	12.6	0.87	0.29	75
mean ± SD	11 ± 1	0.81 ± 0.05	0.32 ± 0.04	

The mean of the attenuation coefficients is close to that for the entire thickness range (Table 16). The standard deviation from the mean is about 9% which is well within the SLAM's measurement uncertainty of 15%. Again, more consistency in the attenuation measurement is found in thickness range II than range I. The higher correlation coefficient (0.81 ± 0.05) is also characteristic of thickness range II.

To study the speed and HI statistically, ANOVA was performed to judge the effect of thickness on these properties. The data files and results are listed in Appendix V. Table 19 summarizes the result.

Table 19. The ANOVA results showing the effect of thickness on ultrasonic speed and heterogeneity index for the rat liver (75 μm to 400 μm).

Property	Degrees of freedom	F-ratio	Significance	Mean ± SD (m/s)
Speed	71	0.944	0.49	1567 ± 3
HI	71	14.4	0.000	2.2 ± 1

Figure VI.5 is an ANOVA variance plot of speed versus thickness. There is no significant effect of thickness on the ultrasonic speed in the liver ($p<0.49$). The low SD (±3 m/s or 0.19%) shows good agreement of the speed measurements between the various thicknesses. This value is within the error estimate of SLAM's evaluation of speed for homogeneous material (±0.4%), as shown in Section 2.2.2.4.

The heterogeneity index, unlike the speed, was very much affected by the thickness of the specimen ($p<0.000$). Figure VI.6, an ANOVA variance plot of HI versus thickness, shows the same pattern as that of the rat myocardium (Figure V.10). In thickness range I, there is an obvious negative correlation of HI and thickness. However, in thickness region II, there does not seem to be a correlation between the two. ANOVA performed on speed and HI for thickness range II further investigates this issue. Table 20 displays the result.

Table 20. The ANOVA results showing the effect of thickness on ultrasonic speed and heterogeneity index for the rat liver (200 μm to 400 μm).

Property	Degrees of freedom	F-ratio	Significance	Mean ± SD (m/s)
Speed	39	1.04	0.40	1570 ± 3
HI	39	0.57	0.69	1.5 ± 0.2

The p-values for both the speed and the HI versus thickness ($p<0.40$ and $p<0.69$) display no significant effect of thickness on either of these properties in the thickness range from 200 μm to 400 μm. The low SD for the HI (±0.2 or 13%) indicates fairly constant HI between the thicknesses.

4.3.2 Rat liver discussion

The rat liver data analysis suggests that the attenuation coefficients of both of the thickness ranges were similar. However, in thickness range I, the uncertainty in A was much greater. Again, this may be due to the wider dynamic range used in range II.

The speed was not affected by the thickness in either range. Also, very little variation exists between the speed values for the different thicknesses. This is a good indication of accurate thickness determination.

The HI shows a strong negative correlation with thickness in thickness range I. However, it is completely uncorrelated with the thickness in range II. An explanation for this observation

is the underestimation of the system SD which will be discussed in more detail in the following section.

4.4 Comparison of Rat Heart and Liver Results

For the liver, attenuation coefficient measurements taken in thickness range I deviated greatly among the four rats and the correlation coefficient was low. Both of these observations were also made of the rat myocardia in the same thickness range. Thus, it can be assumed that the inconsistent attenuation coefficient measurements from the normal canine myocardia are not due to the tissue, but rather to some method or system error.

The speed measurements have been very consistent for both the heart and the liver. This is an indication of an accuracy in the measurement of sample thicknesses as demonstrated by Equation (3) in Section 2.2.2.2.

The analysis of the heterogeneity index data also yielded unexpected observations in thickness region I. For both the rat heart and liver, an obvious decreasing trend in the HI is seen with increasing thickness. This same trend exists in the canine myocardium. Some discussion has been made in Section 4.4.2 about this phenomenon and a possible explanation would be the underestimation of the system SDs for the thicknesses in range I. However, since fairly constant HIs for thickness range II for a homogeneous material are available, it is possible to find the error in the estimation of the system SD for each thickness by taking the difference between its respective HI and the average of the HIs in range II. For the liver, this average is 1.5 m/s

(Table 20). The HIs for thicknesses 75 μm, 100 μm and 150 μm are 4.0 m/s, 3.7 m/s and 2.9 m/s, respectively. Thus, the underestimation in the system SD for each of the thicknesses ranging from thin to thick would be 2.5 m/s, 2.2 m/s and 1.4 m/s, respectively. The average of HI for thickness range II is 1.6 m/s for the rat heart (Table 15). The HIs for 75 μm, 100 μm and 150 μm are 4.3 m/s, 3.4 m/s and 2.6 m/s, respectively. Calculations of the underestimation in the system SD yield 2.7 m/s, 1.8 m/s and 1.0 m/s for the respective thicknesses. Since the values of the underestimation are close for the heart and the liver, they are probably tissue independent.

In thickness range II (200 μm to 400 μm), in contrast to range I, very consistent and repeatable measurements of all the ultrasonic propagation properties have been made for both the liver and the heart. The attenuation coefficients are similar in both tissues; however, the standard deviation is higher for the heart tissue. Also, the correlation coefficient is lower for the heart tissue. Both the high standard deviation and the low correlation coefficient are directly related to the high mean squared variance.

Compared to the rat heart, the regression analysis showed a significantly lower mean squared variance in the insertion loss for the rat liver. Since the insertion loss values for a specific thickness of specimen represent the correlation of data taken in different regions of the tissue, this low variance is an indication of the homogeneity of the rat liver. It is reasonable to expect a higher value for the heterogeneous rat myocardium

since the IL values in different regions of the tissue vary. In the myocardium, the spread in insertion loss is due mainly to the heterogeneity of the tissue whereas in the liver, it is mostly due to the uncertainty in the IL measurements.

The standard deviations of the attenuation coefficient for both the heart and the liver are close to the SLAM's measurement uncertainty, mentioned in Section 2.2.2.4. However, the attenuation coefficient measurement for the heart tissue is less reproducible (higher standard deviation) than for the liver tissue. This is due to its wide spread in the IL values. This wide spread possesses large possibility for error in the determination of the IL versus thickness slope. Figure 8 demonstrates this phenomenon. The vertical bars represent the spread of the IL; the center curve is the best fitted slope while the other two are the worst-case slopes. If the IL spread increases (mean squared variance increases), the two worst-case slopes will become even worse (the flat one will become flatter while the steep one will become steeper). Thus, the range for the uncertainty in the determination of the attenuation coefficient will then increase. The mean squared variance is also associated with the correlation coefficient of the IL versus thickness slope. Since the correlation coefficient is an indication of how well the IL data fit a slope, a wide spread in the IL values means that there is a greater tendency for the data to skew either up or down in value depending upon the number of insertion loss values taken and the location where they are taken. Correspondingly, the low correlation coefficient in

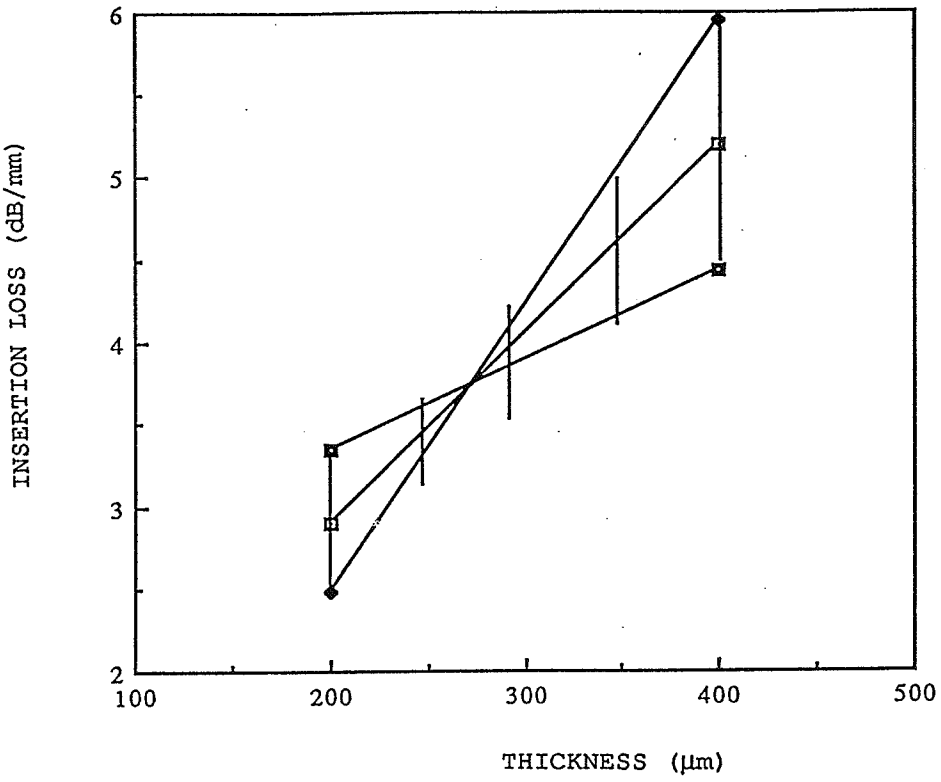

Figure 8. Graphical display of the uncertainty in the attenuation coefficient for given uncertainties in insertion loss for typical rat liver specimens.

therat heart is also associated with high mean squared variance.

4.5 Comparison of Heterogeneity Index for Several Tissues

Heterogeneity index, the standard deviation of the speed measurement in a specimen, is an indication of how heterogeneous the specimen is. Reported here are the heterogeneity indices of different tissues evaluated by the SLAM and a comparison among them to quantitatively study the inhomogeneity of these tissues. The specimens studied include canine skin, wound, and myocardium, and rat myocardium and liver. The results of the canine skin and wound tissues were from studies conducted by Steiger [42]. Agemura studied the ultrasonic propagation properties of the five-hour occluded canine myocardium [16]. The results of the stunned and 90-minute occluded canine myocardium, and the rat liver and heart from the present investigation were presented in the previous sections of this chapter.

The heterogeneity of a tissue is largely dependent on the type and arrangement of cells from which it is constructed and also the different structures that may be present among the tissue cells. The following is an overview of the histology of the various tissues being studied.

The skin consists of two main layers, the surface epithelium, or the epidermis, and the connective tissue layer, or the dermis (Figure 9). The bulk of the epidermis undergoes

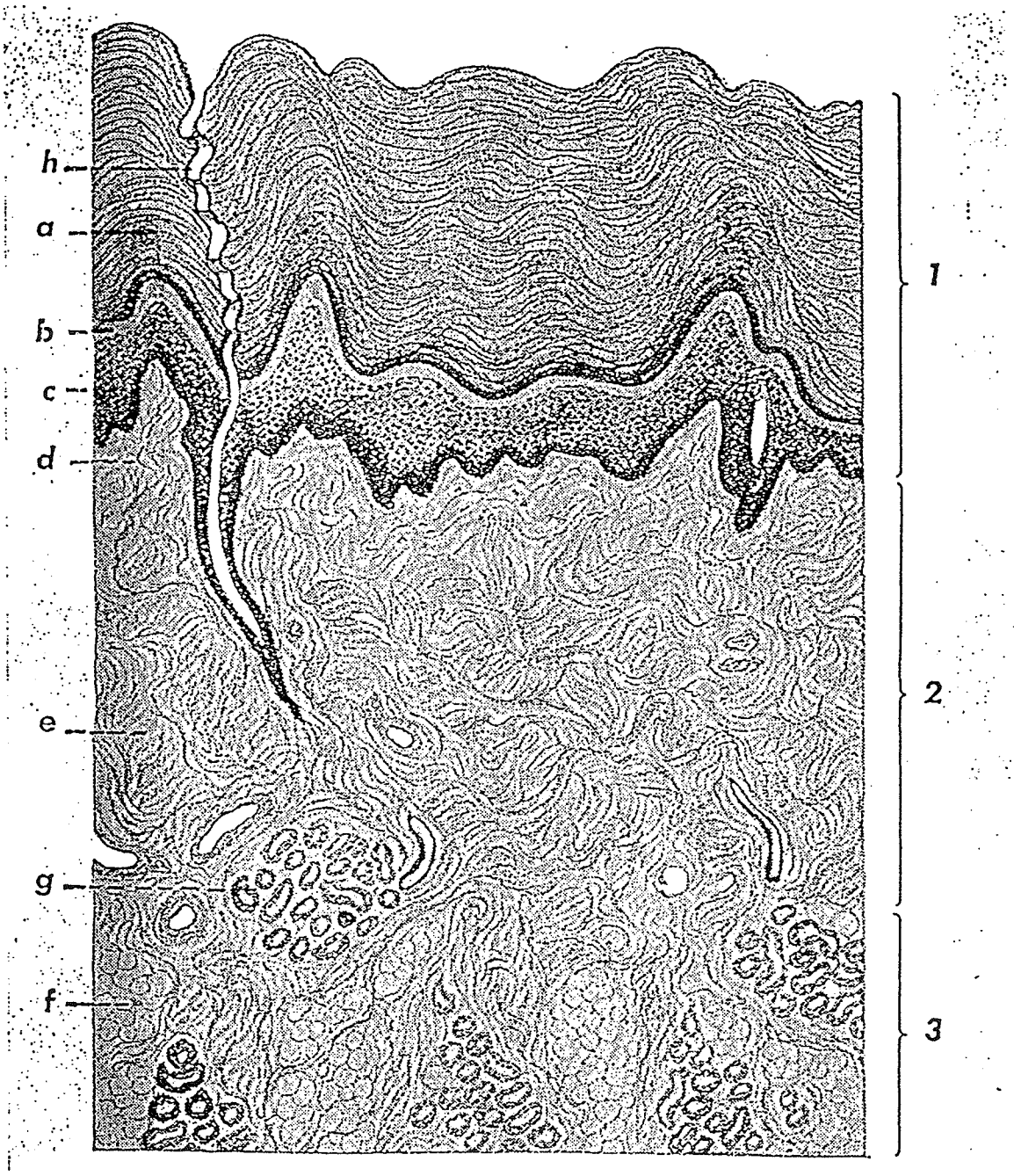

Figure 9. Section through the metacarpal pad of the dog (30x). 1, epidermis; 2, corium; 3, subcutis; a, stratum corneum; b, stratum lucidum; c, stratum profundum; d, papillary body; e, stratum reticulare; f, adipose tissue; g, tubular glands; h, their excretory duct. (From [53].)

keratinization and forms the dead superficial layer of the skin, marked by delicate grooves which create patterns that vary from region to region. Additionally, the epidermis is locally specialized to form hair follicles and sweat and oil glands. These structures also expand to various levels of the dermis. Additionally, in the dermis, there are blood vessels, nerves and nerve endings. All these components in both layers contribute to the heterogeneity of the skin tissue under study. The canine skin in the experiment [42] was taken from the epidermis and part of the dermis.

When the skin is wounded, the collagen fibers, which are responsible for the tensile strength of the skin, are cut. The wound healing involves a three-phase process which is associated with a gradual reconstruction of collagen content and as a result, tensile strength. Phase I of the recovery lasts for four to six days after wounding, and is associated with the removal of cellular debris, such as dead tissues, and infection control. In phase II, which extends from six up to about 16 to 30 days, there is a large increase in the synthesis of collagen and thus increased tensile strength. Phase III, occurring after 16 to 30 days, involves structural changes in the existing collagen fibers resulting in increased tensile strength. However, the wound scar tensile strength seldom equals the tensile strength of unwounded skin. The wound studied by Steiger [42] aged from nine to 49 days.

The myocardium is the middle and thickest layer of the heart, composed of bundles and groups of bundles of cardiac

muscle cells (Figure 10). The striated muscle fibers are composed of separate cellular units joined end to end by surface specializations called intercalated disks which run transversely across the fiber. These fibers bifurcate (split into two branches) and connect with adjacent fibers to from a complex three dimensional network.

The liver is made up of epithelial cells arranged in plates or laminae that are interconnected to form a continuous tridimensional lattice (Figure 11). The laminae are arranged radially around the central veins to form prismatic units of liver parenchyma which make up the liver lobules. On either side of the radially disposed liver cells are the hepatic sinusoids, vascular channels for blood flow. These sinusoids are radially oriented, conforming to the broad surfaces of the celullar laminae. As a result, a labyrinthine system of thin-walled vessels over a large surface area of liver parenchyma is created.

In the skin and wound studies, the heterogeneity indices were calculated for specimen thicknesses of 100 μm and 150 μm. The results for these two thicknesses were combined since it was assumed that no correlation existed between the HI and the thickness [42]. In the canine myocardium studies, the HIs were calculated for thicknesses from 75 μm to 150 μm. In the rat heart and liver studies, the heterogeneity indices were found for thicknesses ranged from 75 μm to 400 μm. Figure 12 shows the HIs versus thickness graph for all the tissue types.

The graph clearly demonstrates significantly higher heterogeneity indices associating with the skin tissues than the

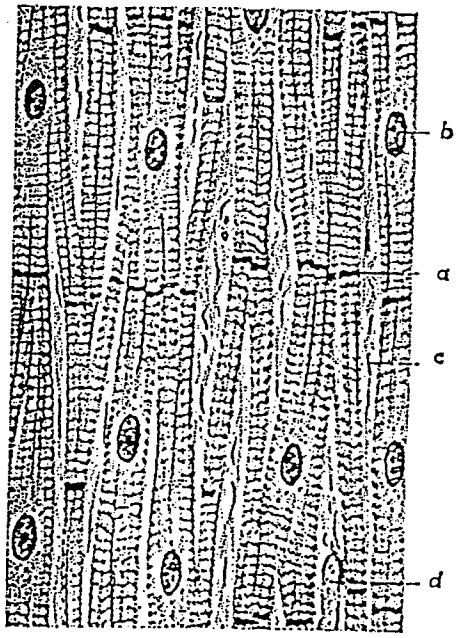

Figure 10. Longitudinal section through cardiac muscle fibers. a, intercalated disc; b, nucleus; c, nucleus of a connective tissue cell; d, blood vessel. (From [53].)

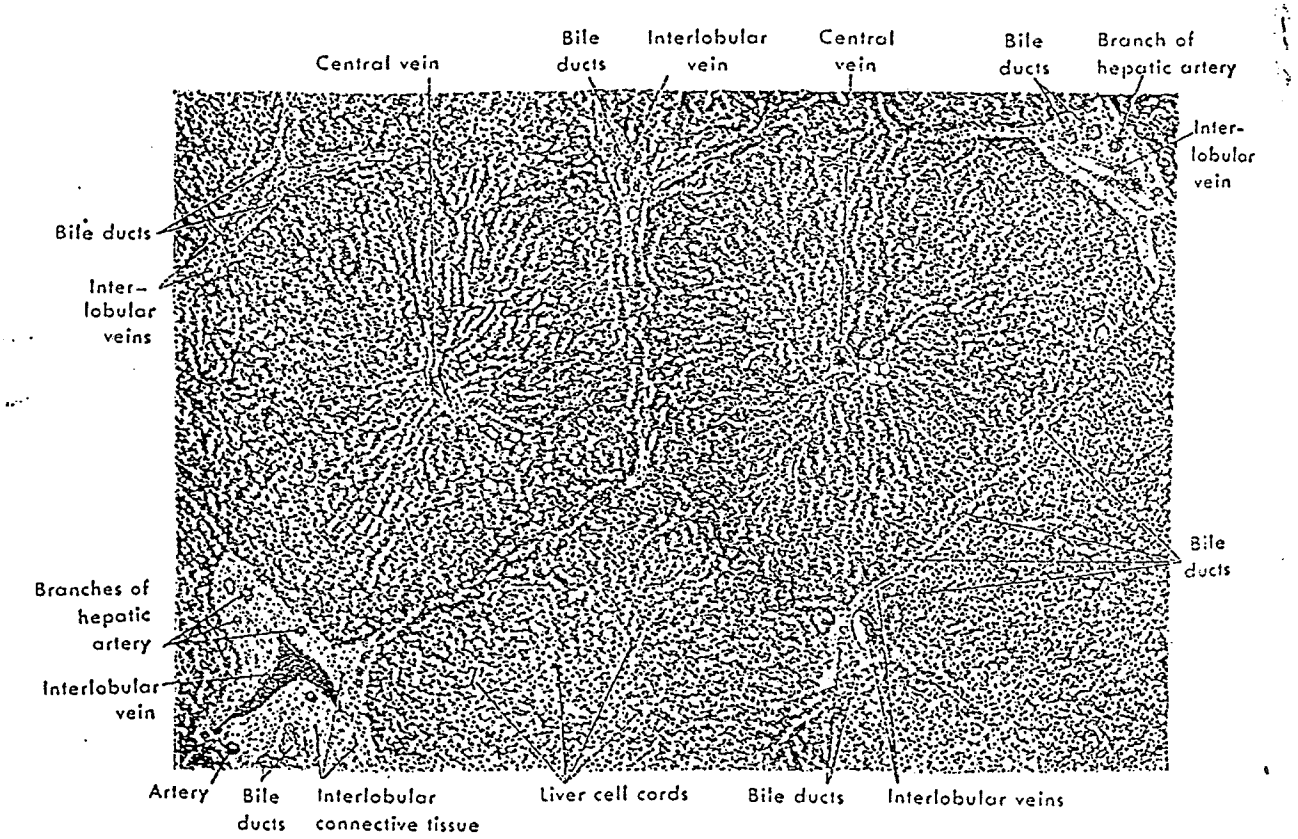

Figure 11. Portion of liver from a 22 year old man (70x). Two complete lobules are surrounded by portions of other lobules. (From [54].)

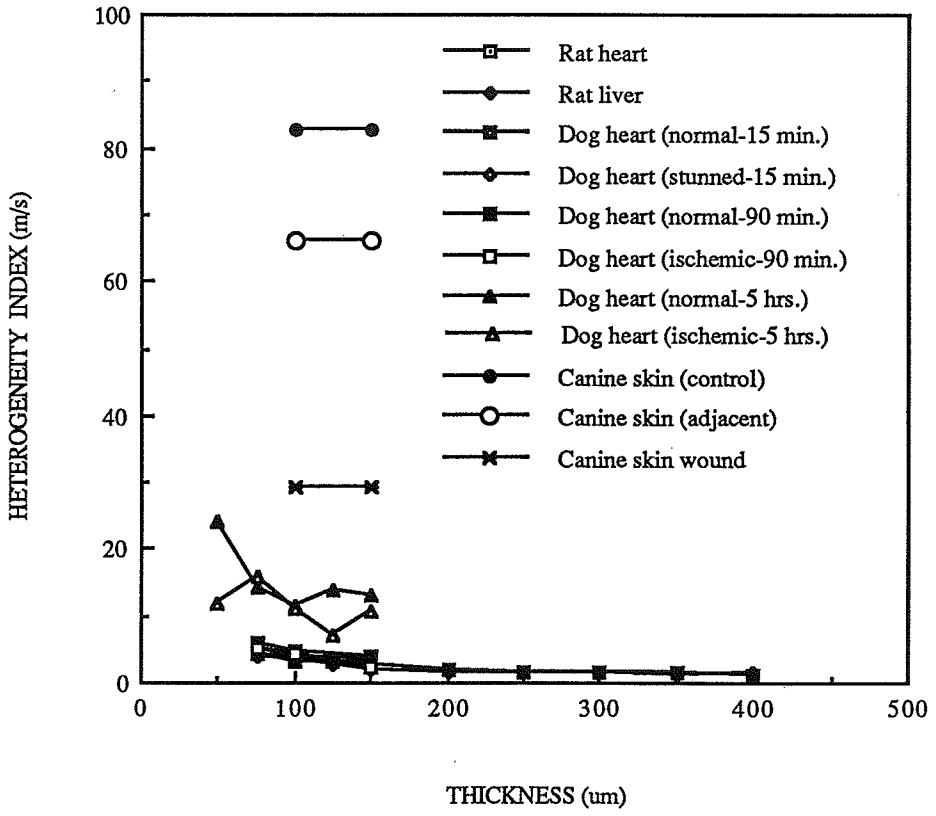

Figure 12. Plot of heterogeneity index versus thickness for normal and infarcted dog myocardium with occlusion period of 15 minutes, 90 minutes, and 5 hours, canine skin, wound and adjacent skin, and normal rat myocardium and rat heart.

rest of the specimens. This is due to the inhomogeneous structures that exit in the epidermis and dermis such as hair follicles and sweat and oil glands. The wound showed much lower heterogeneity than the skin, and the skin adjacent to the wound displayed an HI value in between those of the normal skin and the wound. The wound area is expected to be more homogeneous than the skin since most of it is collagen in the process of rebuilding and not many hair follicles or glands are present. In all three regions, however, the standard deviations of the HI values were large, 50 to 100% for the wound and 40 to 70% for both the normal skin and the adjacent skin. An explanation provided for these high SDs is that an estimated system SD, which varied with the number of values averaged, was used to calculate the HIs. However, an estimated average constant number of values was assumed since the actual number of values averaged was not known [42].

Figure 12 suggests that myocardium and liver are more homogeneous than both the skin and the wound. When the graph is expanded to show only the results for the canine myocardium and the rat tissues (Figure 13), it is seen that the HIs for the normal and ischemic myocardium of the five-hour occlusion are higher than those of the 15-minute and 90-minute occlusions. The reason for this unexpected outcome may be the modification in the system. In the current system, which was used to analyze the tissues for the 15- and 90-minute occlusions, speed values for each of the 480 raster lines are available, as opposed to the 255 from the previous system used for the 5-hour occlusion. The

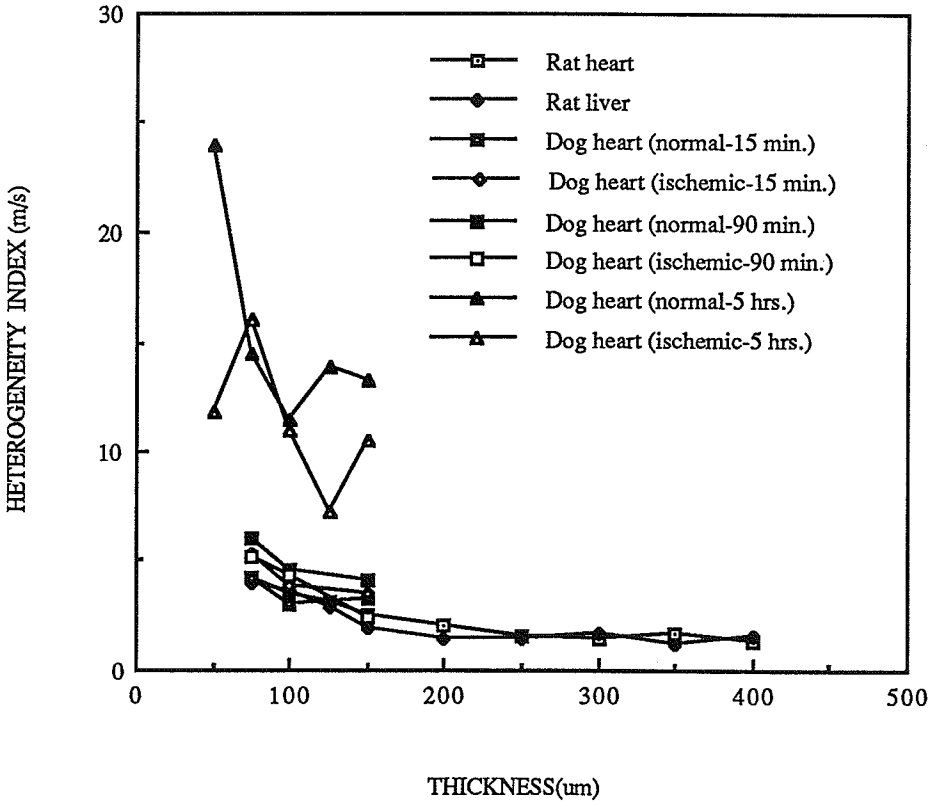

Figure 13. Plot of heterogeneity index for normal and infarcted dog myocardium with occlusion times 15 minutes, 90 minutes, and 5 hours, and normal rat myocardium and rat heart.

standard deviation of the HI for the dog heart is also high; it is anywhere between 20% to 100% of the mean.

Figure 14 shows the HIs for the tissues studied in this thesis. The rat liver exhibited lower HIs than the heart for the most part. The canine myocardium, the rat liver and the heart tissues exhibit negative slopes in the range between 75 μm and 150 μm as mentioned previously. Linear regression analysis was performed on these slopes, and the results are shown below.

Table 21. Linear regression of HI vs. thickness in the range 75 mm to 150 mm for canine myocardium, rat heart and rat liver.

Tissue type	Slope	Intercept	R
Rat heart	-0.021	5.76	0.96
Rat liver	-0.027	6.22	0.96
Dog heart (normal-15 min.)	-0.009	4.52	0.33
Dog heart (stunned-15 min.)	-0.022	6.58	0.77
Dog heart (normal-90 min.)	-0.024	7.50	0.82
Dog heart (isch.-90 min.)	-0.038	8.13	0.99

The slopes are fairly close for all the tissues studied except the normal dog heart for the 15-minute occlusion. This may have been caused by spatial averaging of the heterogeneity with thickness. It is possible that the thinner samples exhibit large heterogeneity; however, as the samples become thicker, this heterogeneity becomes averaged out.

Different types of tissues exhibit different levels of heterogeneity. In the discussion above, it is seen that four

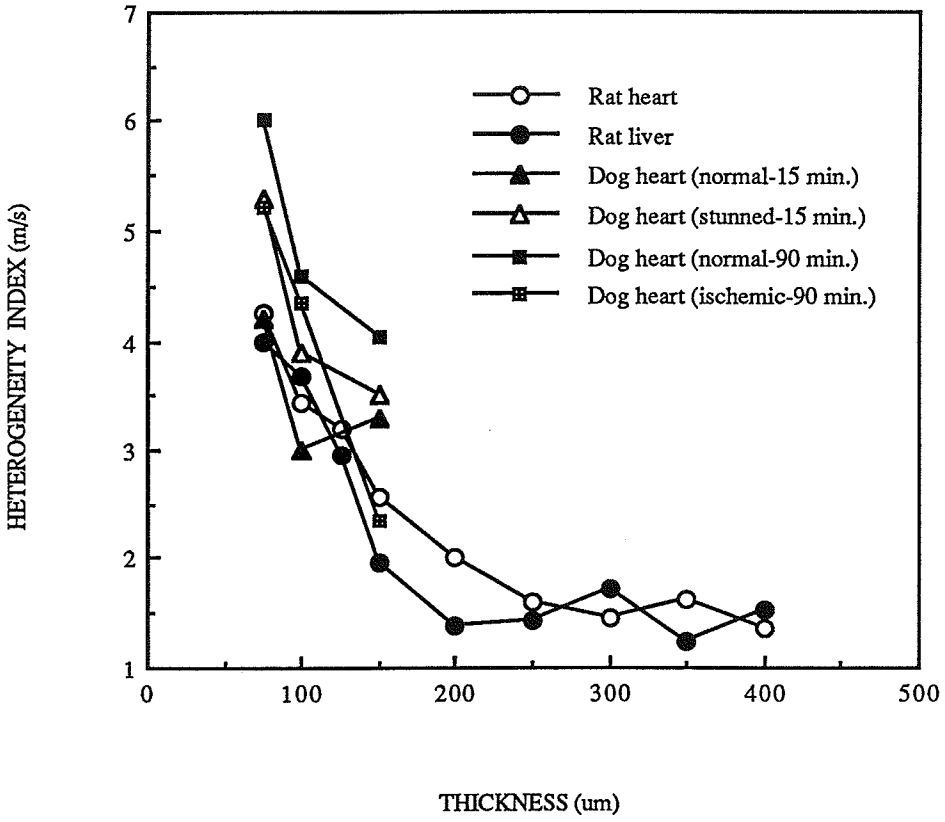

Figure 14. Plot of heterogeneity index for normal and infarcted dog myocardium with occlusion period 15 minutes and 90 minutes, and normal rat myocardium and heart.

very different types of tissue, skin, wound, heart and liver, also display different heterogeneity indices. These indices will allow better understanding of the ultrasound's interaction with different types of tissues and their structures. The heterogeneity of the tissue is related to the amount of scattering that occurs in the tissue. Thus, the IBR5 which measures the scattering inside the tissue should be directly related to the heterogeneity index.

4.6 Future Work

Future studies concerning canine myocardium tissue characterization need to involve a wide dynamic range of thicknesses. A thickness range needs to be found in which consistent measurements are yielded for the canine myocardium following the same procedure used to find the range for the rat myocardium and liver in this thesis. Also, at least five or six thicknesses should be studied so a more accurate assessment can be made. A possible approach to gain better understanding of the acoustic propagation properties of the tissue is to perform SLAM analysis on normal canine LAD and CCX tissues to establish a baseline for future comparisons. Any difference in the acoustical propagation properties or in the biochemistry between those tissues should be known so that it can be accounted for in experiments involving infarcted myocardia. Once methods for obtaining consistent attenuation coefficients are established, then steps can be taken to compare the acoustical properties of the ischemic and normal tissues and correlate these properties

with the tissue constituents associated with the infarction. More consistent values of the heterogeneity index can be obtained so that a comparison can be made with the IBR5s from the normal and the ischemic tissues.

APPENDIX I: STATGRAPHICS ANOVA DATA FILES FOR CANINE MYOCARDIUM, RAT HEART, AND RAT LIVER.

The files of factors and categories needed in the ANOVA are listed for all the tissues studied. The data contained include the attenuation coefficient, speed and heterogeneity index. The abbreviations used are defined below:

Canine myocardium

TISSUE	=	Tissue: 1 = Normal and 2 = Ischemic
ATTEN	=	Attenuation coefficient (dB/mm)
SPDTHIN	=	Speed for thickness 75 μm (m/s)
SPDMED	=	Speed for thickness 100 μm (m/s)
SPDTHICK	=	Speed for thickness 150 μm (m/s)
THICKNORM	=	Thickness for normal tissue data (μm)
THICKISCH	=	Thickness for ischemic tissue data (μm)
HI	=	Heterogeneity index (m/s)
HITHIN	=	HI for thickness 75 μm (m/s)
HIMED	=	HI for thickness 100 μm (m/s)
HITHICK	=	HI for thickness 150 μm (m/s)
SPDNORM	=	Speed for normal tissue (m/s)
SPDISCH	=	Speed for ischemic tissue (m/s)
HINORM	=	HI for normal tissue (m/s)
HIISCH	=	HI for ischemic tissue (m/s)

Rat myocardium and liver

THICK	=	Thickness (μm)
LIVSPD	=	Speed for liver specimen (m/s)
LIVHI	=	Heterogeneity index for liver (m/s)
HRTSPD	=	Speed for heart specimen (m/s)
HRTHI	=	Heterogeneity index for heart (m/s)
RATNO	=	Rat identification

Canine Myocardium (15 min)

File DGHRT15A 11/20/89

row	TISSUE	ATTEN	SPDTHIN	SPDMED	SPDTHICK
1	1	40.2	1620	1588	1576
2	1	32.2	1618	1605	1563
3	1	24.9	1562	1601	1550
4	1	38.6		1580	1600
5	1	42.9	1575	1595	1598
6	1	18.0	1581	1577	1569
7	1	29.4	1562	1573	1576
8	1	51.3	1627	1596	1574
9	1	51.4	1557	1627	1567
10	1	32.3	1611	1565	1567
11	1	27.6	1597	1609	1618
12	1	32.5	1583	1583	1585
13	1	42.1	1566	1562	1549
14	1	21.1		1544	1538
15	1	18.4	1563	1550	1572
16	1	49.4	1568	1565	1572
17	1	33.3	1578	1555	1560
18	1		1570	1569	1567
19	1	14.0	1586	1587	1582
20	1	36.8	1591	1584	1583
21	1	28.5	1556	1567	1554
22	1	32.0	1564	1556	1568
23	1	49.4	1575	1548	1566
24	1	42.3	1567	1584	1560
25	1	42.8	1555	1520	1524
26	1	32.5	1582	1571	1568
27	1	23.7	1559	1552	1563
28	1	45.3	1558	1558	1563
29	2	44.3	1626	1566	1558
30	2	24.6	1569	1579	1573
31	2	33.6	1547	1613	1579
32	2	67.4	1589	1586	
33	2	45.7	1567	1565	1581
34	2	17.6	1564	1556	1579
35	2	29.1	1565	1564	1533
36	2	20.5	1567	1552	
37	2	32.5			
38	2	33.3	1664	1597	1610
39	2	75.0	1614	1582	1582
40	2	19.8	1648	1580	1595
41	2	47.2	1586	1579	1567
42	2	44.2	1559	1575	1559
43	2	41.4	1554	1546	1544
44	2	33.4	1560	1585	1591
45	2	24.1	1591	1561	1591
46	2	26.6	1595	1567	1576
47	2	17.6	1572	1562	1566
48	2	47.7	1559	1567	1563
49	2	23.9	1588	1570	1586
50	2	32.4	1591	1571	1564
51	2	23.9	1565	1569	1567
52	2	47.7	1561	1581	1574
53	2	55.2	1566	1573	1599
54	2	36.4	1566	1576	1565
55	2	54.8	1552	1558	1560

Canine Myocardium (15 min)

File DGHRT15C 11/20/89

row	THICKNORM	SPDNORM	HINORM	THICKISCH	SPDISCH	HIISCH
1	75	1620	12.7	75	1626	5.6
2	75	1618	6.6	75	1569	5.1
3	75	1562	6.7	75	1547	5.1
4	75			75	1589	5.8
5	75	1575	6.1	75	1567	10.0
6	75	1581	4.1	75	1564	4.7
7	75	1562	5.1	75	1565	7.1
8	75	1627	6.6	75	1567	8.6
9	75	1557	4.8	75		
10	75	1611	4.0	75	1664	11.7
11	75	1597	3.6	75	1614	15.5
12	75	1583	1.4	75	1648	20.1
13	75	1566	3.8	75	1586	2.5
14	75			75	1559	2.1
15	75	1563	4.1	75	1554	3.0
16	75	1568	1.7	75	1560	2.9
17	75	1578	3.2	75	1591	3.0
18	75	1570	4.7	75	1595	2.9
19	75	1586	2.1	75	1572	3.6
20	75	1591	2.3	75	1559	1.7
21	75	1556	1.0	75	1588	2.3
22	75	1564	3.7	75	1591	2.9
23	75	1575	4.6	75	1565	2.7
24	75	1567	7.6	75	1561	6.4
25	75	1555	1.8	75	1566	1.9
26	75	1582	3.5	75	1566	2.6
27	75	1559	2.3	75	1552	1.2
28	75	1558	1.3	75	1571	1.3
29	100	1588	11.3	100	1566	2.4
30	100	1605	4.9	100	1579	4.0
31	100	1601	5.4	100	1613	3.0
32	100	1580	1.7	100	1586	6.1
33	100	1595	5.6	100	1565	4.1
34	100	1577	2.7	100	1556	3.1
35	100	1573	5.6	100	1564	4.0
36	100	1596	4.1	100	1552	6.4
37	100	1627	4.6	100		
38	100	1565	1.8	100	1597	10.9
39	100	1609	1.7	100	1582	14.9
40	100	1583	2.8	100	1580	4.8
41	100	1562	1.2	100	1579	3.2
42	100	1544	1.8	100	1575	2.2
43	100	1550	2.5	100	1546	3.6
44	100	1565	1.1	100	1585	4.1
45	100	1555	2.7	100	1561	1.2
46	100	1569	3.4	100	1567	1.1
47	100	1587	1.1	100	1562	5.6
48	100	1584	2.2	100	1567	0.7
49	100	1567	2.1	100	1570	1.3
50	100	1556	2.1	100	1571	1.7
51	100	1548	3.4	100	1569	6.2
52	100	1584	3.3	100	1581	3.9
53	100	1520	2.2	100	1573	1.9
54	100	1571	1.4	100	1576	1.5
55	100	1552	0.9	100	1558	1.4

Canine Myocardium (15 min)

File DGHRT15C 11/20/89

row	THICKNORM	SPDNORM	HINORM	THICKISCH	SPDISCH	HIISCH
58	150	1563	3.2	150	1573	4.2
59	150	1550	1.9	150	1579	2.1
60	150	1600	4.5	150		
61	150	1598	1.5	150	1581	6.0
62	150	1569	2.1	150	1579	3.6
63	150	1576	5.6	150	1533	1.4
64	150	1574	25.3	150		
65	150	1567	2.6	150		
66	150	1567	3.8	150	1610	22.4
67	150	1618	1.6	150	1582	6.6
68	150	1585	2.1	150	1595	8.8
69	150	1549	1.2	150	1567	2.0
70	150	1538	1.8	150	1559	1.0
71	150	1572	2.2	150	1544	2.4
72	150	1572	2.7	150	1591	2.0
73	150	1560	2.3	150	1591	0.8
74	150	1567	4.9	150	1576	2.2
75	150	1582	0.4	150	1566	2.8
76	150	1583	2.4	150	1563	1.4
77	150	1554	0.9	150	1586	1.8
78	150	1568	2.0	150	1564	1.0
79	150	1566	2.2	150	1567	2.7
80	150	1560	2.7	150	1574	2.5
81	150	1524	0.9	150	1599	2.5
82	150	1568	1.0	150	1565	1.1
83	150	1563	1.1	150	1560	1.6
84	150	1563	0.8	150	1558	1.0

Canine Myocardium (90 min)

File DGHRT90A 11/21/89

row	TISSUE	ATTEN	SPDTHIN	SPDMED	SPDTHICK
1	1	53.5	1592	1579	1591
2	1	37.3	1604	1578	1588
3	1	34.2	1617	1596	1583
4	1	86.0	1577	1575	1587
5	1	37.8	1551	1568	1559
6	1	45.5	1574	1603	1591
7	1	22.1	1611	1570	1559
8	1	23.8	1592	1606	1587
9	1	53.8	1654	1613	1566
10	1	24.1	1558	1578	1576
11	1	25.1	1570	1578	1562
12	1	27.5	1560	1563	1573
13	1	19.3	1568	1552	1556
14	1	24.3	1546	1547	1570
15	1	28.2	1552	1561	1570
16	1	41.0	1567	1559	1564
17	1	33.1	1567	1556	1554
18	1	15.0	1569	1557	1574
19	1	24.6	1566	1578	1568
20	2	39.8	1626	1581	1581
21	2	32.5	1562	1602	1602
22	2	29.2	1644	1604	1586
23	2	30.0	1560	1607	1588
24	2	16.1		1551	1537
25	2	26.0	1556	1586	1588
26	2	43.8	1622		1583
27	2	34.2	1664	1639	1565
28	2	50.8	1563	1611	1563
29	2	14.0	1553	1550	1561
30	2	20.1	1560		
31	2	20.3	1565	1552	1553
32	2	25.6	1579	1573	1556
33	2	41.1	1553	1557	1560
34	2	48.9	1583	1578	1562
35	2	29.3	1558	1565	1547
36	2	23.5	1569	1568	1568
37	2	36.6	1574	1588	1579
38	2	37.1	1561	1604	1574

Canine Myocardium (90 min)

File DGHRT90C 11/21/89

row	THICKNORM	SPDNORM	HINORM	THICKISCH	SPDISCH	HIISCH
1	75	1592	4.6	75	1626	6.7
2	75	1604	6.3	75	1562	1.2
3	75	1617	10.4	75	1644	7.8
4	75	1577	6.5	75	1560	14.4
5	75	1551	14.3	75		
6	75	1574	13.0	75	1556	13.4
7	75	1611	7.5	75	1622	11.9
8	75	1592	13.3	75	1664	3.5
9	75	1654	10.2	75	1563	7.1
10	75	1558	4.0	75	1553	3.8
11	75	1570	5.0	75	1560	4.0
12	75	1560	4.7	75	1565	3.5
13	75	1568	3.3	75	1579	5.5
14	75	1546	1.2	75	1553	1.0
15	75	1552	1.8	75	1583	1.4
16	75	1567	1.2	75	1558	1.8
17	75	1567	2.4	75	1569	1.2
18	75	1569	1.6	75	1574	3.8
19	75	1566	2.9	75	1561	2.0
20	100	1579	4.5	100	1581	6.1
21	100	1578	6.7	100	1602	4.8
22	100	1596	4.3	100	1604	7.4
23	100	1575	20.2	100	1607	13.0
24	100	1568	3.8	100	1551	3.5
25	100	1603	3.9	100	1586	6.6
26	100	1570	5.8	100		
27	100	1606	2.8	100	1639	2.6
28	100	1613	9.4	100	1611	2.9
29	100	1578	3.3	100	1550	2.9
30	100	1578	3.3	100		
31	100	1563	3.6	100	1552	7.0
32	100	1552	3.4	100	1573	3.5
33	100	1547	4.7	100	1557	1.2
34	100	1561	1.3	100	1578	1.3
35	100	1559	1.0	100	1565	3.0
36	100	1556	1.3	100	1568	2.3
37	100	1557	2.2	100	1588	3.9
38	100	1578	1.9	100	1604	2.0
39	150	1591	2.3	150	1581	1.7
40	150	1588	1.6	150	1602	2.2
41	150	1583	3.8	150	1586	1.8
42	150	1587	19.9	150	1588	5.8
43	150	1559	2.9	150	1537	1.6
44	150	1591	3.6	150	1588	3.2
45	150	1559	9.4	150	1583	5.4
46	150	1587	3.4	150	1565	1.9
47	150	1566	7.0	150	1563	2.8
48	150	1576	3.2	150	1561	2.8
49	150	1562	3.0	150		
50	150	1573	2.3	150	1553	2.9
51	150	1556	2.7	150	1556	3.2
52	150	1570	2.8	150	1560	0.8
53	150	1570	2.2	150	1562	1.2
54	150	1564	1.5	150	1547	0.7
55	150	1554	1.2	150	1568	1.3

Rat Myocardium and Liver

File RATSPD 11/28/89

row	THICK	LIVSPD	LIVHI	RATNO	HRTSPD	HRTHI
1	75	1549	3.60	1	1569	2.90
2	100	1560	3.60	1	1557	2.80
3	125	1551	5.40	1	1566	2.70
4	150	1588	1.70	1	1568	2.90
5	175			1	1571	1.20
6	200	1579	1.60	1	1576	1.10
7	250	1582	2.20	1	1581	3.20
8	300	1567	1.50	1	1573	1.80
9	350	1576	0.71	1		
10	400	1591	2.40	1	1574	0.62
11	500			1	1566	0.44
12	600			1	1564	0.82
13	75	1577	3.90	1	1567	2.00
14	100	1569	3.50	1	1563	3.20
15	125	1579	3.10	1	1565	2.60
16	150	1584	1.20	1	1568	2.10
17	175			1	1564	2.40
18	200	1577	1.10	1	1571	2.50
19	250	1564	1.70	1	1570	1.30
20	300	1576	4.10	1	1573	1.10
21	350	1577	2.10	1		
22	400	1582	0.97	1	1573	1.00
23	500			1	1565	0.58
24	75	1554	4.30	2	1575	3.40
25	100	1566	4.60	2	1572	2.20
26	125	1545	2.80	2		
27	150	1551	2.60	2	1565	1.60
28	200	1567	1.40	2	1568	2.20
29	250	1575	0.96	2	1574	2.00
30	300	1583	1.40	2	1591	1.40
31	350	1577	1.80	2	1575	1.20
32	400	1584	0.63	2	1584	1.60
33	450			2	1573	0.98
34	75	1577	3.50	2	1578	5.50
35	100	1572	3.20	2	1562	4.00
36	125	1574	2.70	2	1584	4.70
37	150	1560	1.70	2	1572	2.90
38	175			2	1577	1.90
39	200	1571	1.20	2	1567	1.70
40	250	1564	0.87	2	1570	0.99
41	300	1574	1.70	2	1578	1.60
42	350	1560	0.86	2	1577	1.20
43	400	1566	0.86	2	1575	2.10
44	450			2	1581	1.40
45	500			2	1565	1.20
46	75	1562	4.80	3	1576	5.20
47	100	1563	3.00	3	1571	2.10
48	125	1563	1.70	3	1570	3.80
49	150	1568	1.70	3	1572	3.60
50	175			3	1581	1.70
51	200	1554	1.40	3	1580	1.80
52	250	1562	2.00	3	1577	1.80
53	300	1572	1.40	3	1571	1.50
54	350	1566	1.40	3	1577	1.90
55	400	1576	1.70	3	1563	1.60
56	450			3	1573	0.86
57	75	1559	3.40	3	1565	4.90

Rat Myocardium and Liver

File RATSPD 11/28/89

row	THICK	LIVSPD	LIVHI	RATNO	HRTSPD	HRTHI
58	100	1570	2.60	3	1567	2.70
59	125	1560	2.50	3	1566	3.60
60	150	1555	3.10	3	1567	2.90
61	200	1561	1.40	3	1572	2.30
62	250	1563	1.30	3	1572	0.83
63	300	1564	1.30	3	1569	1.10
64	350	1559	1.40	3	1566	1.30
65	400	1559	3.00	3	1585	0.78
66	75	1562	2.50	4	1562	3.30
67	100	1559	3.90	4	1583	5.20
68	125	1570	2.90	4	1570	1.60
69	150	1560	2.20	4	1564	3.00
70	200	1562	1.40	4	1580	1.30
71	250	1570	1.40	4	1556	0.88
72	300	1559	1.30	4	1576	1.70
73	350	1564	0.99	4	1574	1.70
74	400	1563	1.60	4	1589	1.00
75	75	1566	6.10	4	1563	1.90
76	100	1574	5.00	4	1566	3.20
77	125	1568	2.40	4	1577	2.60
78	150	1558	1.50	4	1570	2.50
79	200	1556	1.60	4	1577	1.60
80	250	1565	1.10	4	1568	1.80
81	300	1563	1.04	4	1566	1.20
82	350	1559	0.75	4	1566	3.80
83	400	1572	1.20	4	1588	0.89
84	75			5	1560	8.60
85	75			5	1581	5.00
86	100			5	1547	2.20
87	100			5	1565	4.60
88	125			5	1560	2.80
89	125			5	1564	3.00
90	150			5	1565	1.80
91	150			5	1584	2.60
92	200			5	1581	1.20
93	200			5	1599	4.80
94	250			5	1593	3.30
95	250			5	1576	1.00
96	300			5	1581	2.20
97	300			5	1571	0.88
98	350			5	1580	1.40
99	350			5	1571	1.60
100	400			5	1575	2.40
101	400			5	1573	1.70
102	75			6	1567	3.70
103	75			6	1559	3.30
104	100			6	1574	2.60
105	100			6	1580	3.30
106	125			6	1560	2.10
107	125			6	1576	4.20
108	150			6	1567	2.00
109	150			6	1566	2.80
110	200			6	1567	2.70
111	200			6	1572	1.60
112	250			6	1571	1.90
113	250			6	1572	1.10
114	300			6	1567	1.60

Rat Myocardium and Liver

File RATSPD 11/28/89

row	THICK	LIVSPD	LIVHI	RATNO	HRTSPD	HRTHI
115	300			6	1576	2.10
116	350			6	1572	2.10
117	350			6	1574	1.40
118	400			6	1574	1.40
119	400			6		
120	75			7	1561	4.40
121	75			7	1565	5.10
122	100			7	1557	4.70
123	100			7	1574	5.40
124	125			7	1573	2.90
125	125			7	1567	4.00
126	150			7	1570	1.80
127	150			7	1577	3.60
128	200			7	1572	2.00
129	200			7	1569	2.20
130	250			7	1563	1.10
131	250			7	1576	1.30
132	300			7	1564	1.00
133	300			7	1571	0.88
134	350			7	1577	1.30
135	350			7	1561	1.10
136	400			7	1585	1.20
137	400			7	1595	1.50
138	75			8	1592	5.60
139	75			8	1576	3.40
140	100			8	1560	3.50
141	100			8		
142	125			8	1584	4.10
143	125			8		
144	150			8	1586	2.50
145	150			8		
146	200			8	1580	1.20
147	200			8		
148	250			8	1581	1.60
149	250			8		
150	300			8	1585	1.80
151	300			8		
152	350			8	1577	1.20
153	350			8		
154	400			8	1588	1.10
155	400			8		
156						

APPENDIX II: STATGRAPHICS ANALYSIS OF CANINE MYOCARDIUM

ANOVA results on speed and heterogeneity index are listed in a table which shows the F-ratio and siginificance level. Also, the corresponding graph is displayed below the table. Data files are given in APPENDIX I.

Table II.1. ANOVA results of thickness vs. ultrasonic speed of normal tissue for the 15 min occlusion.

One-Way Analysis of Variance

Data: DGHRT15C.SPDNORM

Level codes: DGHRT15C.THICKNORM

Labels: 3 3 RESHAPE '075100150'

Range test: Conf. Int. Confidence level: 95

Analysis of variance

Source of variation	Sum of Squares	d.f.	Mean square	F-ratio	Sig. level
Between groups	1126.284	2	563.14215	1.288	.2816
Within groups	34545.618	79	437.28631		
Total (corrected)	35671.902	81			

11 missing value(s) have been excluded.

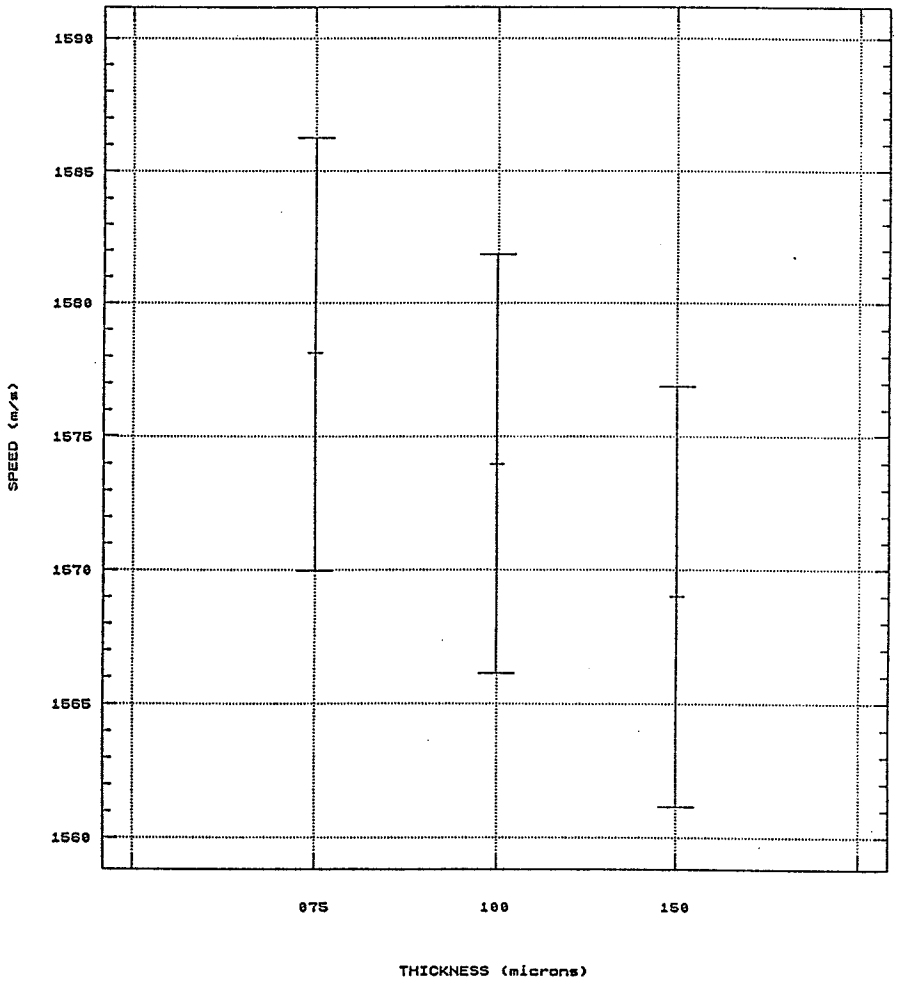

Figure II.1. Statgraphics ANOVA: ultrasonic speed of normal tissue vs. thickness for the 15 min occlusion.

Table II.2. ANOVA results of thickness vs. heterogeneity index of normal tissue for the 15 min occlusion.

One-Way Analysis of Variance

Data: DGHRT15C.HINORM

Level codes: DGHRT15C.THICKNORM

Labels: 3 3 RESHAPE '075100150'

Range test: Conf. Int. Confidence level: 95

Analysis of variance

Source of variation	Sum of Squares	d.f.	Mean square	F-ratio	Sig. level
Between groups	20.41683	2	10.208417	.939	.3955
Within groups	859.15039	79	10.875321		
Total (corrected)	879.56722	81			

11 missing value(s) have been excluded.

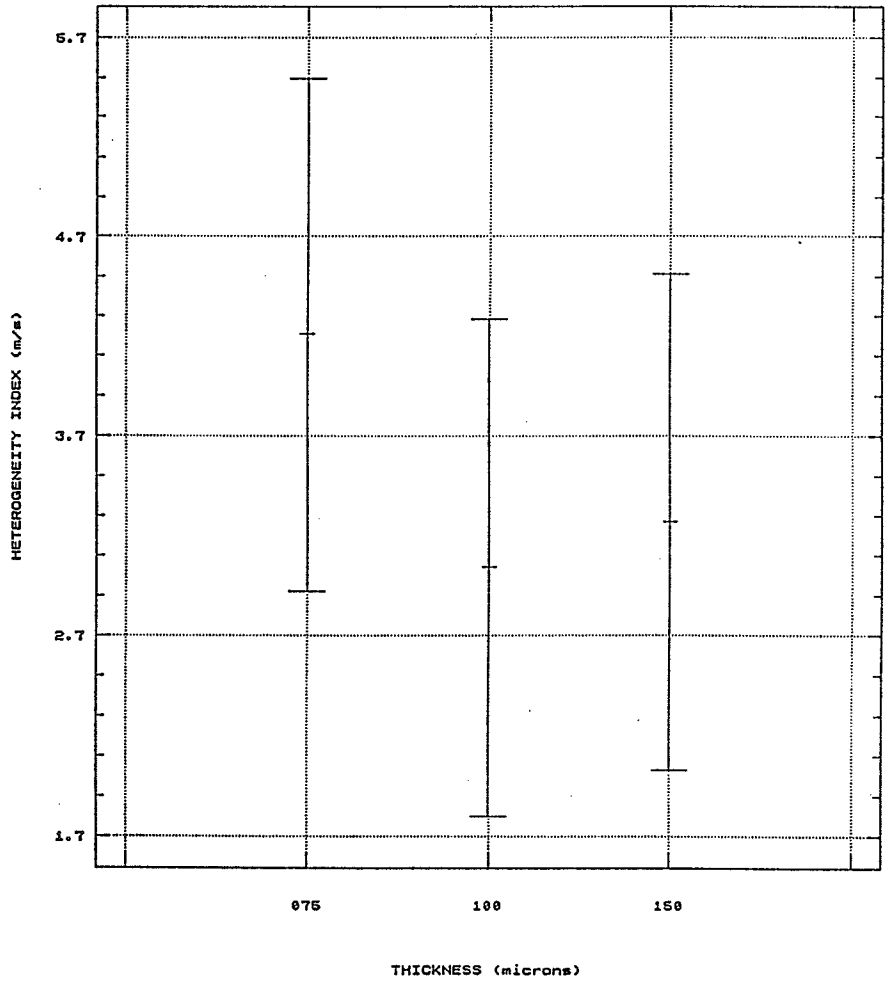

Figure II.2. Statgraphics ANOVA: heterogeneity index of normal tissue vs. thickness for the 15 min occlusion.

Table II.3. ANOVA results of thickness vs. ultrasonic speed of stunned tissue for the 15 min occlusion.

One-Way Analysis of Variance

Data: DGHRT15C.SPDISCH

Level codes: DGHRT15C.THICKISCH

Labels: 3 3 RESHAPE '075100150'

Range test: Conf. Int. Confidence level: 95

Analysis of variance

Source of variation	Sum of Squares	d.f.	Mean square	F-ratio	Sig. level
Between groups	1041.585	2	520.79231	1.167	.3168
Within groups	33912.593	76	446.21832		
Total (corrected)	34954.177	78			

14 missing value(s) have been excluded.

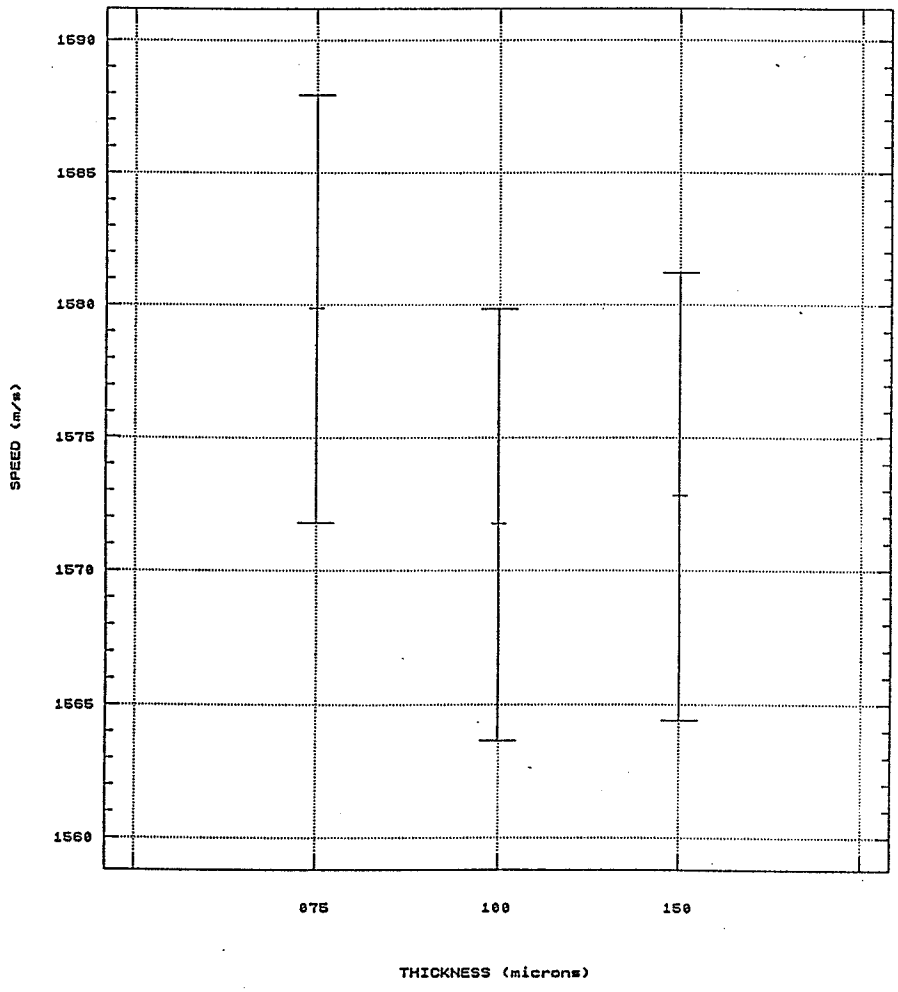

Figure II.3. Statgraphics ANOVA: ultrasonic speed of stunned tissue vs. thickness for the 15 min occlusion.

Table II.4. ANOVA results of thickness vs. heterogeneity index of stunned tissue for the 15 min occlusion.

One-Way Analysis of Variance

Data: DGHRT15C.HIISCH

Level codes: DGHRT15C.THICKISCH

Labels: 3 3 RESHAPE '075100150'

Range test: Conf. Int. Confidence level: 95

Analysis of variance

Source of variation	Sum of Squares	d.f.	Mean square	F-ratio	Sig. level
Between groups	44.8607	2	22.430341	1.363	.2621
Within groups	1250.8133	76	16.458069		
Total (corrected)	1295.6739	78			

14 missing value(s) have been excluded.

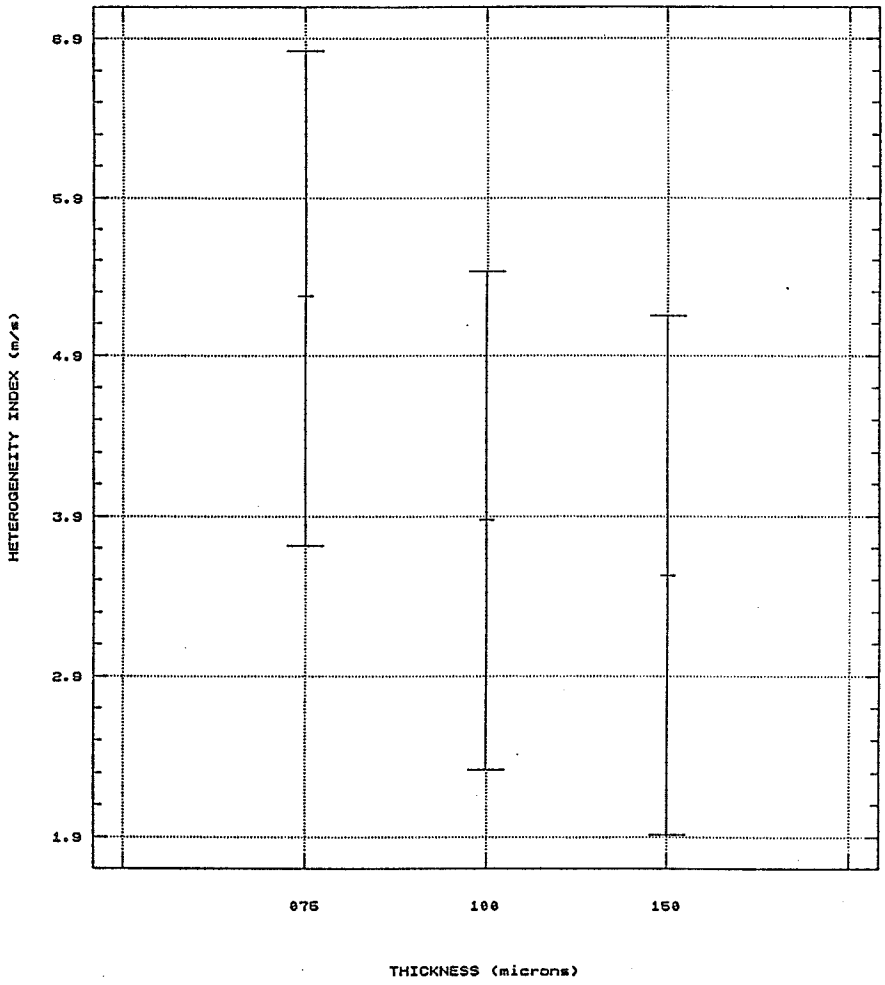

Figure II.4. Statgraphics ANOVA: heterogeneity index of stunned tissue vs. thickness for the 15 min occlusion.

Table II.5. ANOVA results of thickness vs. ultrasonic speed of normal tissue for the 90 min occlusion.

One-Way Analysis of Variance

Data: DGHRT90C.SPDNORM

Level codes: DGHRT90C.THICKNORM

Labels: 3 3 RESHAPE '075100150'

Range test: Conf. Int. Confidence level: 95

Analysis of variance

Source of variation	Sum of Squares	d.f.	Mean square	F-ratio	Sig. level
Between groups	373.579	2	186.78947	.452	.6385
Within groups	22299.474	54	412.95322		
Total (corrected)	22673.053	56			

0 missing value(s) have been excluded.

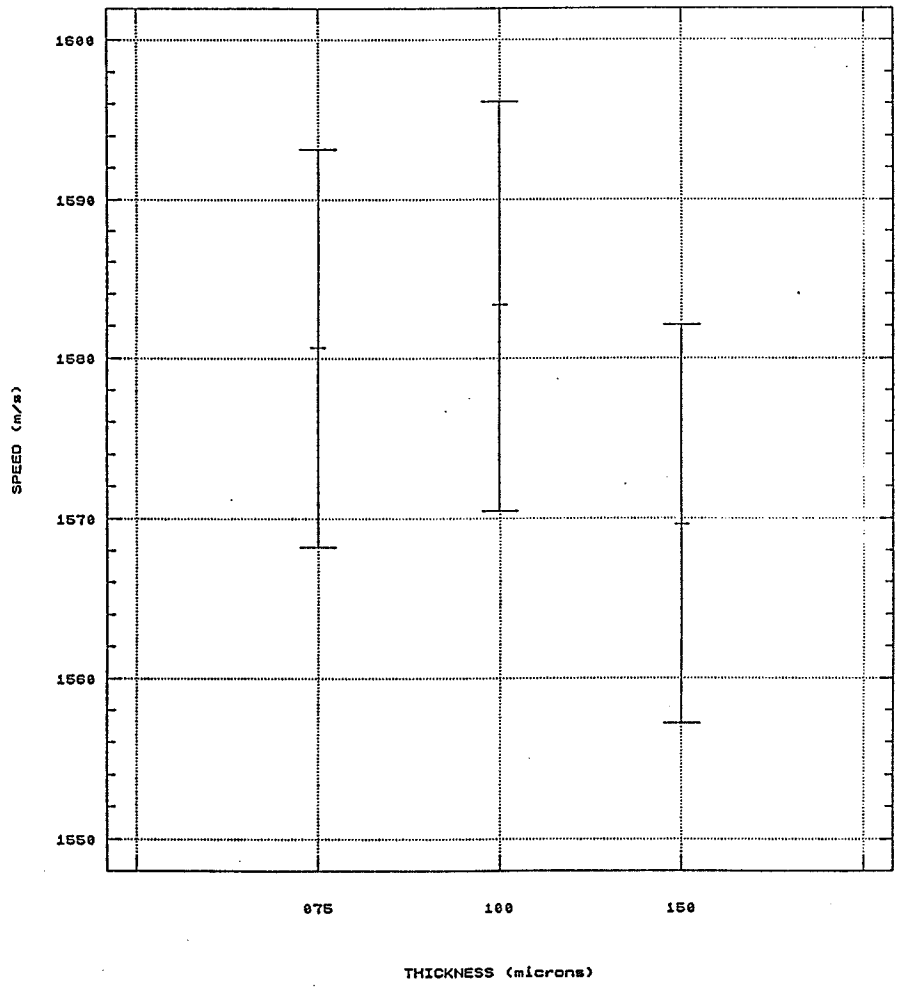

Figure II.5. Statgraphics ANOVA: ultrasonic speed of normal tissue vs. thickness for the 90 min occlusion.

Table II.6. ANOVA results of thickness vs. heterogeneity index of normal tissue for the 90 min. occlusion.

One-Way Analysis of Variance

Data: DGHRT90C.HINORM

Level codes: DGHRT90C.THICKNORM

Labels: 3 3 RESHAPE '075100150'

Range test: Conf. Int. Confidence level: 95

Analysis of variance

Source of variation	Sum of Squares	d.f.	Mean square	F-ratio	Sig. level
Between groups	39.11158	2	19.555789	1.059	.3538
Within groups	997.04421	54	18.463782		
Total (corrected)	1036.1558	56			

0 missing value(s) have been excluded.

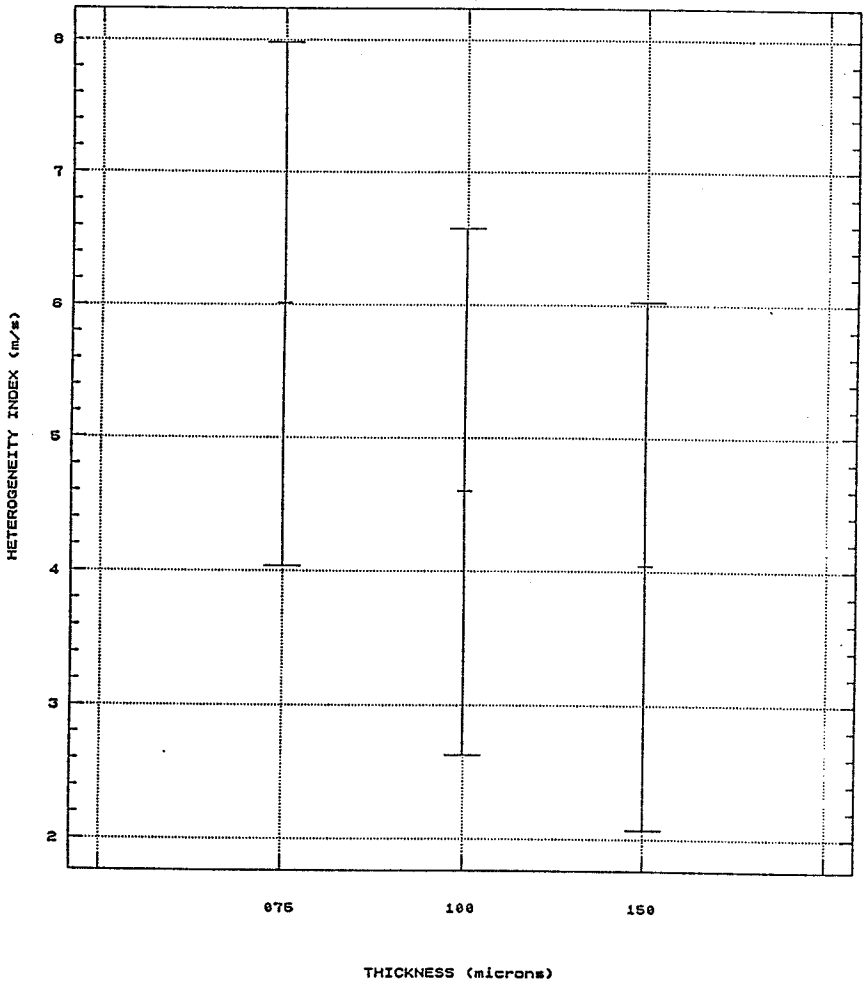

Figure II.6. Statgraphics ANOVA: heterogeneity index of normal tissue vs. thickness for the 90 min occlusion.

Table II.7. ANOVA results of thickness vs. ultrasonic speed of ischemic tissue for the 90 min occlusion.

One-Way Analysis of Variance

Data: DGHRT90C.SPDISCH

Level codes: DGHRT90C.THICKISCH

Labels: 3 3 RESHAPE '075100150'

Range test: Conf. Int. Confidence level: 95

Analysis of variance

Source of variation	Sum of Squares	d.f.	Mean square	F-ratio	Sig. level
Between groups	1868.004	2	934.00207	1.348	.2691
Within groups	34645.807	50	692.91614		
Total (corrected)	36513.811	52			

4 missing value(s) have been excluded.

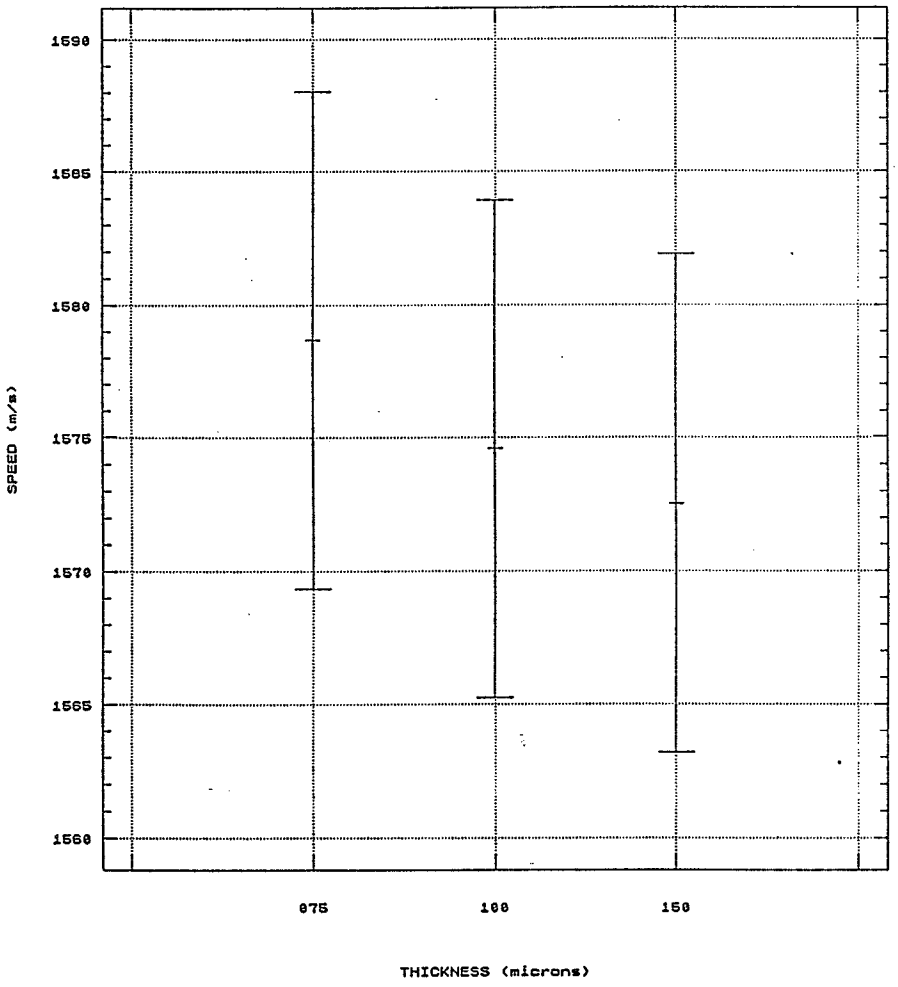

Figure II.7. Statgraphics ANOVA: ultrasonic speed of ischemic tissue vs. thickness for the 90 min. occlusion.

Table II.8. ANOVA results of thickness vs. heterogeneity index of ischemic tissue for the 90 min occlusion.

One-Way Analysis of Variance

Data: DGHRT90C.HIISCH

Level codes: DGHRT90C.THICKISCH

Labels: 3 3 RESHAPE '075100150'

Range test: Conf. Int. Confidence level: 95

Analysis of variance

Source of variation	Sum of Squares	d.f.	Mean square	F-ratio	Sig. level
Between groups	77.15034	2	38.575169	4.025	.0240
Within groups	479.25249	50	9.585050		
Total (corrected)	556.40283	52			

4 missing value(s) have been excluded.

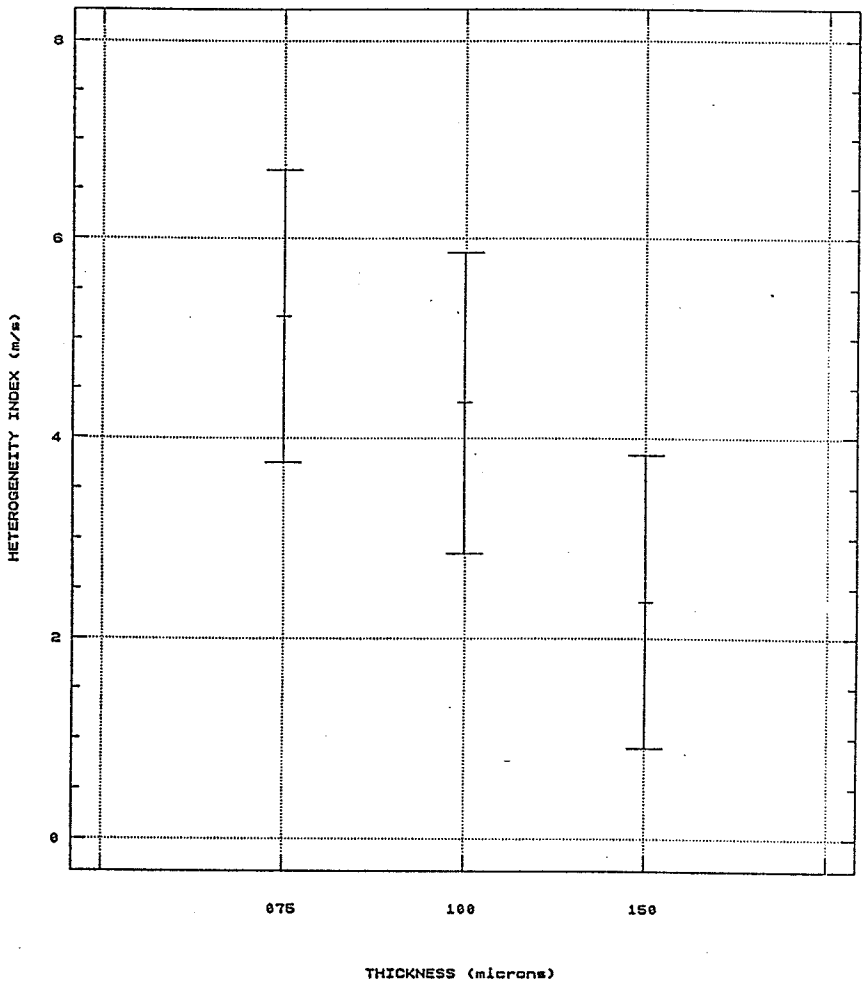

Figure II.8. Statgraphics ANOVA: heterogeneity index of ischemic tissue vs. thickness for the 90 min occlusion.

APPENDIX III: THE IBR5 FOR CANINE MYOCARDIUM (dB)

15 MINUTE INFARCTION

Dog	Normal	Stunned
1	-49.0	-45.7
2	-48.4	-45.4
3	-47.9	-45.2
4	-48.0	-46.3

90 MINUTE INFARCTION

Dog	Normal	Ischemic
1	-47.6	-44.6
2	-48.8	-45
3	-50.6	-46.5

APPENDIX IV: THE WATER, PROTEIN AND LIPID CONCENTRATION OF STUNNED AND NORMAL CANINE MYOCARDIUM

NORMAL TISSUE (CCX)

Dog	Water(%)	Protein(%)	Lipid(%)
1	77.1	16.5	15.3
2	77.2	11.7	11.4
3	76.8	16.8	5.8

STUNNED TISSUE (LAD)

Dog	Water(%)	Protein(%)	Lipid(%)
1	76.9	16.6	5.6
2	77.8	15.4	6.9
3	77.4	16.2	7.1

APPENDIX V: STATGRAPHICS ANALYSIS OF RAT MYOCARDIUM

Regression analysis plot of insertion vs. thickness is displayed for each rat. In the table above each graph, slope and variance analyses are given. ANOVA results for speed and HI vs. thickness are also shown in plots and tables.

Table V.1. Regression analysis results on IL vs. thickness for rat 1.

Regression Analysis - Linear model: Y = a+bX

Dependent variable: RATHRT.R1IL Independent variable: RATHRT.THICKNESS

Parameter	Estimate	Standard Error	T Value	Prob. Level
Intercept	1.10425	0.119344	9.25266	.00000
Slope	9.16634	0.45327	20.2227	.00000

Analysis of Variance

Source	Sum of Squares	Df	Mean Square	F-Ratio	Prob. Level
Model	222.37923	1	222.37923	408.9568	.00000
Error	80.47825	148	.54377		
Total (Corr.)	302.85748	149			

Correlation Coefficient = 0.856896 R-squared = 73.43 percent
Stnd. Error of Est. = 0.737409

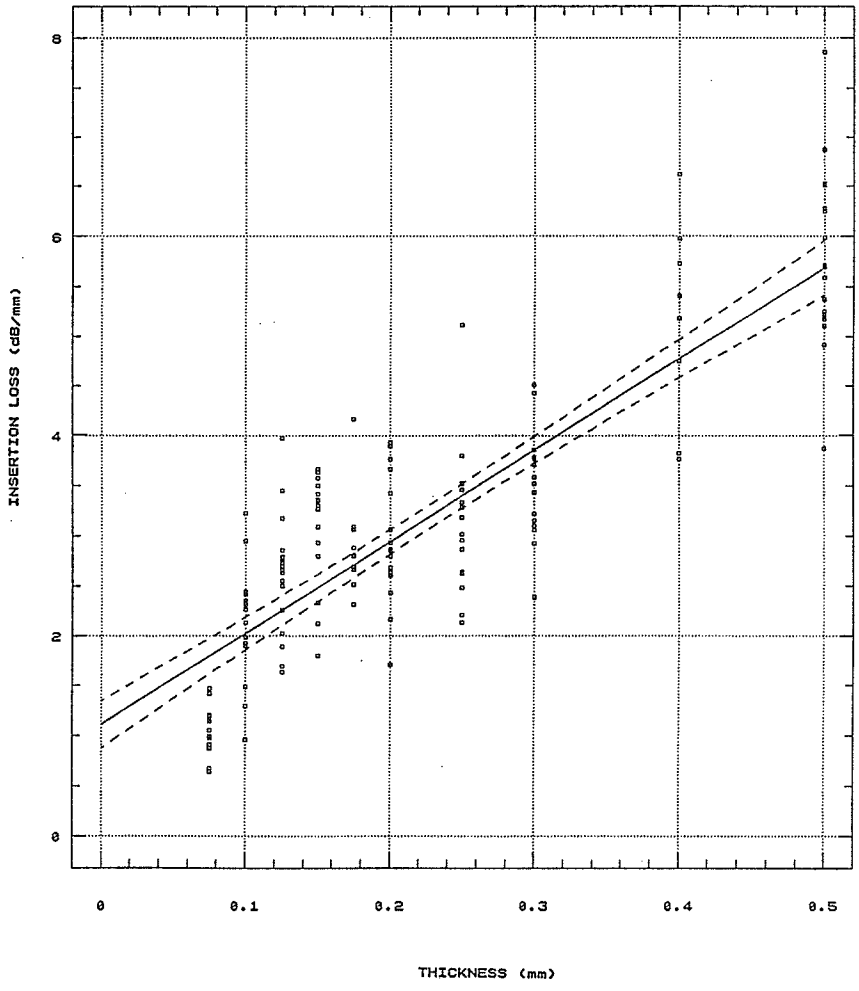

Figure V.1. Statgraphics linear regression plot: IL vs. thicknesses for rat 1. Slope is the atten. coeff.

Table V.2. Regression analysis results on IL vs. thickness for rat 2.

Regression Analysis - Linear model: Y = a+bX

Dependent variable: RATHRT.R2IL Independent variable: RATHRT.THICKNESS

Parameter	Estimate	Standard Error	T Value	Prob. Level
Intercept	1.60068	0.168216	9.51564	.00000
Slope	9.28533	0.646818	14.3554	.00000

Analysis of Variance

Source	Sum of Squares	Df	Mean Square	F-Ratio	Prob. Level
Model	181.02132	1	181.02132	206.0779	.00000
Error	132.64024	151	.87841		
Total (Corr.)	313.66156	152			

Correlation Coefficient = 0.759686 R-squared = 57.71 percent
Stnd. Error of Est. = 0.937236

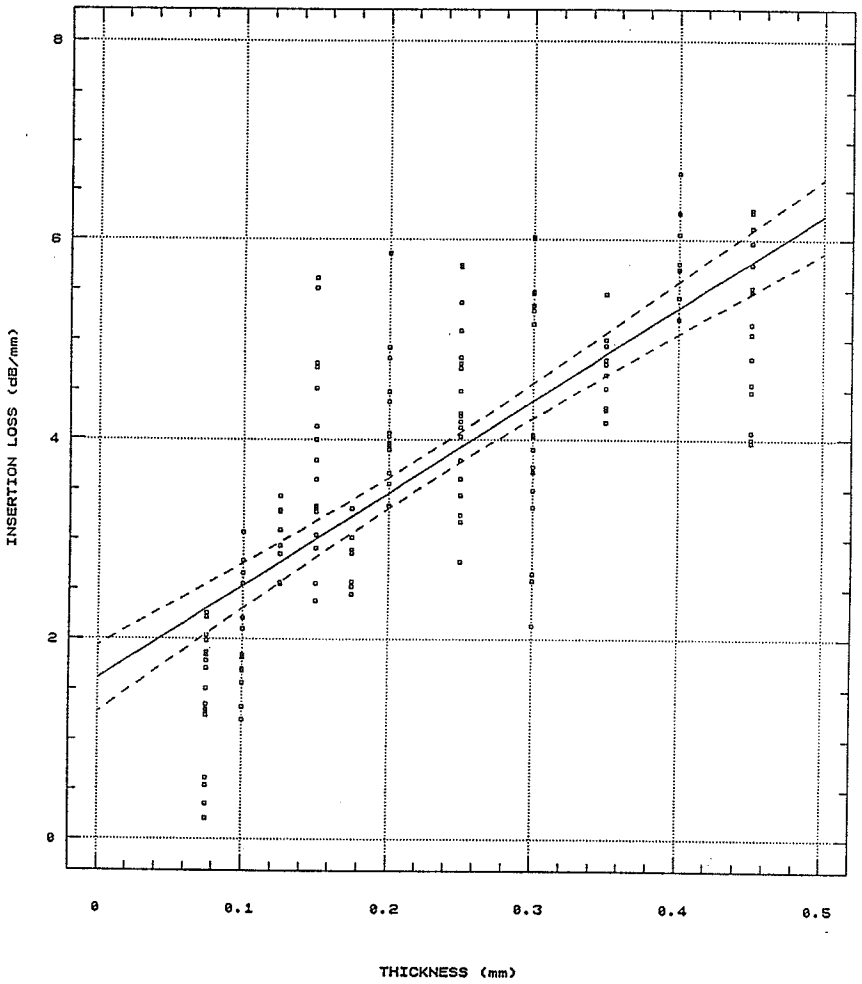

Figure V.2. Statgraphics linear regression plot: IL vs. thicknesses for rat 2. Slope is the atten. coeff.

Table V.3. Regression analysis results on IL vs. thickness for rat 3.

Regression Analysis - Linear model: Y = a+bX

Dependent variable: RATHRT.R3IL Independent variable: RATHRT.THICKNESS

Parameter	Estimate	Standard Error	T Value	Prob. Level
Intercept	1.37152	0.160308	8.55553	.00000
Slope	10.9499	0.640893	17.0854	.00000

Analysis of Variance

Source	Sum of Squares	Df	Mean Square	F-Ratio	Prob. Level
Model	261.13937	1	261.13937	291.9116	.00000
Error	167.28716	187	.89458		
Total (Corr.)	428.42653	188			

Correlation Coefficient = 0.780725 R-squared = 60.95 percent
Stnd. Error of Est. = 0.945824

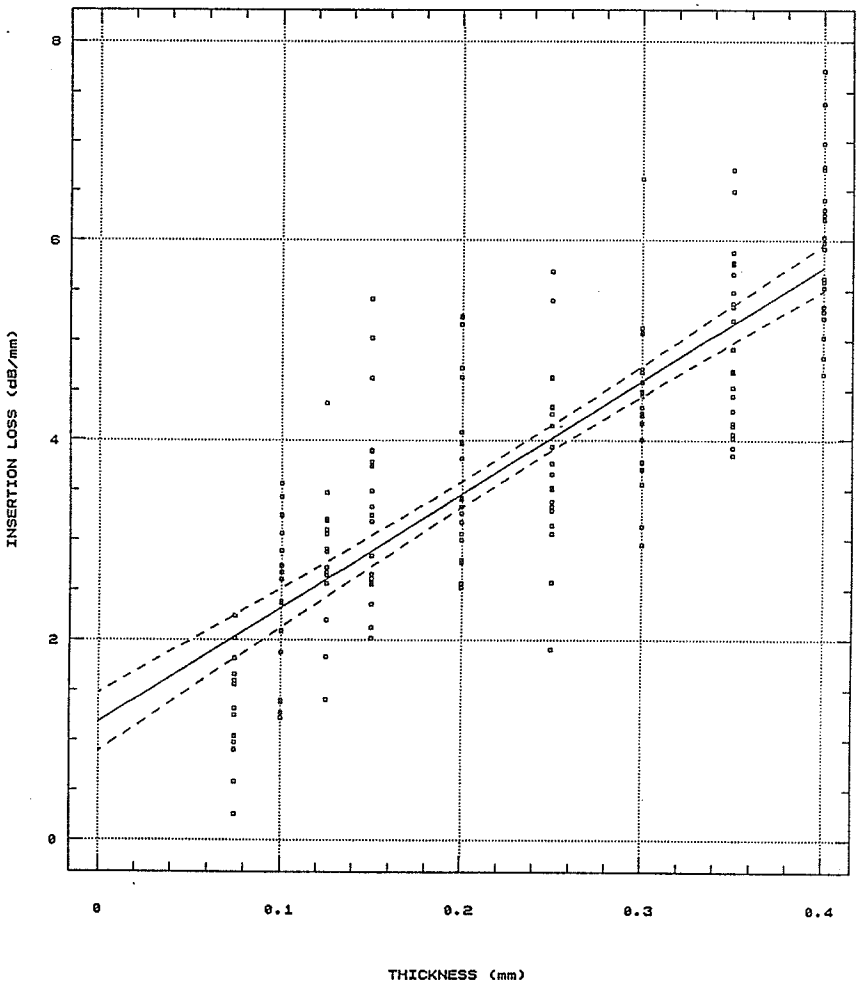

Figure V.3. Statgraphics linear regression plot: IL vs. thicknesses for rat 3. Slope is the atten. coeff.

Table V.4. Regression analysis results on IL vs. thickness for rat 4.

Regression Analysis - Linear model: Y = a+bX

Dependent variable: RATHRT.R4IL Independent variable: RATHRT.THICKNESS

Parameter	Estimate	Standard Error	T Value	Prob. Level
Intercept	1.08204	0.159647	6.77768	.00000
Slope	10.5673	0.686412	15.395	.00000

Analysis of Variance

Source	Sum of Squares	Df	Mean Square	F-Ratio	Prob. Level
Model	202.44966	1	202.44966	237.0052	.00000
Error	131.54666	154	.85420		
Total (Corr.)	333.99633	155			

Correlation Coefficient = 0.778552 R-squared = 60.61 percent
Stnd. Error of Est. = 0.924229

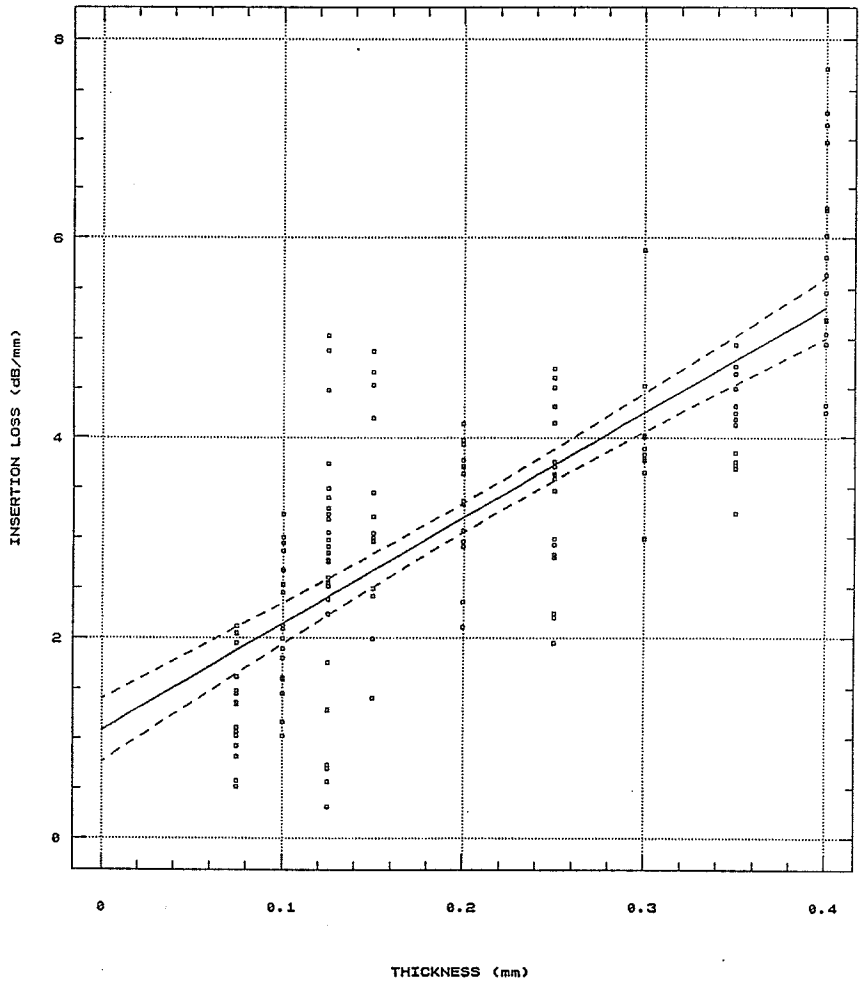

Figure V.4. Statgraphics linear regression plot: IL vs. thicknesses for rat 4. Slope is the atten. coeff.

Table V.5. Regression analysis results on IL vs. thickness for rat 5.

Regression Analysis - Linear model: Y = a+bX

Dependent variable: RATHRT.R5IL Independent variable: RATHRT.THICKNESS

Parameter	Estimate	Standard Error	T Value	Prob. Level
Intercept	0.660952	0.155065	4.26242	.00004
Slope	11.8675	0.631245	18.8001	.00000

Analysis of Variance

Source	Sum of Squares	Df	Mean Square	F-Ratio	Prob. Level
Model	189.49638	1	189.49638	353.4423	.00000
Error	58.43983	109	.53615		
Total (Corr.)	247.93621	110			

Correlation Coefficient = 0.87424 R-squared = 76.43 percent
Stnd. Error of Est. = 0.732219

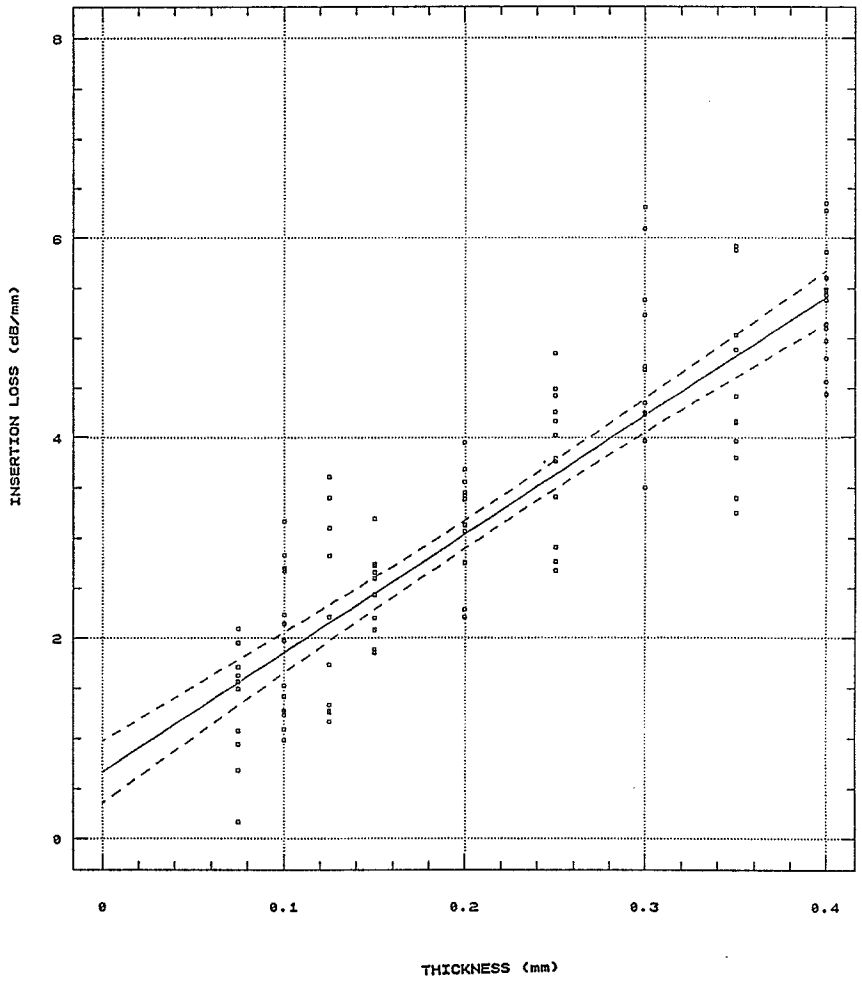

Figure V.5. Statgraphics linear regression plot: IL vs. thicknesses for rat 5. Slope is the atten. coeff.

Table V.6. Regression analysis results on IL vs. thickness for rat 6.

Regression Analysis - Linear model: Y = a+bX

Dependent variable: RATHRT.R6IL Independent variable: RATHRT.THICKNESS

Parameter	Estimate	Standard Error	T Value	Prob. Level
Intercept	0.190697	0.134258	1.42038	.15825
Slope	13.4166	0.557555	24.0632	.00000

Analysis of Variance

Source	Sum of Squares	Df	Mean Square	F-Ratio	Prob. Level
Model	247.27683	1	247.27683	579.0387	.00000
Error	48.25633	113	.42705		
Total (Corr.)	295.53316	114			

Correlation Coefficient = 0.914721 R-squared = 83.67 percent
Stnd. Error of Est. = 0.653488

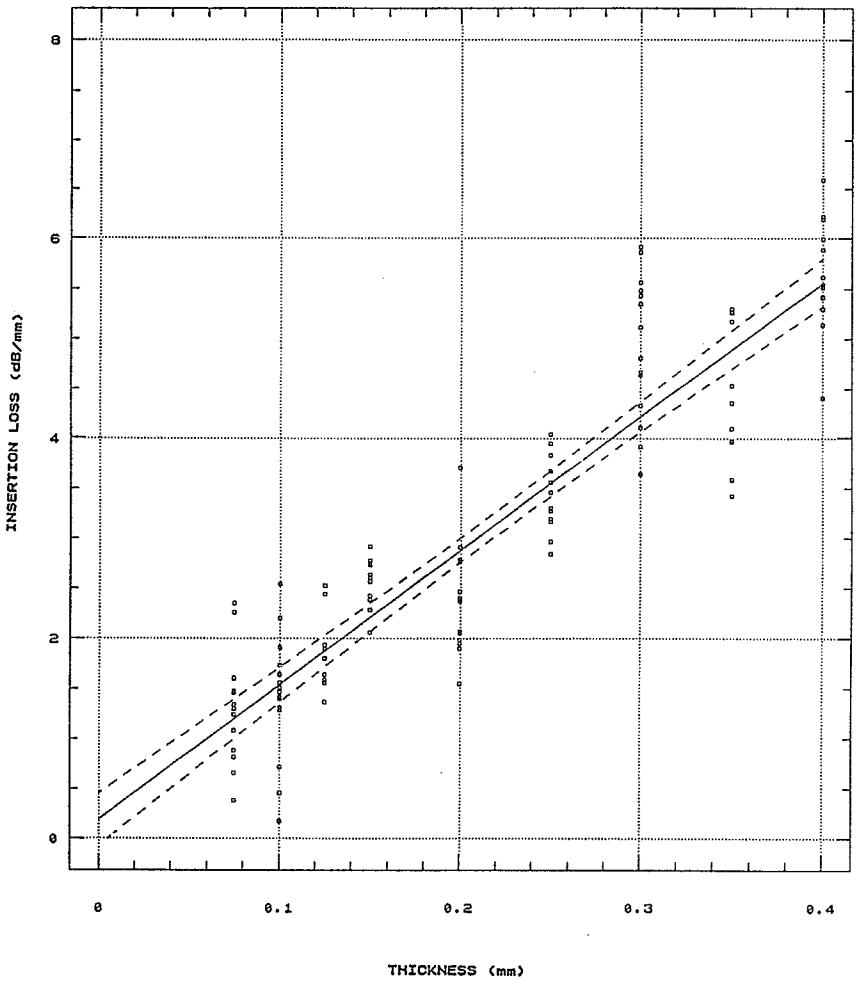

Figure V.6. Statgraphics linear regression plot: IL vs. thicknesses for rat 6. Slope is the atten. coeff.

Table V.7. Regression analysis results on IL vs. thickness for rat 7.

Regression Analysis - Linear model: Y = a+bX

Dependent variable: RATHRT.R7IL Independent variable: RATHRT.THICKNESS

Parameter	Estimate	Standard Error	T Value	Prob. Level
Intercept	0.648127	0.181135	3.57814	.00054
Slope	10.6806	0.776654	13.752	.00000

Analysis of Variance

Source	Sum of Squares	Df	Mean Square	F-Ratio	Prob. Level
Model	110.96937	1	110.96937	189.1184	.00000
Error	56.916868	97	.586772		
Total (Corr.)	167.88623	98			

Correlation Coefficient = 0.813006 R-squared = 66.10 percent
Stnd. Error of Est. = 0.76601

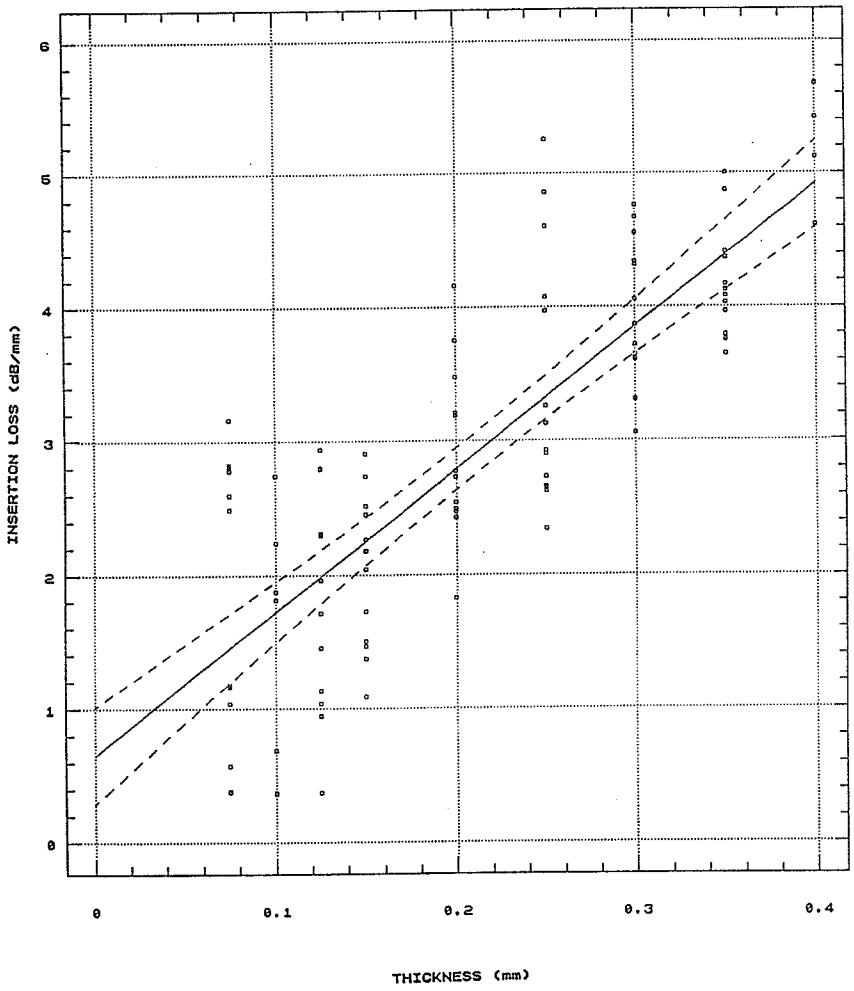

Figure V.7. Statgraphics linear regression plot: IL vs. thicknesses for rat 7. Slope is the atten. coeff.

Table V.8. Regression analysis results on IL vs. thickness for rat 8.

Regression Analysis - Linear model: Y = a+bX

Dependent variable: RATHRT.R8IL Independent variable: RATHRT.THICKNESS

Parameter	Estimate	Standard Error	T Value	Prob. Level
Intercept	0.0591653	0.196221	0.301524	.76372
Slope	15.5157	0.825325	18.7995	.00000

Analysis of Variance

Source	Sum of Squares	Df	Mean Square	F-Ratio	Prob. Level
Model	252.88351	1	252.88351	353.4218	.00000
Error	63.682077	89	.715529		
Total (Corr.)	316.56559	90			

Correlation Coefficient = 0.893775 R-squared = 79.88 percent
Stnd. Error of Est. = 0.845889

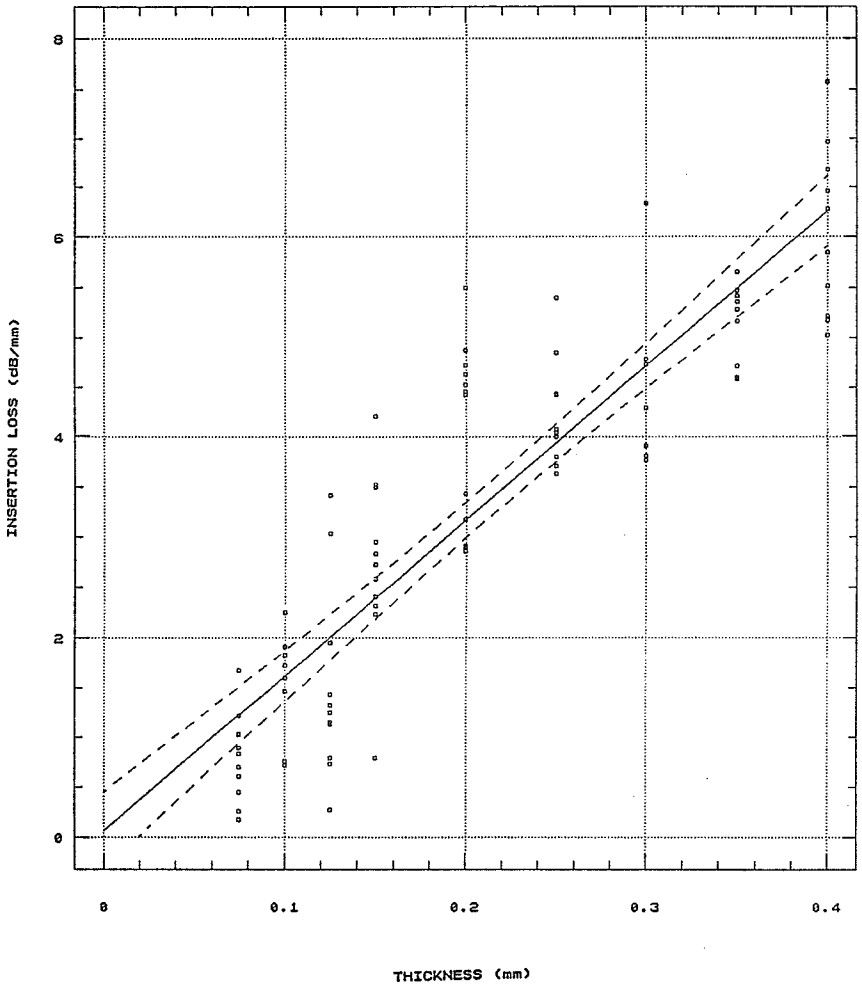

Figure V.8. Statgraphics linear regression plot: IL vs. thicknesses for rat 8. Slope is the atten. coeff.

Table V.9. ANOVA results for the effect of thickness on ultrasonic speed of the rat heart tissue.

One-Way Analysis of Variance

Data: RATSPD.HRTSPD

Level codes: RATSPD.THICK

Labels:

Range test: Conf. Int. Confidence level: 95

Analysis of variance

Source of variation	Sum of Squares	d.f.	Mean square	F-ratio	Sig. level
Between groups	2016.3391	12	168.02826	2.664	.0031
Within groups	8198.7518	130	63.06732		
Total (corrected)	10215.091	142			

13 missing value(s) have been excluded.

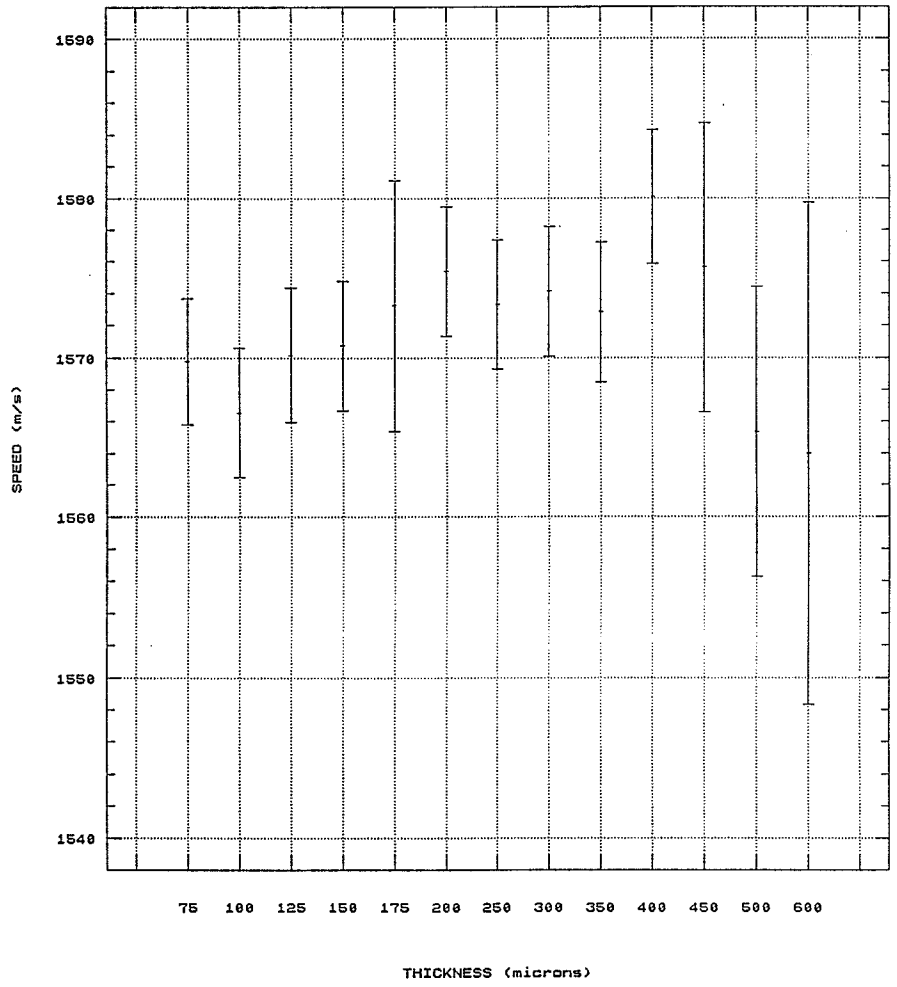

Figure V.9. Statgraphics ANOVA: ultrasonic speed of rat heart tissue vs. thickness.

Table V.10. ANOVA results for the effect of thickness on heterogeneity index of the rat heart tissue.

One-Way Analysis of Variance

Data: RATSPD.HRTHI

Level codes: RATSPD.THICK

Labels: 13 4 RESHAPE ' 75 100 125 150 175 200 250 300 350 400 450 500 600'

Range test: Conf. Int. Confidence level: 95

Analysis of variance

Source of variation	Sum of Squares	d.f.	Mean square	F-ratio	Sig. level
Between groups	146.04033	12	12.170027	14.829	.0000
Within groups	106.68760	130	.820674		
Total (corrected)	252.72793	142			

13 missing value(s) have been excluded.

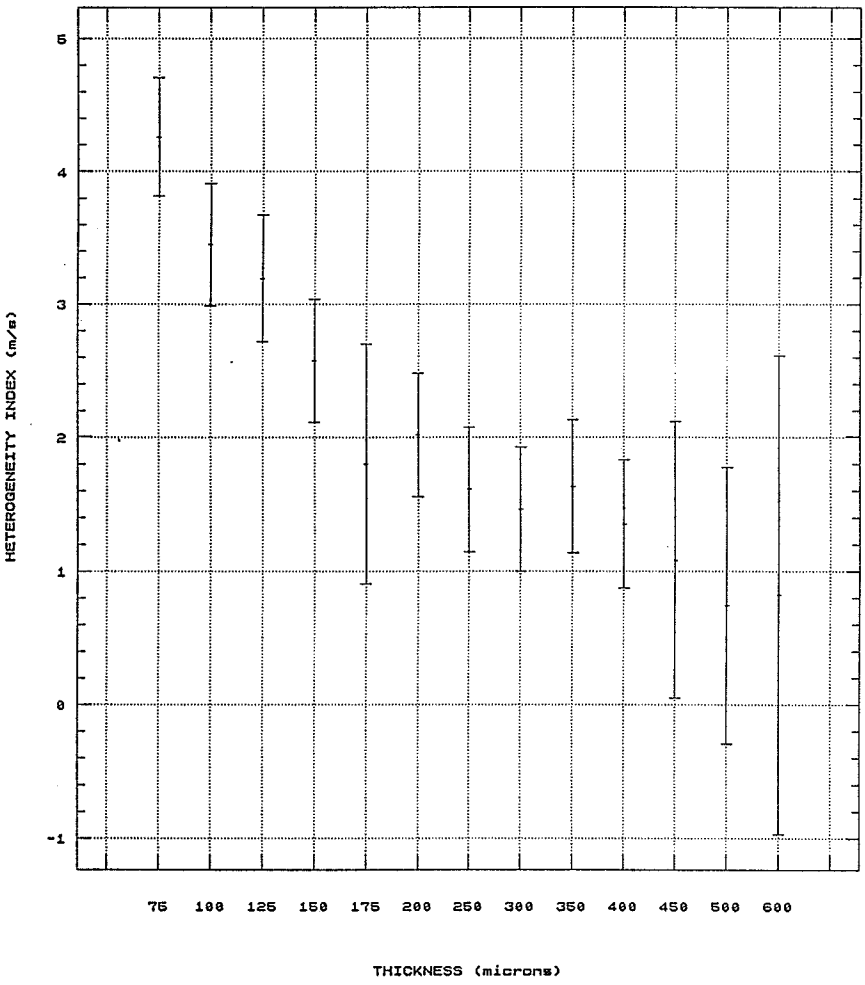

Figure V.10. Statgraphics ANOVA: heterogeneity index of rat heart tissue vs. thickness.

APPENDIX VI: STATGRAPHICS ANALYSIS OF RAT LIVER

Tables containing the result of the regression analysis are displayed. Below each table, the corresponding insertion loss versus thickness plot is displayed. The slope of the plot is the attenuation coefficient.

Table VI.1. Regression analysis results on IL vs. thickness for rat 1.

Regression Analysis - Linear model: Y = a+bX

Dependent variable: RATLIV.R1IL Independent variable: RATLIV.THICKNESS

Parameter	Estimate	Standard Error	T Value	Prob. Level
Intercept	0.101987	0.111793	0.912282	.36320
Slope	9.03914	0.453704	19.923	.00000

Analysis of Variance

Source	Sum of Squares	Df	Mean Square	F-Ratio	Prob. Level
Model	136.27387	1	136.27387	396.9261	.00000
Error	47.72190	139	.34332		
Total (Corr.)	183.99577	140			

Correlation Coefficient = 0.860602 R-squared = 74.06 percent
Stnd. Error of Est. = 0.585938

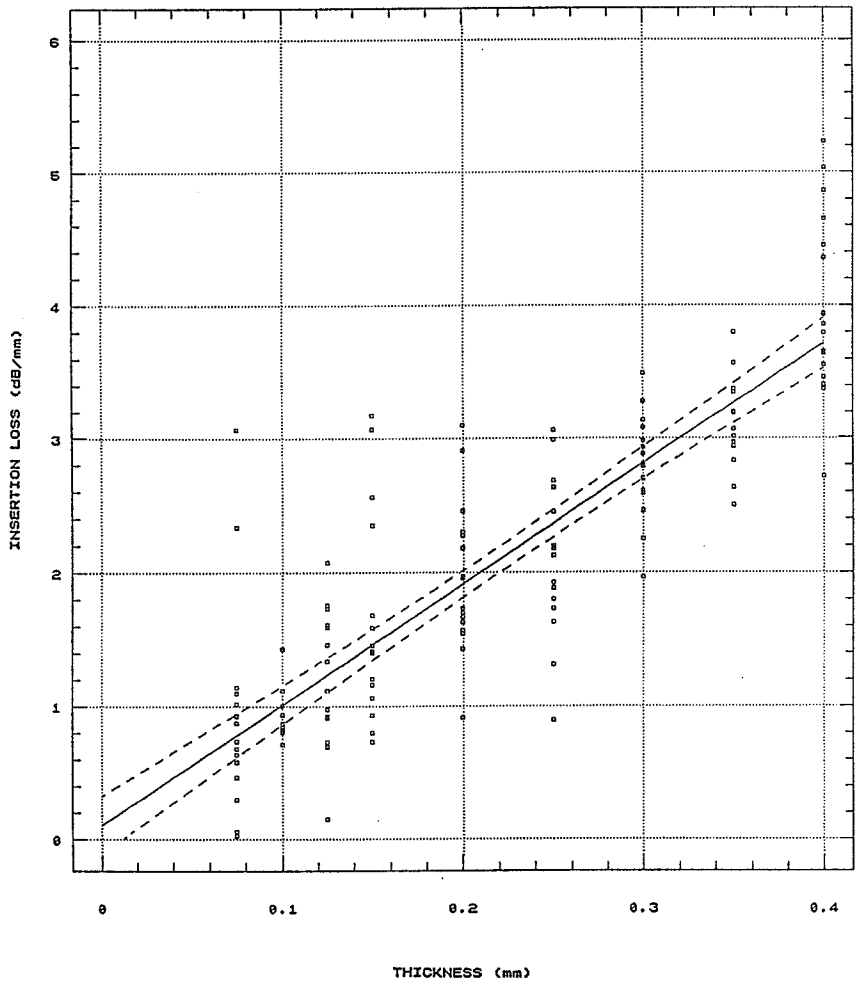

Figure VI.1. Statgraphics linear regression plot: IL vs. thicknesses for rat 1.

Table VI.2. Regression analysis results on IL vs. thickness for rat 2.

Regression Analysis - Linear model: Y = a+bX

Dependent variable: RATLIV.R2IL Independent variable: RATLIV.THICKNESS

Parameter	Estimate	Standard Error	T Value	Prob. Level
Intercept	0.0987458	0.12582	0.784815	.43398
Slope	9.08028	0.490433	18.5148	.00000

Analysis of Variance

Source	Sum of Squares	Df	Mean Square	F-Ratio	Prob. Level
Model	118.28919	1	118.28919	342.7985	.00000
Error	45.20406	131	.34507		
Total (Corr.)	163.49324	132			

Correlation Coefficient = 0.850595 R-squared = 72.35 percent
Stnd. Error of Est. = 0.587426

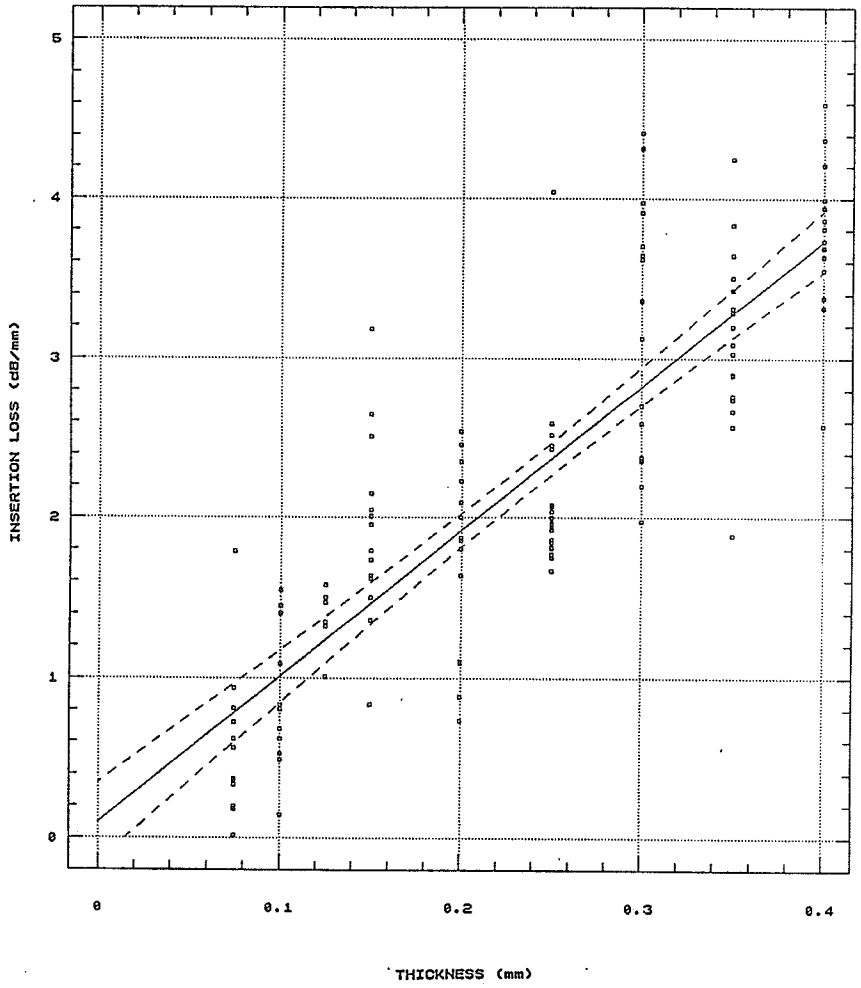

Figure VI.2. Statgraphics linear regression plot: IL vs. thicknesses for rat 2.

Table VI.3. Regression analysis results on IL vs. thickness for rat 3.

Regression Analysis - Linear model: Y = a+bX

Dependent variable: RATLIV.R3IL Independent variable: RATLIV.THICKNESS

Parameter	Estimate	Standard Error	T Value	Prob. Level
Intercept	-0.0785003	0.100009	-0.784934	.43382
Slope	9.86797	0.409231	24.1134	.00000

Analysis of Variance

Source	Sum of Squares	Df	Mean Square	F-Ratio	Prob. Level
Model	161.48297	1	161.48297	581.4577	.00000
Error	38.88093	140	.27772		
Total (Corr.)	200.36390	141			

Correlation Coefficient = 0.897746 R-squared = 80.59 percent
Stnd. Error of Est. = 0.526992

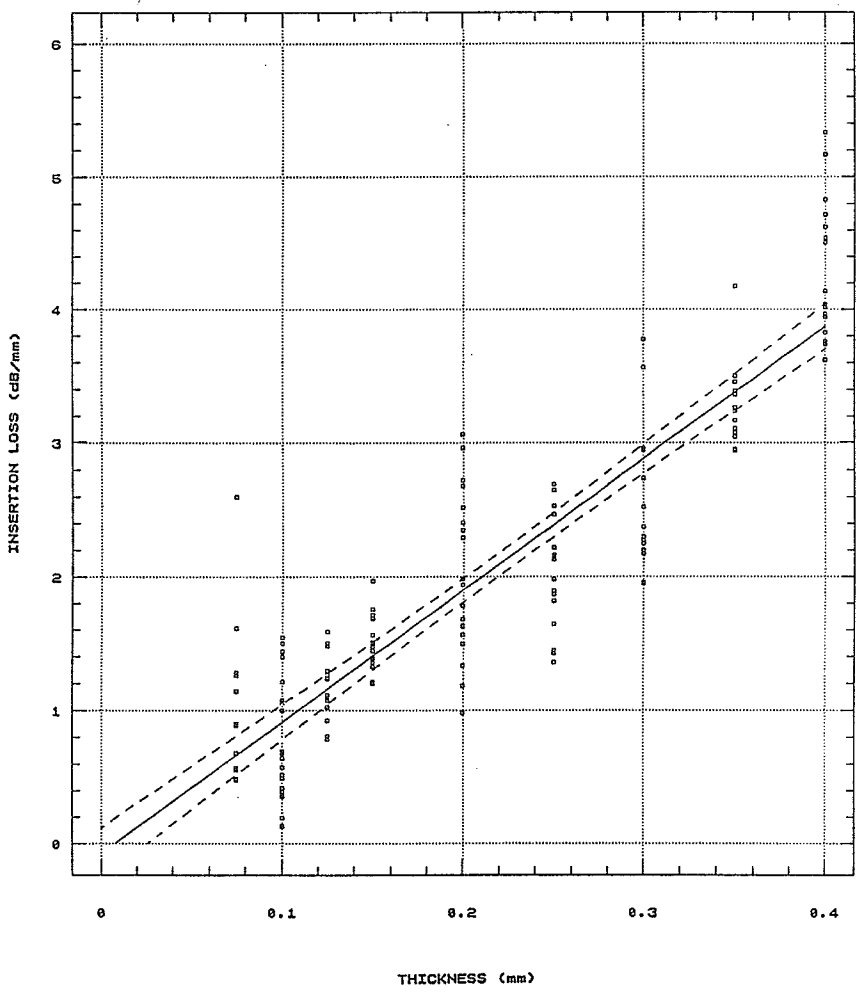

Figure VI.3. Statgraphics linear regression plot: IL vs. thicknesses for rat 3.

Table VI.4. Regression analysis results on IL vs. thickness for rat 4.

Regression Analysis - Linear model: Y = a+bX

Dependent variable: RATLIV.R4IL Independent variable: RATLIV.THICKNESS

Parameter	Estimate	Standard Error	T Value	Prob. Level
Intercept	-0.323503	0.128139	-2.52463	.01280
Slope	10.2986	0.521248	19.7576	.00000

Analysis of Variance

Source	Sum of Squares	Df	Mean Square	F-Ratio	Prob. Level
Model	154.18823	1	154.18823	390.3610	.00000
Error	50.55857	128	.39499		
Total (Corr.)	204.74680	129			

Correlation Coefficient = 0.867795 R-squared = 75.31 percent
Stnd. Error of Est. = 0.628481

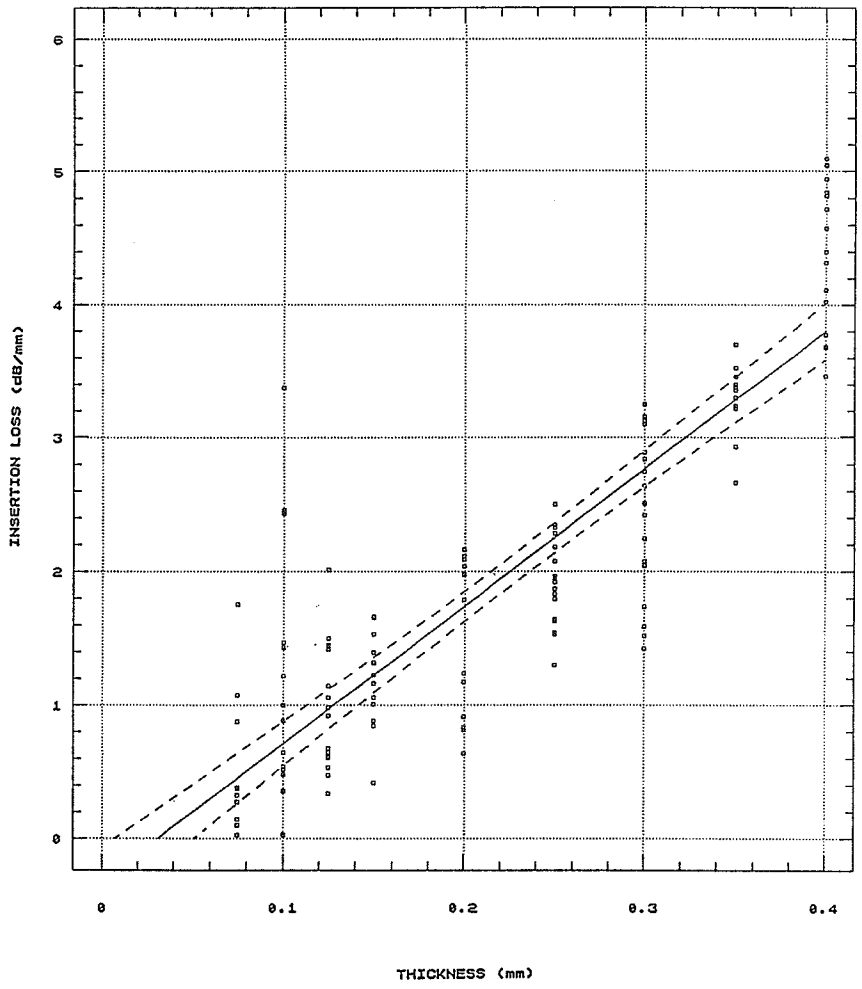

Figure VI.4. Statgraphics linear regression plot: IL vs. thicknesses for rat 4.

Table VI.5. ANOVA results for the effect of thickness on ultrasonic speed (speed for the 4 rats combined).

One-Way Analysis of Variance

Data: RATSPD.LIVSPD

Level codes: RATSPD.THICK

Labels: 9 4 RESHAPE ' 75 100 125 150 200 250 300 350 400 '

Range test: Conf. Int. Confidence level: 95

Analysis of variance

Source of variation	Sum of Squares	d.f.	Mean square	F-ratio	Sig. level
Between groups	702.1111	8	87.763889	.944	.4873
Within groups	5856.5000	63	92.960317		
Total (corrected)	6558.6111	71			

84 missing value(s) have been excluded.

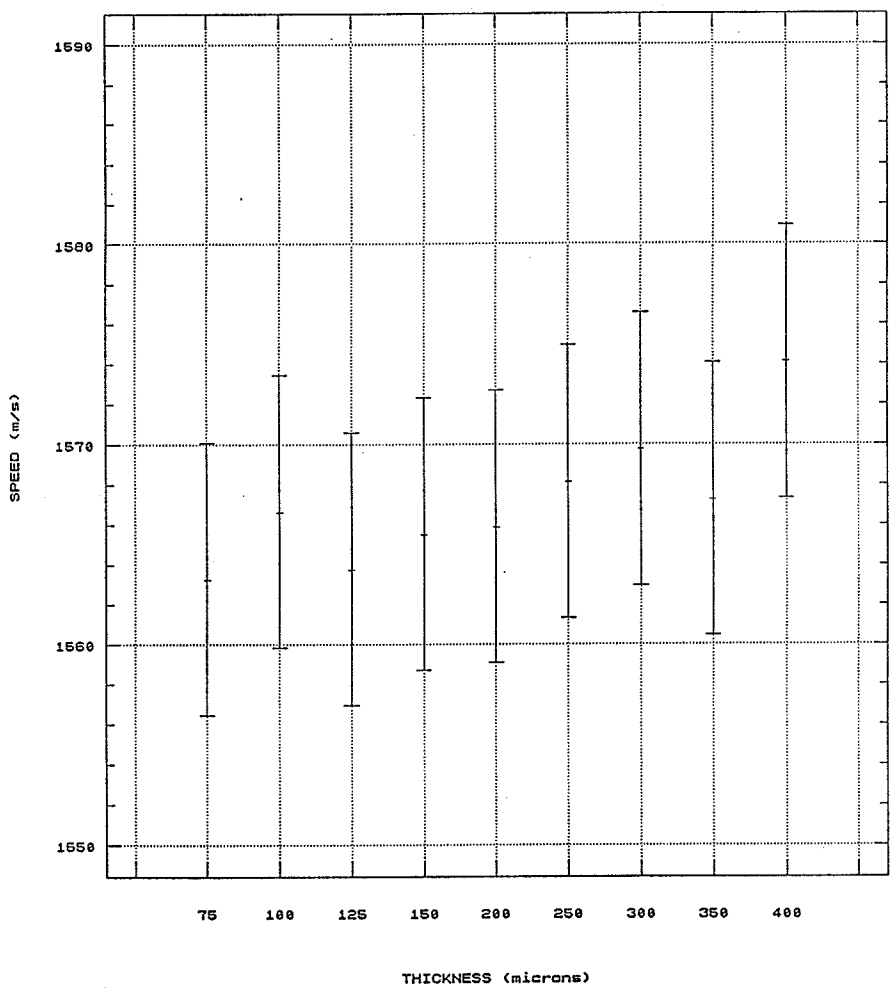

Figure VI.5. Statgraphics ANOVA: ultrasonic speed of rat heart tissue vs. thickness.

Table VI.6. ANOVA results for the effect of thickness on heterogeneity index (HI for the 4 rats combined).

One-Way Analysis of Variance

Data: RATSPD.LIVHI

Level codes: RATSPD.THICK

Labels:

Range test: Conf. Int. Confidence level: 95

Analysis of variance

Source of variation	Sum of Squares	d.f.	Mean square	F-ratio	Sig. level
Between groups	70.856253	8	8.8570316	14.420	.0000
Within groups	38.696525	63	.6142306		
Total (corrected)	109.55278	71			

84 missing value(s) have been excluded.

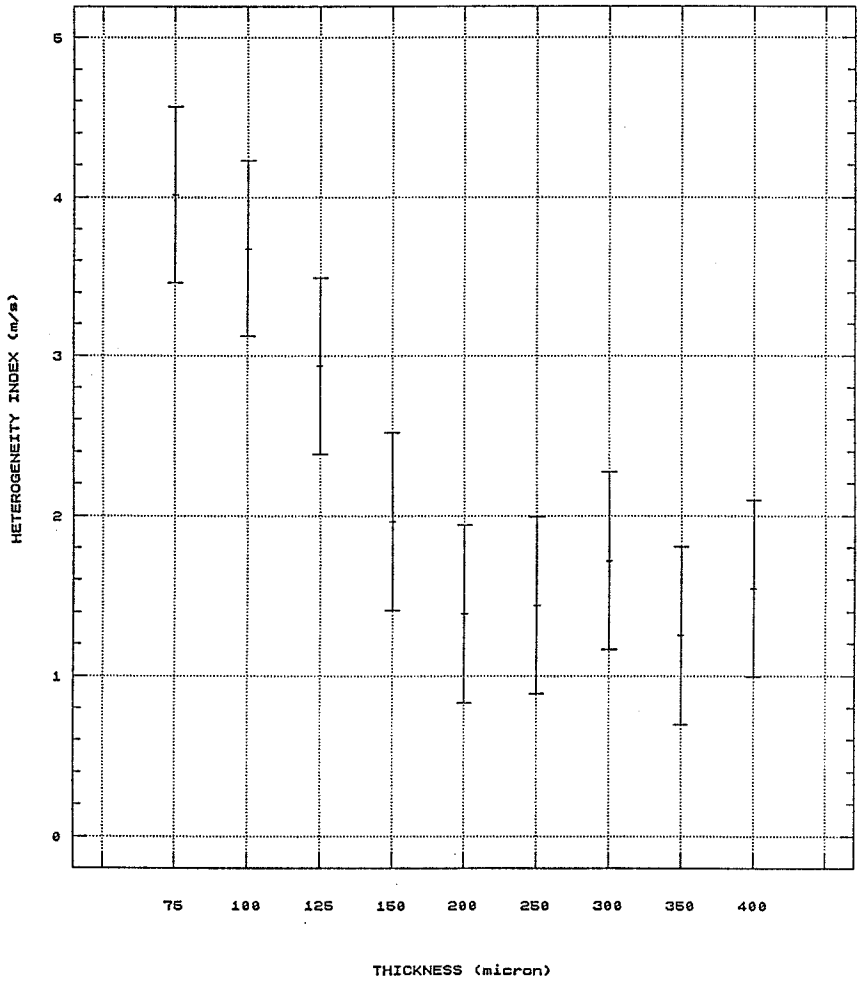

Figure VI.6. Statgraphics ANOVA: heterogeneity index of rat heart tissue vs. thickness.

REFERENCES

[1] Miller, J. G. and B. E. Sobel, "Cardiac Ultrasonic Tissue Characterization," Hosp. Prac., Jan. 1982, pp. 143-151.

[2] Pohlman, R., "Uber die Absorption des Ultraschalls im menschlichen Gewenben und ihre Abhangigkeit von des Frequenz," Phys. Z., vol. 40, pp. 159-161, 1939.

[3] Carstensen, E. L., K. Li, and H. P. Schwan, "Determination of the Acoustic Properties of Blood and its Components," J. Acoust. Soc. Amer., vol. 25, pp. 286-289, 1953.

[4] Carstensen, E. L. and H. P. Schwan, "Acoustic Properties of Hemoglobin Solutions," J. Acoust. Soc. Amer., vol. 31, p. 305, 1959.

[5] Pauly, H. and H. P. Schwan, "Mechanism of Absorption of Ultrasound in Liver Tissue," J. Acoust. Soc. Amer., vol. 50, pp. 692-699, 1971.

[6] Bamber, J. C., J. J. Fry, C. R. Hill, and F. Dunn, "Ultrasonic Attenuation and Backscatter by Mammalian Organs as a Function of Time After Excision," Ultrasound Med. Biol., vol. 3, p. 15, 1977.

[7] Frucht, A. H., "Die Schallgeschwindigkeit in menschlichen and tierischen Geweben," Z. ges. exp. Med., vol. 120, pp. 526-557, 1953.

[8] Goss, S. A., "The Role of Collagen in the Ultrasonic Properties of Tissue," Ph.D. dissertation, University of Illinois, Urbana, IL, 1978.

[9] Dussik, K. T. and D. J. Fritch, "Determination of Sound Attenuation and Sound Velocity in the Structures Constituting the Joints, and of the Ultrasonic Field Distribution within the Joints on Living Tissues and Anatomical Preparations, both in Normal and Pathological Conditions," Public Health Service, National Institute of Health Project A454, Progress Report, April 15, 1956.

[10] Dussik, K. T. and D. J. Fritch, "Determination of Sound Attenuation and Sound Velocity in the Structures Constituting the Joints, and of the Ultrasonic Field Distribution within the Joints on Living Tissues and Anatomical Preparations, both in Normal and Pathological Conditions," Public Health Service, National Institute of Health Project A454, Progress Report, September 15, 1956.

[11] Pohlhammer, J. and W. D. O'Brien Jr., "The Relationship Between Ultrasonic Attenuation and Speed in Tissues and the Constituents: Water, Collagen, Protein and Fat," Med. Phy. of CT Ultras.: Tissue Imaging and Characterization, G. D. Fullerton and J. A. Zagzebski, editors, pp. 409-435, 1980.

[12] Goss, S. A., L. A. Frizzell, F. Dunn, and K. A. Dines, "Dependence of the Ultrasonic Properties of Biological Tissue on Constituent Proteins," J. Acoust. Soc. Amer., vol. 67, pp. 1041-1044, 1980.

[13] Fields, S. and F. Dunn, "Correlation of Echographic Visualizability of Tissue with Biological Compositions and Physiological State," J. Acoust. Soc. Amer., vol. 54, pp. 809-812, 1973.

[14] Goss, S. A. and W. D. O'Brien Jr., "Direct Ultrasonic Velocity Measurements of Mammalian Collagen Threads," J. Acoust. Soc. Amer., vol. 65, pp. 507-511, 1979.

[15] O'Brien, W. D. Jr., J. W. Erdman, and T. B. Hebner, "Ultrasonic Propagation Properties (@ 100 MHz) in Excessively Fatty Rat Liver," J. Acoust. Soc. Amer., vol. 83, pp. 1159-1166, 1988.

[16] Agemura, D. H., "Ultrasonic Propagation Properties of Canine Myocardium and Bovine Articular Cartilage at 100 MHz," M.S. thesis, University of Illinois, Urbana, IL, 1988.

[17] Spain, D. M. and V. A. Bradess, "Sudden Death from Coronary Heart Disease: Survival Time, Frequency of Thrombi, and Cigarette Smoking," Chest, vol. 58, pp. 107-110, 1970.

[18] Wild, J. J., M. D. Crafford, and J. M. Reid, "Visualization of the Excised Human Heart by Means of Reflected Ultrasound or Echography," Amer. Heart J., vol. 54, pp. 903-906, 1957.

[19] Rasmussen S., B. C. Cohya, H. Feigenbaum, and S. B. Knoebel, "Detection of Myocardial Scar Tissue by M-mode Echocardiography," Circ., vol. 57, pp. 230-237, 1978.

[20] Bhandari A. K. and N. L. Nanda, "Myocardial Texture Characterization by Two-dimensional Echocardiography," Amer. J. Cardio., vol. 51, pp. 817-825, 1983.

[21] Martin, P. R., H. Rakowski, J. French, and R. L. Popp, "Idiopathic Hypertrophic Subaortic Stenosis Viewed by Wide-angle Phased Array Echocardiography," Circ., vol. 59, pp. 1206-1217, 1979.

[22] Skorton, D. J., S. M. Collins, J. Nichols, N. G. Pandian, J. A. Bean, and R. E. Kerber, "Quantitative Texture Analysis in Two-dimensional Echocardiography: Application to the Diagnosis of Experimental Myocardial Contusion," Circ., vol. 68, pp. 217-223, 1983.

[23] Skorton, D. J., H. E. Melton, N. G. Pandian, J. Nichols, S. Koyanagi, M. L. Marcus, S. M. Collins, and R. E. Kerber, "Detection of Acute Myocardial Infarction in Closed Chest Dogs by Analysis of Regional Two-dimensional Echocardiographic Grey-level Distributions," Circ. Res., vol. 52, pp. 36-44, 1983.

[24] Haendchen, R. V., K. Ong, M. C. Fishbein, W. Zwehl, S. Meerbaum, and E. Corday, "Early Differentiation of Infarcted and Noninfarcted Reperfused Myocardium in Dogs by Quantitative Analysis of Regional Myocardium Echo Amplitudes. Circ. Res., vol. 57, pp. 718-728, 1985.

[25] Miller, J. G., J. E. Perez, and B. E. Sobel, "Ultrasonic Characterization of Myocardium," Prog. in Cardio. Diseases, vol. 28 no. 2, pp. 85-110, 1985.

[26] Lele, P. P. and J. Namery, "A Computer-based Ultrasonic System for the Detection and Mapping of Myocardial Infarcts," Proc. San Diego Biomed. Symp., vol. 13, pp. 121-132, 1974.

[27] Mimbs, J. W., D. E. Yuhas, A. N. Weiss, and B. E. Sobel, "Detection of Myocardial Infarction in Vitro Based on Altered Attenuation of Ultrasound," Circ. Res., vol. 4, pp. 192-198, 1977.

[28] O'Donnell, M., J. W. Mimbs, J. G. Miller, and B. E. Sobel, "Ultrasonic Attenuation in Normal and Ischemic Myocardium," Ultras. Tissue Charac. II, M. Linzer, editor, National Bureau of Standards, Special Publication 525, U.S. Government Printing Office, Washington, D.C., pp. 63-71, 1979.

[29] Mimbs, J. W., D. Bauwens, R. D. Cohen, M. O'Donnell, and J. G. Miller, "Effects of Myocardial Ischemia on Quantitative Ultrasonic Backscatter and Identification of Responsible Determinants," Circ. Res., vol. 49, pp. 89-96, 1981.

[30] Rhyne, T. L., K. B. Sagar, L. S. Wann, and G. Haasler, "The Myocardial Signature: Absolute Backscatter, Cyclic Variation, Frequency Variation and Statistics," Ultrason. Imaging, vol. 8, pp. 107-120, 1986.

[31] Rhyne, T. L., K. B. Sagar, L. S. Wann, and G. Haasler, "A Myocardial Backscatter Parameter with Maximal Sensitivity to Cyclic Variation," IEEE Ultrason. Symp. Proc., IEEE Catalog No. 86H23775-4:909, 1986.

[32] Sagar, K. B., T. L. Rhyne, D. C. Warltier, L. Pelc, and L.S. Wann, "Intramyocardial Variability in Integrated Backscatter: Effects of Coronary Occlusion and Reperfusion," Circ. Res., vol. 75, pp. 436-442, 1987.

[33] Whitman, R. L. and A. Korpel, "Probing of Acoustic Surface Perturbations by Coherent Light," Appl. Opt., vol. 8, pp. 1567-1576, 1969.

[34] Korpel, A. and P. Desmares, "Rapid Sampling of Acoustic Holograms by Laser-Scanning Techniques," J. Acoust. Soc. Amer., vol. 45, pp. 881-884, 1969.

[35] Kessler, L. W., P. R. Palermo, and A. Korpel, "Practical High Resolution Acoustic Microscopy," Acoust. Holography, G. Wade, editor, vol. 4, Plenum Press, New York, pp. 51-71, 1972.

[36] Kessler, L. W., "Review in Progress and Applications of Acoustic Microscopy," J. Acoust. Soc. Amer., vol. 55, pp. 909-918, 1974.

[37] Kessler, L. W., "Introduction to Acoustic Imaging Systems," Acoustic Imaging, G. Wade, editor, Plenum Press, New York, pp. 43-63, 1976.

[38] Kessler, L. W., "Imaging with Dynamic-Ripple Diffraction," Acoustic Imaging, G. Wade, editor, Plenum Press, New York, pp. 229-239, 1976.

[39] Kessler, L. W., "Acoustic Microscopy Commentary: SLAM and SAM," IEEE Trans. Sonics Ultrason., vol. SU-32, pp. 136-137, 1985.

[40] Yuhas D. E. and L. W. Kessler, "Acoustic Microscopy of Excised Tissues," Proc. Soc. Opt. Inst. Eng., vol. 152, pp. 47-53, 1978.

[41] Nicozisin, D. D., "An Automated Imaging Data Acquisition and Analysis System for the Scanning Laser Acoustic Microscope," M.S. thesis, University of Illinois, Urbana, IL, 1989.

[42] Steiger, D. L., "Ultrasonic Assessment of Skin and Wounds with the Scanning Laser Acoustic Microscope," M.S. thesis, University of Illinois, Urbana, IL, 1986.

[43] Foster, S., "An Image Digitizing System for a Scanning Laser Acoustic Microscope," M.S. thesis, University of Illinois, Urbana, IL, 1981.

[44] Embree, P. M., S. G. Forster, G. Bright, and W. D. O'Brien Jr., "Ultrasonic Velocity Spatial Distribution Analysis of Biological Materials with the Scanning Laser Acoustic Microscope," Acoustical Imaging, M. Kaveh, R. K. Mueller and J. F. Greenleaf, editors, vol. 13, Plenum Press, New York, pp. 203-216, 1984.

[45] Embree, P. M., K. M. U. Tervola, S. G. Foster, and W. D. O'Brien Jr., "Spatial Distribution of the Speed of Sound in Biological Materials with the Scanning Laser Acoustic Microscope," IEEE Trans. Sonics Ultrason., vol. SU-32, pp. 341-350, 1985.

[46] Tervola, K. M. U. and W. D. O'Brien Jr., "Spatial Frequency Domain Technique: An Approach for Analyzing the Scanning Laser Acoustic Microscope Interferogram Images," IEEE Trans. Sonics Ultrason., vol. SU-32, pp. 544-554, 1985.

[47] Steiger, D. L., W. D. O'Brien Jr., J. E. Olerud, M. A. Riederer-Henderson, and G. F. Odland, "Measurement Uncertainty Assessment of the Scanning Laser Acoustic Microscope and Application to Canine Skin and Wound," IEEE Trans. Ultrason., Ferroelec. and Freq., vol. 35, pp. 741-748, 1988.

[48] Sagar, K. B., L. Pelc, T. L. Rhyne, L. S. Wann, and D. C. Warltier, "Influence of Heart Rate, Preload, Afterload and Inotropic State on Integrated Backscatter. Circ. Res., vol. 77, pp. 478-483, 1988.

[49] Marangoni R. D., A. A. Glaser, J. S. Must, G. S. Brody, T. G. Beckwith, G. R. Walker, and W. L. White, "Effect of Storage and Handling Techniques on Skin Tissue Properties," Ann. N.Y. Acad. Sc., vol. 136, pp. 439-454, 1966.

[50] Geleskie, J. V. and K. K. Shung, "Further Studies on Acoutstic Impedance of Major Bovine Blood Vessel Walls," J. Acoust. Soc. Amer., vol. 71, pp. 467-470, 1982.

[51] Wear, K. A., T. A. Shoup, and R. L. Popp, "Ultrasonic Characterization of Canine Myocardium," IEEE Trans. Sonics Ultrason., vol. SU-33, p. 247, 1986.

[52] Kloner, R. A., R. E. Rude, N. Carlson, P. R. Maroko, L. W. V. DeBoer, and E. Braunwald, "Ultrastructural Evidence of Microvascular Damage and Myocardial Cell Injury After Coronary Artery Occlusion: Which Comes First?" Circ. Res., vol. 62, p.945, 1980.

[53] Trautmann, A. and J. Fiebiger, Fundamentals of the Histology of Domestic Animals, Comstock Publishing Assoc., New York, pp. 70 and 335, 1957.

[54] Bloom W. and D. W. Fawcett, A Textbook of Histology, ninth ed., W. B. Saunders Company, Philadelphia, p. 586, 1968.